SECOND ORDER ORBIT PERTURBATIONS and DISTRIBUTIONS OF ORBITING PARTICLES

by

CHARLES WILLIAM PERKINS

B. of A. E., Rensselaer Polytechnic Institute
(1959)

S. M., Massachusetts Institute of Technology
(1960)

SUBMITTED IN PARTIAL FULFILLMENT
OF THE REQUIREMENTS FOR THE
DEGREE OF DOCTOR OF SCIENCE

at the

MASSACHUSETTS INSTITUTE OF TECHNOLOGY
December, 1963

Signature of Author Signature redacted
Department of Aeronautics
and Astronautics, December 1963

Certified by Signature redacted
Thesis Supervisor

Accepted by Signature redacted
Chairman, Departmental
Graduate Committee

SECOND ORDER ORBIT PERTURBATIONS AND DISTRIBUTIONS OF ORBITING PARTICLES

by

Charles W. Perkins

Submitted to the Department of Aeronautics and Astronautics on December 6, 1963, in partial fulfillment of the requirements for the degree of Doctor of Science.

ABSTRACT

Second-order analytic expressions are derived for the satellite orbit perturbations caused by the second zonal harmonic of the gravitational field of the earth. These expressions are incorporated into an existing digital computer program which is capable of predicting orbit behavior over many orbital periods. Detailed studies were carried out, with the aid of this program, for the orbits of 1960 Iota 2 (the Echo I rocket case) and 1961 Delta 1 (a 12 ft. diameter, rigid balloon). The computed orbital elements are shown to compare within the order of the theory to the precisely-reduced photographic data prepared by the Smithsonian Astrophysical Observatory for 1960 Iota 2 and 1961 Delta 1. For example, the maximum error in the computed eccentricity for the orbit of 1960 Iota 2 during a 200 day interval is 2×10^{-5} compared to 8×10^{-4} if the second-order theory is neglected. The program was further applied to the improvement of empirical atmospheric density models using the 1961 Delta 1 data. The demise of 1961 Delta 1 is predicted to occur on or about March 28, 1964. The second-order theory is also used to explain an oscillation of amplitude 100 seconds and period 300 days in the time of nodal crossing of a heavy satellite observed by radar.

The distributions of orbiting particles are treated both analytically and by Monte Carlo techniques with specific application to the West Ford dipole ensemble. Comparisons are made to radar and optical observations of the belt.

Thesis Supervisor: Marten T. Landahl

Title: Professor of Aeronautics and Astronautics

ACKNOWLEDGEMENTS

The author wishes to express his appreciation to the following persons: Professors M. Landahl and W. Wrigley for their supervision, Professors R. Halfman, P. Sandorff and H. G. Stever for serving on the committee, and Miss J. Dickhaut, Mrs. C. Mawdsley, and Miss J. Kula who typed the manuscript.

The author especially wishes to thank Dr. I. Shapiro and Dr. H. Jones for their continued direction and encouragement.

The author also wishes to thank M. I. T. Lincoln Laboratory* under whose auspices this work was carried out.

*Operated with support from the U. S. Air Force.

TABLE OF CONTENTS

PRINCIPAL NOTATIONS

a	semi-major axis (see Fig. 1.1)
a_p, A_p	geomagnetic planetary indices (see. Figs. 3.4, 3.5)
A/M	area-to-mass ratio
$b = e \cdot \cos(\Omega + \omega)$	see Chapter 4
C_D	drag coefficient
D	coefficient of the fourth zonal harmonic (see Eq. (1.14))
e	eccentricity (see Fig. 1.1)
E	eccentric anomaly
$E_1 \cdots E_{11}$	(see Eq. (1.21))
$\mathcal{E}$	total orbital energy per unit mass of a satellite (see Eq. (1.11))
$F_{10.7}$, $\bar{F}_{10.7}$	10.7 cm solar flux (see Figs. 3.4, 3.5)
GM	gravitational constant
i	inclination (see Fig. 1.2)
J	coefficient of the second zonal harmonic (see Eq. (1.14))
K	coefficient of the third zonal harmonic (see Eq. (1.14))
l	orbital angular momentum per unit mass of a satellite*
M	mean anomaly
n	mean motion
n	density of dipoles (see Chapter 4)
N	total number of dipoles
p	semi-latus rectum (see Fig. 1.1)
p_μ, etc.	probability density function of μ, etc. (see Chapter 4)
P	orbital period
$P_1 \cdots P_7$	(see Eq. (1.20))

*unless otherwise noted

r	instantaneous orbit radius (see Fig. 1.1)
$\tilde{R}, \tilde{S}$, and $\tilde{W}$	components of the perturbing accelerations
t	time
T	time of nodal crossing
T_N	night-time top temperature (see Eq. (3.1))
T	top temperature (see Eq. (3.2))
u	argument of latitude (see Fig. 1.2)
$u = \mu/V_{max}$	(see Chapter 4)
$U' = -U$	potential energy per unit mass of a satellite (see Eqs. (1.11) and (1.14))
v	true anomaly (see Fig. 1.2)
V	dipole dispensing speed (see Chapter 4)
V_R, V_S, and V_W	components of dispensing velocity (see Chapter 4)
$W = \Omega + \omega$	(see Chapter 4)
$W_1 \cdots W_{12}$	(see Eq. (1.22))
$x = \sigma/\sigma_m$	(see Chapter 4)
$y = \rho/\rho_m$	(see Chapter 4)
δp, etc.	first-order perturbations in p, etc.
Δp, etc.	second-order perturbations in p, etc.
η	component of dispensing velocity perpendicular to orbit plane (see Chapter 4)
$\lambda = \cos \Omega$	(see Chapter 4)
μ	component of dispensing velocity in orbit plane (see Chapter 4)
$\nu \overset{\Delta}{=} u - \omega_o$	
ρ	(see Eq. (4.40))
σ	dipole position along the orbit (see Eq. (4.10))
τ	(see Eq. (4.31))

ϕ	location angle of Intersection Plane (see Fig. 4.2)
ψ	(see Eq. (3.1))
ω	argument of perigee (see Figs. 1.2 and 4.2)
$\vec{\omega}_s$	dipole dispenser angular momentum vector (see Chapter 4)
Ω	right ascension of the ascending node (see Fig. 1.2)
Ω	dipole release point (see Fig. 4.2)

Subscripts

o	denotes osculating elements at nodal crossing (e.g., p_o)
o	denotes dispenser elements in Chapter 4
m	denotes SAO mean elements
Max or m	denotes maximum value in Chapter 4
N and S	denote north and south auroral bulges in Chapter 3

INTRODUCTION

Applications of orbit perturbation computations include the prediction of satellite orbits and the analysis of orbital data. The prediction problem can be further divided into predicting where to find a satellite at some time in the future and predicting when events such as final orbital decay will occur. The comparison of orbit perturbations, computed from theory, with observed changes in orbital elements tests the adequacy of the theory and provides a means with which to study the physical effects which cause perturbing accelerations.

Consider, for example, the problem of acquiring (finding) an orbiting satellite with a radar. The position of the satellite must be predicted as a function of time with sufficient accuracy that the "volume" of uncertainty can be searched by the radar while the satellite is above the horizon. If the allowable Doppler uncertainty is also limited, this volume is four dimensional (typically, azimuth, elevation, range and Doppler). Ideally the satellite should fall within the radar beam without elaborate searching. As the antenna size and operating frequencies of high precision radars increase, the beamwidths of these radars decrease. Hence, the volume that such instruments can search for a target decreases. This problem of finding a satellite is already difficult for existing 1/10 degree beamwidth radars, such as the Project West Ford radars, if the satellite is sensitive to erratic atmospheric density fluctuations as is the 12 ft. balloon, 1961 Delta 1. With the advent of milliradian beam radars such as the Haystack facility and eventually laser "radars", the problem will become acute.

The following chapters treat (without specific reference to the acquisition problem) aspects of the problem of orbit-perturbation computation accuracy which are important to large classes of satellites.

Second-order analytic expressions are derived in Chapter I for the orbit perturbations caused by the second zonal harmonic of the gravitational field of the earth. Comparisons are made in Chapter II between observed orbital parameters and parameters computed with a

digital computer program that incorporates this second order theory. This computer program is further extended to the study of semi-empirical atmospheric density models in Chapter III.

The distributions of orbiting particles in the West Ford dipole ensemble are treated in Chapter IV both analytically and by Monte Carlo techniques. Comparisons are made to distributions which were determined from radar and optical observations of the experimental dipole belt.

CHAPTER I

Second-Order Orbit Perturbations Caused by the Second Zonal Harmonic of the Gravitational Field of the Earth

1.1 Introduction

Each force that perturbs a satellite of the earth from a Keplerian elliptical orbit is usually small compared with the central gravitational field. Any attempt to classify these perturbing forces in order of their importance is complicated, however, by the dissimilarity of the effects on the orbit, by the dependence of these effects on the particular satellite orbit, by the physical properties of the satellite, etc. and by a variety of other special conditions. The primary importance of the second zonal spherical harmonic of the gravitational field of the earth[1.1 *] can be demonstrated despite this difficulty of classification by comparing the magnitudes of each perturbing force.

The ratio of the force exerted by the second zonal spherical harmonic (commonly called" the equatorial bulge") to the central field is of order J, where $J \sim 10^{-3}$ is the empirically determined coefficient of this harmonic.[1.1] The order of magnitude of the ratios of other perturbing forces to the central force such as the higher gravitational harmonics, drag, solar radiation pressure and the gravitational attraction of the sun and moon are, in general, of order J^2 and higher for a large class of earth satellites. For example, the following table compares a set of computed** perturbations of the argument of perigee (ω) (see Fig. 1.1) for one orbital period of 1961 Delta 1 (a 12 ft diameter balloon satellite).

---

*Refers to references at end of chapter.

**See Chapters II and III for the details of these computations.

Perturbing force	ω perturbation
Solar radiation pressure	$1.89^\circ \times 10^{-3}$
Atmospheric drag	$-7.21^\circ \times 10^{-5}$
Zonal Harmonics	
First order, second harmonic	$3.89^\circ \times 10^{-1}$
Second order, second harmonic	$2.36^\circ \times 10^{-3}$
Third harmonic	$1.47^\circ \times 10^{-3}$
Fourth harmonic	$-1.68^\circ \times 10^{-4}$
Fifth harmonic	$-2.93^\circ \times 10^{-5}$
Lunar gravitation	$2.62^\circ \times 10^{-5}$
Solar gravitation	$-3.35^\circ \times 10^{-6}$

A perturbation theory which accounts for perturbations such as drag, etc. to first order should therefore account for perturbations from the second harmonic to second order in J. This theory need not account for the cross terms between the second harmonic and the other perturbing forces because these terms will be of order J^3 and higher.

Here we develop analytically, to order J^2, the orbit perturbations caused by the second harmonic between two successive ascending crossings of the equator by the satellite (a nodal period). These solutions are included in a high-speed digital computer program (see Appendix II) which computes the net effects of other perturbing forces averaged over a nodal period. By iteration, the orbital elements after each of a large number of successive nodal cycles are computed.

The perturbation equations could of course be integrated numerically by the computer directly but this procedure consumes too much computer operating time and makes it more difficult to obtain a qualitative description of the perturbations which follows directly from analytic solutions.

1.2 General Method of Solution

With a known force law, only six independent constants are necessary to completely describe the position and velocity vectors of a satellite as functions of time. If the satellite were moving in a simple central gravitational field, a convenient set of constants would be a set

of six independent elements of a Keplerian ellipse. If the force law is complicated by small "perturbing" forces such a set of six independent elements will be slowly varying with time (slow in comparison to the rapid variation of the position and velocity vectors). A convenient set of elements, termed osculating elements, is a set which completely describesthe ellipse that can be constructed at each instant of time given the instantaneous position and velocity vectors and neglecting all forces except the primary central force. This set will then change with time because of the action of the perturbing forces.

The exact perturbation equations of a set of six independent osculating elements of a satellite orbit are first-order, but non-linear. Exact closed form solutions to this set of equations, in terms of well-known functions, cannot in general be obtained.

The procedure used in this chapter to derive approximate analytic solutions to the set of perturbation equations is characterized by the following generalized example:

Let f_N, $N = 1, 2, \ldots, 6$, represent six independent osculating orbital elements and let

$$\frac{df_N}{du} = F_N(f_1, f_2, \ldots, f_6, J, u) \qquad N = 1, 2, \ldots, 6 \tag{1.1}$$

represent the corresponding perturbation equations for the second harmonic of the earth* where u is an independent variable.

A first approximation to the solution of this set of equations is:

$$\delta f_N(J, u) = \int_0^u F_N(f_1|_{u=0}, f_2|_{u=0}, \ldots, f_6|_{u=0}, J, u)du \quad N = 1, 2, \ldots, 6 \tag{1.2}$$

This process gives the perturbations of the elements (including the short period perturbations which have zero averages over one nodal period) that are accurate only to order J.

---

*To order J^2, each perturbing acceleration can be treated independently from the other perturbing accelerations if the others are of order J^2.

Perturbations over one orbit cycle, accurate to J^2, are derived as follows:

$$\Delta f_N = \int_0^{2\pi} F_N \left[(f_1|_{u=0} + \delta f_1(J, u)), \ldots, (f_6|_{u=0} + \delta f_6(J, u)), J, u \right] du$$

$$N = 1, 2, \ldots, 6 \qquad (1.3)$$

The gravitational field of the earth as represented by the zonal spherical harmonics is conservative and rotationally symmetric about the polar axis. Therefore, the labor of performing two of the above integrations can be reduced by using explicitly the conservation of energy and the conservation of angular momentum about the axis of symmetry.

1.3 Orbital Elements

The particular set of osculating orbital elements used in this analysis are: the semi-latus rectum (p) (and alternatively the semi-major axis (a)), the eccentricity (e), the argument of perigee (ω), the right ascension of the ascending node (Ω), the inclination (i), and the time of nodal crossing (T) [see Figs. 1.1 and 1.2]. The osculating elements at nodal crossing are designated by a zero subscript (for example, p_o).

The argument of latitude (u) [see Fig. 1.2] is used as an independent variable in place of time. The angle (ν) (defined as $\nu = u - \omega_o$) is sometimes used as an independent variable when the transformation serves to simplify the integration of the perturbation equations.

In addition, the instantaneous radius (r), the true anomaly (v) [see Fig. 1.1] and the eccentric anomaly ($E = 2\tan^{-1}\left(\sqrt{\frac{1-e}{1+e}}\tan\frac{v}{2}\right)$) are used as intermediate variables.

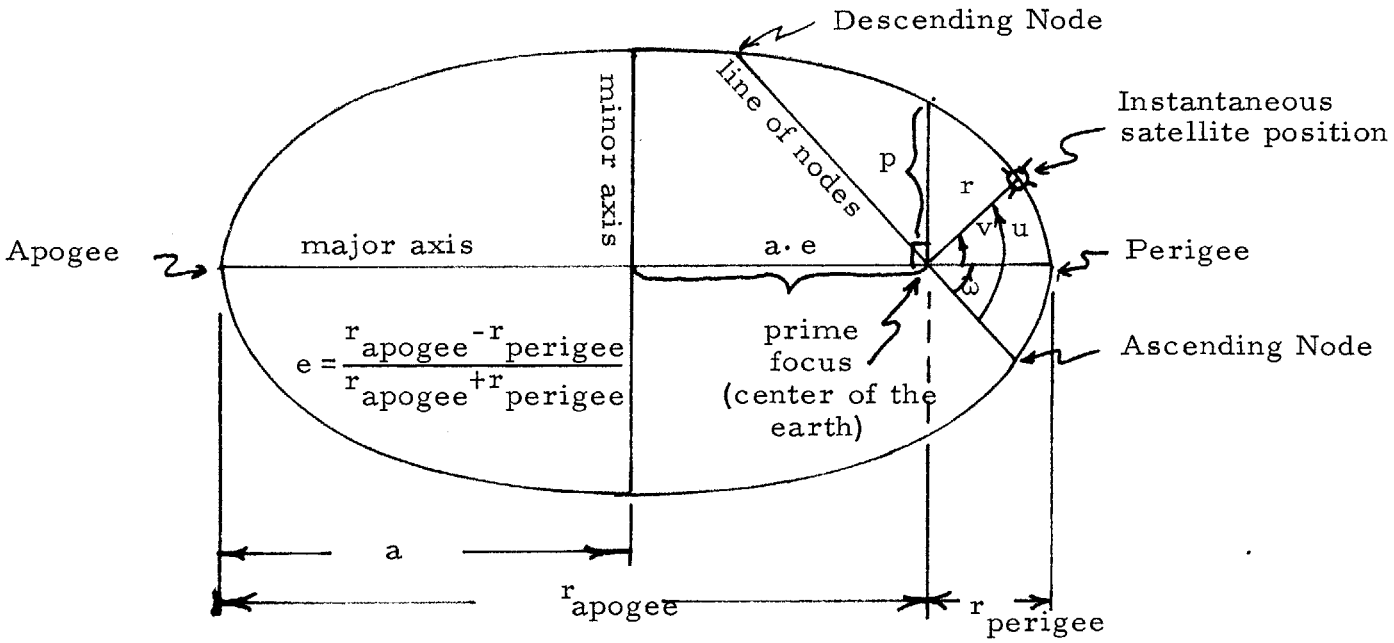

Figure 1.1

The plan view of an orbit

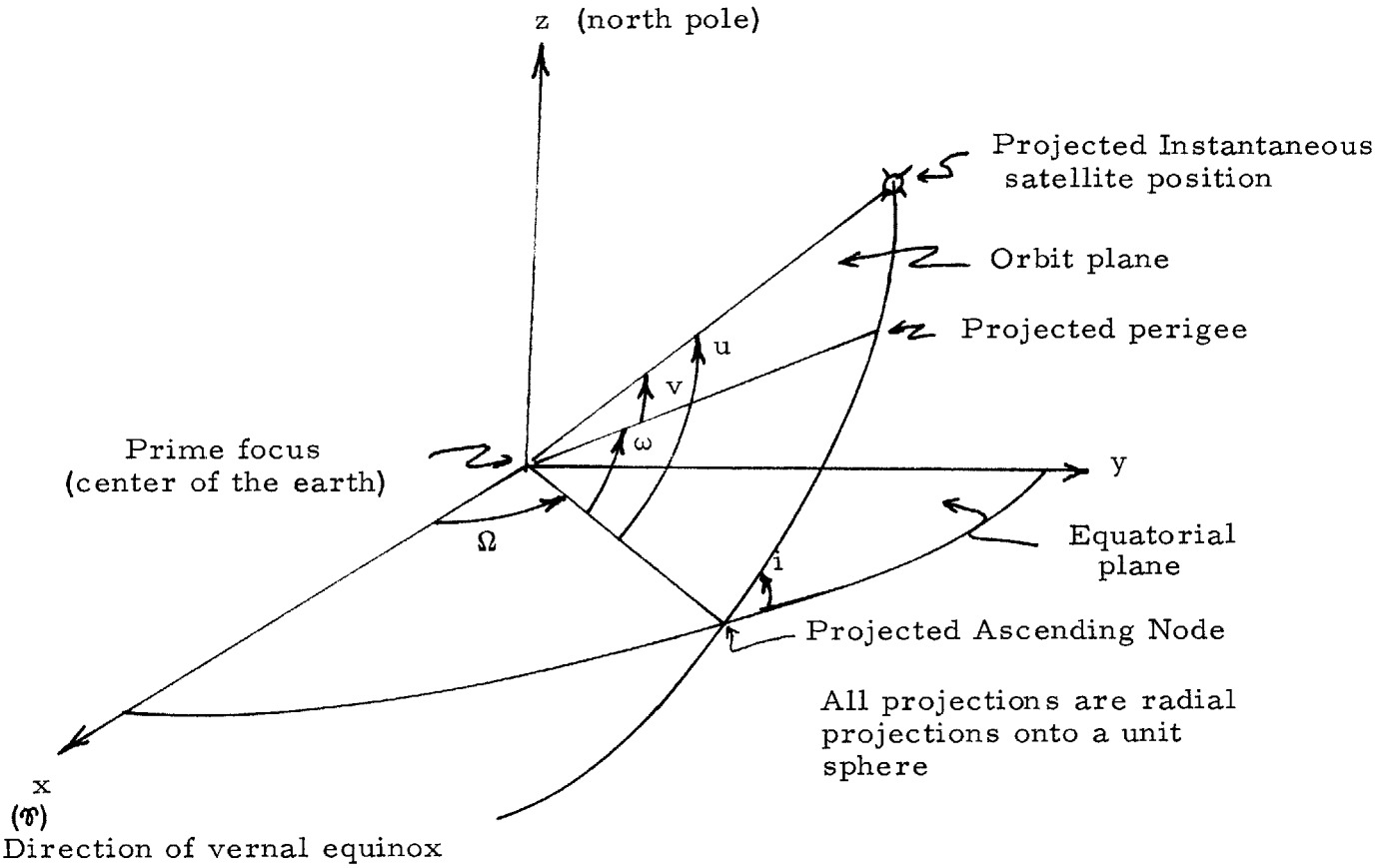

Figure 1.2

The geocentric coordinate system of the orbit in space

1.4 Perturbation Equations

Five of the perturbation equations with time as the independent variable are as follows:[1.3]

$$\frac{dp}{dt} = 2r\sqrt{\frac{p}{GM}}\,\tilde{S}$$

$$\frac{de}{dt} = \sqrt{\frac{p}{GM}}\,\sin v\cdot\tilde{R} + \sqrt{\frac{p}{GM}}\left[\left(1+\frac{r}{p}\right)\cos v + e\,\frac{r}{p}\right]\tilde{S}$$

$$\frac{d\omega}{dt} = -\sqrt{\frac{p}{GM}}\,\frac{\cos v}{e}\,\tilde{R} + \sqrt{\frac{p}{GM}}\left(1+\frac{r}{p}\right)\frac{\sin v}{e}\,\tilde{S} - \sqrt{\frac{p}{GM}}\left(\frac{r}{p}\right)\cot i\cdot\sin u\cdot\tilde{W}$$

$$\frac{d\Omega}{dt} = \sqrt{\frac{p}{GM}}\left(\frac{r}{p}\right)\frac{\sin u}{\sin i}\,\tilde{W}$$

$$\frac{di}{dt} = \sqrt{\frac{p}{GM}}\,\frac{r}{p}\,\cos u\cdot\tilde{W} \qquad (1.4)$$

where $\tilde{R}$, $\tilde{W}$, and $\tilde{S}$ are the components of the perturbing accelerations along the instantaneous radius vector ($\vec{R}$), perpendicular to the orbit plane in the direction of the orbital angular momentum vector ($\vec{W}$) and in the $\vec{W} \times \vec{R}$ direction ($\vec{S}$) respectively. For the second zonal harmonic, $\tilde{R}$, $\tilde{W}$, and $\tilde{S}$ are proportional to J. In addition, GM is the gravitational constant of the earth.

The sixth element is treated in a slightly different manner. Since the five elements given above are sufficient to completely describe the orbit, the sixth element need only relate the position of the satellite in the orbit to time. The time of nodal crossing (T) is used here as the sixth element.

The change in time of nodal crossing can be found by integrating $\frac{dt}{du}$ over the orbital cycle (nodal crossing to nodal crossing). Applying the normal first-order method (Eq. (1.2)) gives a zeroth order (in J) change in T; namely, T is incremented by a Keplerian period. Likewise, applying the second-order method (Eq. (1.3)) will yield only a zeroth-order and a first-order term.*

*However, to simplify the terminology, mention of "second-order effects" will be taken to mean effects on T to only first order in J, unless otherwise noted.

The rate $\frac{dt}{du}$ can be obtained in a simple manner from the following diagram[1.4] which represents the radial projection of arcs onto a unit sphere.

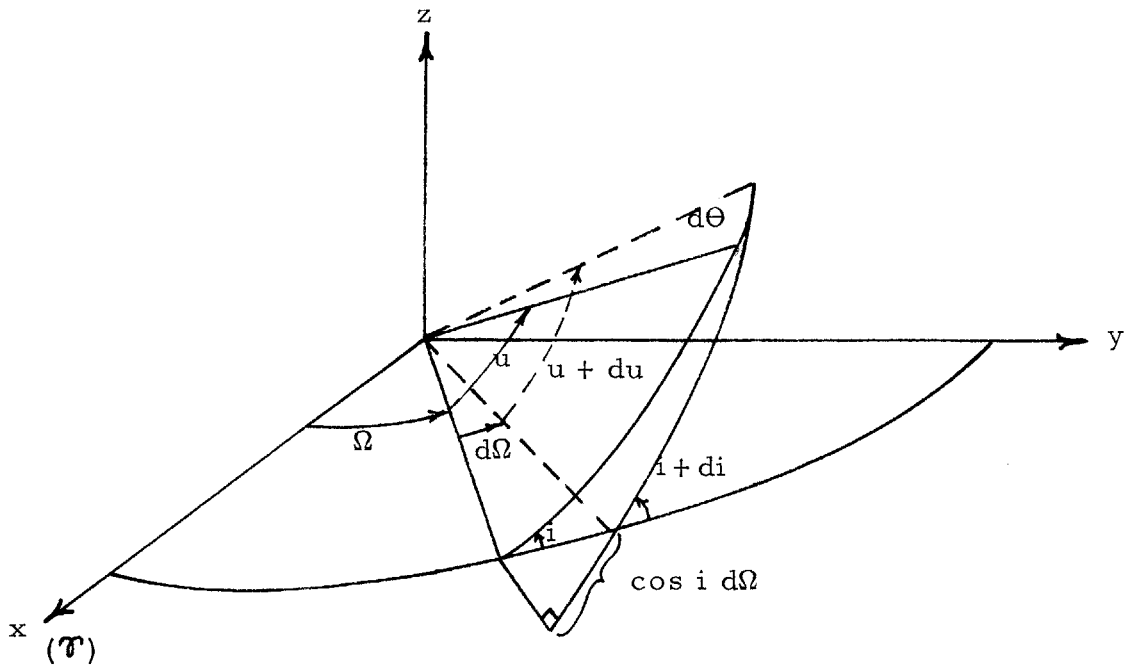

Figure 1.3
Angular Rate

In the limit of differential increments,

$$du = d\Theta - \cos i \, d\Omega \tag{1.5}$$

where $\frac{d\Theta}{dt}$ is the instantaneous angular rate of the satellite position unit vector. This rate determines the osculating semi-latus rectum (p).[1.5]

$$\frac{d\Theta}{dt} = \frac{\sqrt{GMp}}{r^2} \tag{1.6}$$

Substituting this and $\frac{d\Omega}{dt}$ from the perturbation equations into (1.5) yields:

$$\frac{dt}{du} = \frac{r^2}{\sqrt{GMp}\ \left(1 - \frac{r^3}{GMp} \cot i \cdot \sin u \cdot \tilde{W}\right)} \tag{1.7}$$

In a first-order theory, $\frac{dt}{du}$ is approximated by:

$$\frac{dt}{du} \approx \frac{r^2}{\sqrt{GMp}} \tag{1.8}$$

In a second-order theory, terms must be kept which are of the same order as the short-period perturbations of the elements. Expanding the denominator in a power series of $\tilde{W}$ and retaining terms to first order (J) yields:

$$\frac{dt}{du} \approx \frac{r^2}{\sqrt{GMp}} + \frac{r^5}{(GMp)^{3/2}} \cot i \cdot \sin u \cdot \tilde{W} \tag{1.9}$$

In addition to yielding the change of T, the rate $\frac{dt}{du}$ is also used to change the independent variable of the perturbation equations from t to u. The perturbation equations in terms of u, and consistent to second order, are

$$\frac{dp}{du} = \frac{2r^3}{GM} \tilde{S} + \frac{2r^6}{p(GM)^2} \cot i \cdot \sin u \cdot \tilde{S}\tilde{W}$$

$$\frac{de}{du} = \frac{r^2}{GM} \sin v \cdot \tilde{R} + \frac{r^2}{GM} \left[\left(1 + \frac{r}{p}\right) \cos v + e\frac{r}{p} \right] \tilde{S}$$

$$+ \frac{r^5}{p(GM)^2} \cot i \cdot \sin u \cdot \sin v \cdot \tilde{R}\tilde{W} + \frac{r^5}{p(GM)^2} \cot i \left[\left(1+\frac{r}{p}\right)\cos v + e\frac{r}{p} \right] \sin u \cdot \tilde{S}\tilde{W}$$

$$\frac{d\omega}{du} = -\frac{r^2}{GM} \frac{\cos v}{e} \tilde{R} + \frac{r^2}{GM} \left(1+\frac{r}{p}\right) \frac{\sin v}{e} \tilde{S} - \frac{r^3}{GMp} \cot i \sin u \tilde{W}$$

$$+ \frac{r^5}{p(GM)^2} \cot i \cdot \sin u \cdot \tilde{W} \left[-\frac{\cos v}{e} \tilde{R} + \left(1+\frac{r}{p}\right) \frac{\sin v}{e} \tilde{S} - \left(\frac{r}{p}\right) \cot i \sin u \tilde{W} \right]$$

$$\frac{d\Omega}{du} = \frac{r^3}{GMp} \frac{\sin u}{\sin i} \tilde{W} + \frac{r^6}{(GM)^2 p^2} \frac{\cot i}{\sin i} \sin^2 u \, \tilde{W}^2$$

(continued)

$$\left.\begin{aligned} \frac{di}{du} &= \frac{r^3}{GMp}\cos u\,\tilde{W} + \frac{r^6}{(GM)^2 p^2}\cot i\cdot\sin u\cdot\cos u\cdot\tilde{W}^2 \\ \frac{dt}{du} &= \frac{r^2}{\sqrt{GMp}} + \frac{r^5\cot i\cdot\sin u}{\sqrt{(GMp)^3}}\,\tilde{W} \end{aligned}\right\} \qquad (1.10)$$

1.5 Orbital Energy and Angular Momentum Relations

The total orbital energy per unit mass of a satellite is:

$$\mathcal{E} = \tfrac{1}{2}V^2 + U' \qquad (1.11)$$

where U' is the local potential energy and V is the instantaneous orbital velocity. The velocity V can be expressed at each instant in terms of the osculating semi-major axis (a) and the true radius (r):[1.5]

$$\tfrac{1}{2}V^2 = GM\left(\frac{1}{r} - \frac{1}{2a}\right) \qquad (1.12)$$

The instantaneous orbital angular momentum per unit mass is a function only of the osculating semi-latus rectum (p):[1.5]

$$\ell = \sqrt{GMp}$$

The component of this angular momentum along the polar axis of the earth, which is conserved, is:

$$\ell\cos i$$

Therefore,

$$p\cos^2 i = \text{constant} \qquad (1.13)$$

1.6 Perturbing Accelerations

Traditionally, the potential function of the gravitational field of the earth (defined by astronomers as the negative of the potential energy) has been expanded in terms of spherical harmonics. This expansion up to and including the fourth zonal harmonic is:[1.1]

$$U = \frac{GM}{r}\left\{1 + \frac{J}{r^2}\left(\frac{1}{3} - \sin^2\delta\right) + \frac{K}{r^3}\left(\frac{5}{2}\sin^3\delta - \frac{3}{2}\sin\delta\right)\right.$$

$$\left. + \frac{D}{r^4}\left(\frac{3}{35} + \frac{1}{7}\sin^2\delta - \frac{1}{4}\sin^2 2\delta\right)..\right\} \qquad (1.14)^*$$

where δ is the latitude ($\sin\delta = \sin u \cdot \sin i$) and r is the orbit radius in units of equatorial earth radii** and $GM \approx 1.54 \times 10^{-6}$ (earth radii)^3/sec^2. The potential function for the second zonal harmonic only is simply:

$$U_2 = \frac{GMJ}{r^3}\left(\frac{1}{3} - \sin^2 i \cdot \sin^2 u\right) \qquad (1.15)$$

The perturbing accelerations $\tilde{R}, \tilde{S}$, and $\tilde{W}$ are obtained from this function by taking partial derivatives in the $\vec{R}$, $\vec{S}$, and $\vec{W}$ directions respectively.

---

*Other common notations for these coefficients with r in earth radii units are:

Jeffreys[1.1]		Kozai[1.6]		IAU[1.7]
J	=	A_2	=	$\frac{3}{2} J_2$
K	=	A_3	=	$-J_3$
D	=	A_4	=	$-\frac{35}{8} J_4$

**For the remainder of this paper, unless otherwise noted, r, p, and a are measured in units of equatorial earth radii.

$$\tilde{R} = \frac{\partial U_2}{\partial r} = -\frac{3GMJ}{r^4}\left(\frac{1}{3} - \sin^2 i \cdot \sin^2 u\right)$$

$$\tilde{S} = \frac{1}{r}\frac{\partial U_2}{\partial u} = -\frac{2GMJ}{r^4}\left(\sin^2 i \cdot \sin u \cdot \cos u\right)$$

$$\tilde{W} = \frac{1}{r \sin u}\frac{\partial U_2}{\partial i} = -\frac{2GMJ}{r^4} \sin i \cdot \cos i \cdot \sin u \qquad (1.16)$$

1.7 The Effect of the Second Harmonic of the Earth

The components of acceleration $\tilde{R}$, $\tilde{S}$, and $\tilde{W}$ can now be introduced into Eq. (1.10) to yield the second-order equations for the second harmonic of the earth. The result of this substitution is:

$$\frac{dp}{du} = -\frac{4J}{r} \sin^2 i \cos u \sin u + \frac{8J^2}{p_o r^2} \cos^2 i_o \sin^2 i_o \sin^3 u \cos u$$

$$\frac{de}{du} = -J\left[\frac{\sin v}{r^2} + \sin^2 i\left(-\frac{3}{2}\frac{\sin v}{r^2} + \frac{3}{2}\frac{\sin v \cos 2u}{r^2} + \frac{\cos v \sin 2u}{r^2}\right.\right.$$

$$\left.\left. + \frac{\cos v \sin 2u}{rp} + \frac{e \sin 2u}{rp}\right)\right] + \frac{2J^2 \cos^2 i_o}{p_o}\left[\frac{\sin v \sin^2 u}{r^3}\right.$$

$$\left. - 3 \sin^2 i_o \frac{\sin v \sin^4 u}{r^3} + 2 \sin^2 i_o \frac{\cos v \sin^3 u \cos u}{r^3}\right.$$

$$\left. + \frac{2 \sin^2 i_o \cos v \sin^3 u \cos u}{p_o r^2} + \frac{2e_o \sin^2 i_o \sin^3 u \cos u}{p_o r^2}\right]$$

$$\frac{d\omega}{du} = J\left[\frac{\cos v}{er^2} - \frac{\sin^2 i}{e}\left(\frac{3}{2}\frac{\cos v}{r^2} - \frac{3}{2}\frac{\cos v \cos 2u}{r^2} + \frac{\sin v \sin 2u}{r^2}\right.\right.$$

$$\left.\left. + \frac{\sin v \sin 2u}{pr}\right)\right] - \cos i_o \frac{d\Omega}{du} - J\left[\frac{2 \cos i_o \sin i_o}{p_o}\frac{\sin^2 u}{r}\right] \cdot \delta i$$

(continued)

$$
\left.
\begin{aligned}
&- \frac{2J^2}{e_o p_o} \cos^2 i_o \left[\frac{\sin^2 u \cos v}{r^3} - \frac{3 \sin^2 i_o \sin^4 u \cos v}{r^3} \right. \\
&\left. - 2 \sin^2 i_o \frac{\sin^3 u \cos u \sin v}{r^3} - 2 \sin^2 i_o \frac{\sin^3 u \cos u \sin v}{p_o r^2} \right] \\
\frac{d\Omega}{du} &= - 2J \left[\frac{\cos i \sin^2 u}{pr} \right] + \frac{4J^2 \cos^3 i_o}{p_o^2} \left[\frac{\sin^4 u}{r^2} \right] \\
\frac{di}{du} &= - 2J \left[\frac{\cos i \sin i \cos u \sin u}{pr} \right] + \frac{4J^2 \cos^3 i_o \sin i_o}{p_o^2} \left[\frac{\sin^3 u \cos u}{r^2} \right] \\
\frac{dt}{du} &= \frac{r^2}{\sqrt{GMp}} - \frac{2J \cos^2 i_o}{\sqrt{GMp_o}} \frac{r}{p_o} \sin^2 u
\end{aligned}
\right\} \quad (1.17)
$$

The substitution of Eq. (1.12) and the negative of the potential function ($U' = -U$), Eq. (1.15), into the energy equation, (1.11), gives:

$$\mathcal{E} = - GM \left[\frac{1}{2a} + \frac{J}{r^3} \left(\frac{1}{3} - \sin^2 i \sin^2 u \right) \right] = \text{constant} \qquad (1.18)$$

At nodal crossing:

$$\frac{1}{a} + \frac{2J}{3r^3} = \text{constant} \qquad (1.19)$$

1.8 First-Order Perturbations

The perturbations of p, e, and ω to first order are found by integrating their respective perturbation equations from 0 to u and discarding terms of second order (J^2) and higher. Alternatively, δe could be derived from δp and δa where δa is derived from the conservation of energy, but this offers no significant saving in labor at this stage over the straightforward integration. The short period perturbation of i is derived most simply from the conservation of the component of angular momentum along the polar axis.

The perturbation equations for the second harmonic are independent of Ω and T. The first order perturbations of these elements are

therefore not required and have been omitted here (they are given in Appendix I for reference).

The determination of δp is given here as an example of the method used. A transformation to the independent variable ν is made to simplify later integrals. To first order:

$$\frac{dp}{du} = -\frac{2J}{r} \sin^2 i_o \sin 2u$$

and

$$du = d\nu$$

Therefore,

$$\delta p = -\frac{2J \sin^2 i}{p_o} \int_{-\omega_o}^{\nu} [\cos 2\omega_o \sin \nu + \sin 2\omega_o \cos 2\nu$$

$$+ \tfrac{1}{2} e_o \cos 2\omega_o \sin \nu + \tfrac{1}{2} e_o \cos 2\omega_o \sin 3\nu$$

$$+ \tfrac{1}{2} e_o \sin 2\omega_o \cos \nu + \tfrac{1}{2} e_o \sin 2\omega_o \cos 3\nu] d\nu$$

Integration yields:

$$\delta p = -\frac{2}{3} \frac{J}{p_o} \sin^2 i_o [P_1 + P_2 \sin \nu + P_3 \sin 2\nu + P_4 \sin 3\nu$$

$$+ P_5 \cos \nu + P_6 \cos 2\nu + P_7 \cos 3\nu]$$

where

$$P_1 = \frac{3}{2} + 2e_o \cos \omega_o$$

$$P_2 = \frac{3}{2} e_o \sin 2\omega_o$$

$$P_3 = \frac{3}{2} \sin 2\omega_o$$

(continued)

$$P_4 = \frac{1}{2} e_o \sin 2\omega_o$$

$$P_5 = -\frac{3}{2} e_o \cos 2\omega_o$$

$$P_6 = -\frac{3}{2} \cos 2\omega_o$$

$$P_7 = -\frac{1}{2} e_o \cos 2\omega_o \qquad (1.20)$$

A similar but longer process yields the first-order perturbations of e and ω. The details of this procedure can be found in Appendix I. The first-order perturbation of e is

$$\delta e = -\frac{J}{p_o^2}[E_1 + E_2 \sin\nu + E_3 \sin 2\nu + E_4 \sin 3\nu + E_5 \sin 4\nu + E_6 \sin 5\nu + E_7 \cos\nu + E_8 \cos 2\nu + E_9 \cos 3\nu + E_{10} \cos 4\nu + E_{11} \cos 5\nu]$$

where

$$E_1 = \cos\omega_o - \frac{2}{3} \sin^2 i_o \cos\omega_o + e_o(\frac{1}{2}\cos 2\omega_o + \sin^2 i_o(\frac{5}{4} - \frac{3}{8}\cos 2\omega_o)) + e_o^2(\frac{1}{3}\cos^3\omega_o + \sin^2 i_o(\frac{2}{3}\cos\omega_o))$$

$$E_2 = \frac{1}{4} \sin^2 i_o \sin 2\omega_o + \frac{5}{8} e_o^2 \sin^2 i_o \sin 2\omega_o$$

$$E_3 = \frac{5}{4} e_o \sin^2 i_o \sin 2\omega_o$$

$$E_4 = \frac{7}{12} \sin^2 i_o \sin 2\omega_o + \frac{17}{48} e_o^2 \sin^2 i_o \sin 2\omega_o$$

$$E_5 = \frac{3}{8} e_o \sin^2 i_o \sin 2\omega_o$$

$$E_6 = \frac{1}{16} e_o^2 \sin^2 i_o \sin 2\omega_o \qquad \text{(continued)}$$

$$E_7 = -1 + \sin^2 i_o\left(\frac{3}{2} - \frac{1}{4}\cos 2\omega_o\right) + e_o^2\left(-\frac{1}{4} + \frac{3}{8}\sin^2 i_o(1 - 2\cos 2\omega_o)\right)$$

$$E_8 = -\frac{1}{2}e_o + e_o \sin^2 i_o\left(\frac{3}{4} - \frac{5}{4}\cos 2\omega_o\right)$$

$$E_9 = -\frac{7}{12}\sin^2 i_o \cos 2\omega_o + e_o^2\left(-\frac{1}{12} + \sin^2 i_o\left(\frac{1}{8} - \frac{17}{48}\cos 2\omega_o\right)\right)$$

$$E_{10} = -\frac{3}{8}e_o \sin^2 i_o \cos 2\omega_o$$

$$E_{11} = -\frac{1}{16}e_o^2 \sin^2 i_o \cos 2\omega_o \qquad (1.21)$$

The first-order perturbation of ω is

$$\delta\omega = -\frac{J}{e_o p_o^2}\left[W_1 + W_2\nu + W_3 \sin\nu + W_4 \sin 2\nu + W_5 \sin 3\nu + W_6 \sin 4\nu\right.$$
$$+ W_7 \sin 5\nu + W_8 \cos\nu + W_9 \cos 2\nu + W_{10} \cos 3\nu + W_{11} \cos 4\nu$$
$$\left. + W_{12} \cos 5\nu\right]$$

where

$$W_1 = -\sin\omega_o + \frac{2}{3}\sin^2 i_o \sin\omega_o + e_o\left(-2\omega_o - \frac{1}{2}\sin 2\omega_o + \sin^2 i_o \cdot\left(\frac{5}{2}\omega_o + \frac{3}{8}\sin 2\omega_o\right)\right) + e_o^2\left(-2\sin\omega_o - \frac{1}{3}\cos^2\omega_o \sin\omega_o\right.$$
$$\left. + \sin^2 i_o\left(\frac{8}{3}\sin\omega_o\right)\right)$$

$$W_2 = e_o\left(-2 + \frac{5}{2}\sin^2 i_o\right)^*$$

$$W_3 = -1 + \sin^2 i_o\left(\frac{3}{2} + \frac{1}{4}\cos 2\omega_o\right) + e_o^2\left(-\frac{7}{4} + \frac{1}{2}\cos 2\omega_o\right.$$
$$\left. + \sin^2 i_o\left(\frac{17}{8} - \cos 2\omega_o\right)\right)$$

(continued)

*Coefficient of the first-order secular perturbation.

$$W_4 = e_o(-\frac{1}{2}+\frac{1}{2}\cos 2\omega_o + \sin^2 i_o(\frac{3}{4} - \frac{5}{4}\cos 2\omega_o))$$

$$W_5 = -\frac{7}{12}\sin^2 i_o \cos 2\omega_o + e_o^2(-\frac{1}{12}+\frac{1}{6}\cos 2\omega_o + \sin^2 i_o(\frac{1}{8} - \frac{19}{48}\cos 2\omega_o))$$

$$W_6 = -\frac{3}{8} e_o \sin^2 i_o \cos 2\omega_o$$

$$W_7 = -\frac{1}{16} e_o^2 \sin^2 i_o \cos 2\omega_o$$

$$W_8 = \frac{1}{4}\sin^2 i_o \sin 2\omega_o + e_o^2(\frac{1}{2}\sin 2\omega_o - \frac{7}{8}\sin^2 i_o \sin 2\omega_o)$$

$$W_9 = e_o(\frac{1}{2}\sin 2\omega_o - \frac{5}{4}\sin^2 i_o \sin 2\omega_o)$$

$$W_{10} = -\frac{7}{12}\sin^2 i_o \sin 2\omega_o + e_o^2(\frac{1}{6}\sin 2\omega_o - \frac{19}{48}\sin^2 i_o \sin 2\omega_o)$$

$$W_{11} = -\frac{3}{8} e_o \sin^2 i_o \sin 2\omega_o$$

$$W_{12} = -\frac{1}{16} e_o^2 \sin^2 i_o \sin 2\omega_o \qquad (1.22)$$

The conservation of the component of angular momentum along the polar axis provides an exact relation between p and i at each instant of time. Differentiating Eq. (1.13) leads to:

$$di = \frac{1}{2p}\cot i \, dp \qquad (1.23)$$

The first-order perturbation of i is therefore simply

$$\delta i = \frac{1}{2p_o}\cot i_o \, \delta p \qquad (1.24)$$

1.9 Second Order Perturbations

The first-order perturbations can now be added to the nodal osculating elements in the perturbation equations and the final integration over a nodal cycle completed. As in the first-order integration, an abbreviated derivation of Δp is presented as an example (the details of these integrations are presented in Appendix I). Since:

$$\left.\begin{aligned} p &= p_o + \delta p \\ e &= e_o + \delta e \\ \omega &= \omega_o + \delta\omega \\ i &= i_o + \delta i \end{aligned}\right] \qquad (1.25)$$

substitution into Eq. (1.17) and expansion in the variable ν yields:

$$\begin{aligned} \frac{dp}{du} = &-\frac{2J}{p_o}\,[\sin^2 i_o(\cos 2\omega_o \sin 2\nu \cos\nu + \sin 2\omega_o \cos 2\nu \cos\nu)\delta e \\ &+ \sin^2 i_o(e_o \cos 2\omega_o \sin 2\nu \sin\nu + e_o \sin 2\omega_o \cos 2\nu \sin\nu)\delta\omega \\ &+ \cos 2i_o(\cos 2\omega_o \sin 2\nu + \sin 2\omega_o \cos 2\nu + e_o \cos 2\omega_o \sin 2\nu \cos\nu \\ &+ e_o \sin 2\omega_o \cos 2\nu \cos\nu)\frac{\delta p}{p_o} \\ &+ \text{Higher Order Terms} + \text{Terms that will vanish upon integration}] \\ &+ \frac{8J^2 \cos^2 i_o \sin^2 i_o}{p_o^3}\,[2e_o^2 \cos\omega_o \sin\omega_o \sin^4 u \cos^2 u \\ &+ \text{Terms that will vanish upon integration}] \end{aligned} \qquad (1.26)$$

Hence, to second order, the change in p over one cycle is

$$\Delta p \equiv \int_{-\omega_o}^{2\pi-\omega_o} \frac{dp}{du}\, d\nu$$

$$= \frac{2\pi J^2}{p_o^3} \sin^2 i_o \left[\frac{1}{2}\cos 2\omega_o(E_2 + E_4) + \frac{1}{2}\sin 2\omega_o(E_7 + E_9)\right.$$

$$+ \frac{1}{2}\cos 2\omega_o(W_8 - W_{10}) + \frac{1}{2}\sin 2\omega_o(W_5 - W_3) + \frac{4}{3}\sin\omega_o(W_2)$$

$$+ \frac{1}{3}\cos 2i_o(\cos 2\omega_o P_3 + \sin 2\omega_o P_6 + \frac{1}{2}e_o \cos 2\omega_o(P_2 + P_4)$$

$$\left. + \frac{1}{2} e_o \sin 2\omega_o(P_5 + P_7)) + e_o^2 \cos^2 i \cos\omega_o \sin\omega_o \right] \qquad (1.27)$$

which reduces to the final form:

$$\Delta p = \frac{\pi J^2}{p_o^3} \sin^2 i_o [e_o \sin\omega_o(-\frac{16}{3} + \frac{20}{3}\sin^2 i_o)$$

$$+ e_o^2 \sin 2\omega_o(\frac{7}{3} - \frac{5}{2}\sin^2 i_o)] \qquad (1.28)$$

The integrations of $\frac{d\Omega}{du}$, $\frac{d\omega}{du}$, and $\frac{dT}{du}$ are tedious. Only the results of these integrations are given here, since the details of the analysis are presented in Appendix I. Thus

$$\Delta\Omega = -\frac{2\pi J \cos i_o}{p_o^2} + \frac{\pi J^2}{p_o^4}\cos i_o \left[1 - \frac{20}{3}\sin^2 i_o\right.$$

$$+ e_o \cos\omega_o(\frac{16}{3} - \frac{40}{3}\sin^2 i_o) + e_o^2(-\frac{1}{3} - \frac{7}{6}\cos 2\omega_o$$

$$\left. + \sin^2 i_o(-\frac{5}{12} + \frac{5}{2}\cos 2\omega_o))\right] \qquad (1.29)$$

$$\Delta\omega = \frac{\pi J}{p_o^2}(3\cos^2 i_o - 1) - \cos i_o\,\Delta\Omega$$

$$+ \frac{\pi J^2}{p_o^4}\left[\frac{1}{e_o}\cos\omega_o\left(-4 + \frac{23}{3}\sin^2 i_o - \frac{10}{3}\sin^4 i_o\right)\right.$$

$$+ \left(1 - 4\cos 2\omega_o + \sin^2 i_o\left(\frac{49}{6} + \frac{23}{6}\cos 2\omega_o\right) + \sin^4 i_o\left(-\frac{95}{8} + \frac{5}{4}\cos 2\omega_o\right)\right)$$

$$+ e_o\cos\omega_o\left(-4\cos^2\omega_o + \sin^2 i_o(16 + 5\cos^2\omega_o) - 20\sin^4 i_o\right)$$

$$\left. + e_o^2\left(\frac{5}{6} + \sin^2 i_o\left(-\frac{5}{6} - \frac{35}{12}\cos 2\omega_o\right) + \sin^4 i_o\left(-\frac{25}{48} + \frac{25}{8}\cos 2\omega_o\right)\right)\right] \tag{1.30}$$

$$\Delta T = 2\pi\sqrt{\frac{p_o^3}{GM(1-e_o^2)^3}} + \frac{2\pi J}{\sqrt{GMp_o}}\left[-\frac{(1+e_o\cos\omega_o)^3}{(1-e_o^2)^{5/2}} + \frac{\left(-2+\frac{5}{2}\sin^2 i_o\right)}{(1+e_o\cos\omega_o)^2}\right] \tag{1.31}$$

The change after a nodal period in eccentricity, accurate to second order, is derived most easily from the law of conservation of energy. The relation $p = a(1-e^2)$ is exact at each instant for the osculating ellipse. Taking differentials of this expression gives:

$$\Delta e = \frac{1-e_o^2}{2p_o e_o}\left[(1-e_o^2)\,\Delta a - \Delta p\right] + \text{Higher Order Terms} \tag{1.32}$$

where Δa is derived directly from the expression for orbital energy at nodal crossing (Eq. (1.19)), and Δp is given by Equation (1.28). From Eq. (1.19) it follows that

$$\Delta a = -2\frac{Ja_o^2 e_o}{p_o^3}(1 + e_o\cos\omega_o)^2\sin\omega_o\,\Delta\omega$$

and

$$\Delta a = -\frac{2\pi J^2}{p_o^3}\frac{1}{(1-e_o^2)^2} e_o \sin\omega_o(1 + e_o\cos\omega_o)^2(4 - 5\sin^2 i_o)$$
$$+ \text{Higher order terms} \qquad (1.33)$$

Substituting Eqs. (1.33) and (1.28) into Eq. (1.32) gives:

$$\Delta e = \frac{\pi J^2}{p_o^4}\left[\sin\omega_o(-4 + \frac{23}{3}\sin^2 i_o - \frac{10}{3}\sin^4 i_o)\right.$$
$$+ e_o \sin 2\omega_o(-4 + \frac{23}{6}\sin^2 i_o + \frac{5}{4}\sin^4 i_o)$$
$$+ e_o^2 \sin\omega_o(-4\cos^2\omega_o + \sin^2 i_o(\frac{7}{3} - 5\sin^2\omega_o) + \frac{10}{3}\sin^4 i_o)$$
$$\left. + e_o^3 \sin 2\omega_o(\frac{7}{6}\sin^2 i_o - \frac{5}{4}\sin^4 i_o)\right] \qquad (1.34)$$

The net change in inclination over a nodal cycle follows directly from the exact relation between p and i (Eq. (1.13)). Taking finite differences and neglecting terms of order J^3 and higher gives:

$$\Delta i = \frac{1}{2p_o}\cot i_o \Delta p \qquad (1.35)$$

1.10 Validation of the Equations

These integrated forms were checked for accuracy both by a duplicate, but independent, integration of the equations and by a sensitive numerical comparison against a Runge-Kutta integration of the original simultaneous differential equations.

Theoretically (and without considering the convergence question), the solution of the original differential equations can be represented as a set of six infinite series each of the form:

$$\Delta f = \alpha_o + \alpha_1 J + \alpha_2 J^2 + \alpha_3 J^3 + \alpha_4 J^4 + \cdots \tag{1.36}$$

whereas the second-order solution found above yields equations of the form:

$$\Delta f_{\text{second order}} = \alpha_o + \alpha_1 J + \alpha_2 J^2 \tag{1.37}$$

Since J^3 is 10^3 times larger than J^4, the difference between these two forms is:

$$\Delta f - \Delta f_{so} \approx \alpha_3 J^3 \tag{1.38}$$

Thus if Δf and Δf_{so} are computed for several different, non-physical values of J, the ratio of these differences is approximately equal to the ratio of the J's cubed.

$$\frac{\Delta f(J_1) - \Delta f_{so}(J_1)}{\Delta f_{(J_2)} - \Delta f_{so}(J_2)} \approx \frac{\alpha_3 J_1^3}{\alpha_3 J_2^3} = \left(\frac{J_1}{J_2}\right)^3 \tag{1.39}$$

If the value of α_2 in the second-order form is incorrect, then this ratio is:

$$\frac{\alpha'_2 J_1^2 + \alpha_3 J_1^3}{\alpha'_2 J_2^2 + \alpha_3 J_2^3} \neq \left(\frac{J_1}{J_2}\right)^3 \tag{1.40}$$

where α'_2 is the error in α_2.

The Δf's were evaluated numerically on an IBM 7094 computer that used a Runge-Kutta integration of the six exact simultaneous equations. These computations were made in double precision (16 significant figures) giving an accuracy comparable to keeping terms of order J^5 in Eq. (1.36). The Δf_{so}'s are simply Δp, Δe, etc. with the appropriate first and zeroth order terms included. These ratios were evaluated and order of

magnitude checks were made for over forty sets of initial conditions. Care was taken that errors were not masked by degenerate combinations of coefficients equalling zero because of a poor choice of initial conditions. In addition, several ratios were evaluated for actual nodal crossing elements for 1960 Iota 2, the rocket casing of Echo I.

Each of the six second-order changes have passed these tests. A typical set of numerical checks is presented in Table I for one set of initial conditions. Column 1, 2, and 4 in Table I give perturbations computed with J, J/2, and J/4, respectively. The ratio of the differences between the Runge-Kutta integration and the analytic solutions, after Eq. (1.39), are listed in Columns 3 and 5. This ratio should be 8 in Column 3 and 64 in Column 5 (except for ΔT where the ratios should be 4 and 16, respectively). The large values of these ratios (8.5 and 70) for the perturbation of ω indicate that the third order effect for this set of initial conditions is small (note the large number of significant figures in the direct comparison of $\Delta\omega$ computed by Runge-Kutta integration and from Eq. (1.30)).

Detailed comparison of this theory with experiment is given in Chapter II.

While the derivation of the second-order theory in this chapter has been carried out independently, it should be pointed out that a number of second-order theories and approximate second-order theories have appeared in the literature. Of particular note are Merson,[1.9] Blitzer,[1.10] and Kozai.[1.11] Merson's work is correct except for a typographical error in his Eq. 56. Blitzer's work is correct but does not include the time of nodal crossing equation. Kozai includes secular terms to order J^3. His equations are in a form which is very difficult to compare with Eqs. (1.28) – (1.35).

TABLE I

A Typical Numerical Check of Second Order Second Harmonic Perturbations

Initial Conditions:

p_o = 1.67 earth radii
e_o = 0.5
ω_o = 22.5°
i_o = 45.°

	Column 1 $J = 1.62327 \times 10^{-3}$ (see Ref. 1.8 for example)	Column 2 $J = 8.11635 \times 10^{-4}$	Column 3 Ratio $\frac{\text{Column 1}}{\text{Column 2}}$	Column 4 $J = 4.058175 \times 10^{-4}$	Column 5 Ratio $\frac{\text{Column 1}}{\text{Column 4}}$
Δp (in earth radii)					
Runge Kutta	$-1.7221186-7$*	$-4.2891012-8$	4.015	$-1.0702560-8$	16.091
2nd Order	$-1.7091771-7$	$-4.2729427-8$	4.000	$-1.0682357-8$	16.000
Difference	$-.0129415-7$	$-.0161585-8$	8.009	$-.0020203-8$	64.057
Δe (dimensionless)					
Runge Kutta	$-1.2457768-6$	$-3.1063427-7$	4.010	$-7.7557401-8$	16.063
2nd Order	$-1.2393004-6$	$-3.0982510-7$	4.000	$-7.7456275-8$	16.000
Difference	$-.0064764-6$	$-.0080917-7$	8.004	$-.0101126-8$	64.043
$\Delta\omega$ minus first order effect					
Runge Kutta (radians)	$1.3904468-6$	$3.4759631-7$	4.000	$8.6897333-8$	16.001
2nd Order	$1.3903309-6$	$3.4758272-7$	4.000	$8.6895683-8$	16.000
Difference	$.0001159-6$	$.0001359-7$	8.528	$.0001651-8$	70.200
$\Delta\Omega$ minus first order effect					
Runge Kutta (radians)	$-2.3272977-6$	$-5.8202487-7$	3.999	$-1.4553129-7$	15.992
2nd Order	$-2.3289009-6$	$-5.8222523-7$	4.000	$-1.4555631-7$	16.000
Difference	$.0016032-6$	$.0020036-7$	8.001	$.0002502-7$	64.076
Δi (radians)					
Runge Kutta	$-2.9601042-6$	$-7.3724236-7$	4.015	$-1.8396365-7$	16.091
2nd Order	$-2.9378591-6$	$-7.3446476-7$	4.000	$-1.8361619-7$	16.000
Difference	$.0222451-6$	$.0277760-7$	8.009	$.0034746-7$	64.022

Table I continued

ΔT minus zero order period					
Runge Kutta (Universal days)	− 4. 9768438 − 4	− 2. 4917468 − 4	1. 997	− 1. 2468543 − 4	3. 991
2nd Order	− 4. 9909386 − 4	− 2. 4954693 − 4	2. 000	− 1. 2477347 − 4	4. 000
Difference	. 0140948 − 4	. 0035225 − 4	4. 001	. 0008804 − 4	16. 009

* This notation signifies $-1.7221186 \times 10^{-7}$.

REFERENCES

1.1 H. Jeffreys, The Earth (Cambridge, 1959).

1.2 I.I. Shapiro, "The Prediction of Satellite Orbits," ed. M. Roy, IUTAM Dynamics of Satellites Symposium, Paris, May 28-30, 1962, (Academic Press, 1963).

1.3 F.R. Moulton, An Introduction to Celestial Mechanics (The MacMillan Company, New York, 1960).

1.4 H. Jones, "Satellite Perturbations," unpublished.

1.5 K.A. Ehricke, Space Flight, Vol. I (D. Van Norstrand Co., Inc., New York, 1960).

1.6 Y. Kozai, "The Motion of a Close Earth Satellite," The Astronomical Journal 64, No. 9 (November, 1959)~ No. 1274.

1.7 Y. Kozai, "Numerical Results from Orbits," Special Report No. 101, Smithsonian Astrophysical Observatory, Research in Space Science (31 July 1962).

1.8 C. Allen, Astrophysical Quantities (Athlone Press, 2nd edition, University of London, 1963).

1.9 R. Merson, "The Motion of a Satellite in an Axi-symmetric Gravitational Field," Geophysical Journal of the Royal Astronomical Society 4 (1961), pp. 17-52.

1.10 L. Blitzer, "The Orbit of a Satellite in the Gravitational Field of the Earth," Space Technology Laboratories (August 1960).

1.11 Y. Kozai, "Second-Order Solution of Artificial Satellite Theory without Air Drag," The Astronomical Journal 67, No. 7 (November, 1962),~ No. 1302.

CHAPTER II

Second-Order Orbit Perturbation Computations and Comparisons with Observed Satellite Orbital Data

2.1 Introduction

The true test of the second-order perturbation theory derived in Chapter I is of course a comparison with observed orbital perturbations. To make this comparison and to provide for future usage of this theory in orbit perturbation investigations, the second-order perturbations derived in Chapter I have been included in the high-speed digital computer program described in Appendix II.

This General Perturbation Program is provided with observed nodal crossing osculating elements at a single nodal crossing epoch as initial conditions. The program then generates osculating elements at each succeeding nodal crossing from perturbation theory alone without further recourse to observed orbital data. The accuracy of the computation and of the theoretical model is then determined by comparing these computed orbital elements with observed orbital elements for succeeding epochs.

The orbital data of 1960 IOTA 2 [2.1] and 1961 Delta 1 [2.2], used here for comparisons and for orbital studies, were prepared by the Smithsonian Astrophysical Observatory (SAO) from precisely reduced* photographic observations. [2.3] This type of photo-reduced orbital data is perhaps the most accurate obtainable at the present time. Each observation is accurate to ± 20 sec of arc and ± 20 msec in time or better [2.4] and up to 40 observations per day per satellite are made. [2.2]

The orbital elements derived by SAO are not osculating elements at nodal crossing but mean elements. [2.1] These are mean in two senses; first, the first-order short-period effects of the second harmonic of the

*Not to be confused with field-reduced photographic data which are of much lower accuracy. [2.5]

gravitational field are removed from the data, and second, the data are smoothed over time intervals of several days. [2.6] A more precise definition of SAO mean elements and the procedure for conversion to nodal osculating elements are given in detail in Appendix III. The computed nodal crossing osculating elements at each epoch of interest are converted independently to SAO mean elements to facilitate comparison.

In addition to the perturbations caused by the second zonal harmonic of the earth, our computations include the effects of solar radiation pressure, atmospheric drag, the third through fifth zonal harmonics, lunar gravity and solar gravity (see Appendix II).

2.2 1961 IOTA 2

A good set of satellites to test the second-order theory and, in general, to improve geodetic constants would be one which contained satellites whose orbits are completely insensitive to nongravitational perturbations and whose experimentally determined orbital elements are as accurate as or possible more accurate than the SAO photo-reduced data. Such satellites do not yet exist. *

The rocket casing of ECHO I (1961 IOTA 2) was chosen here (on the recommendation of L. Jacchia of SAO) in lieu of an "ideal" satellite because of the extensive orbital data compiled for it and because the perigee height is large enough ($\sim$ 1500 km) so that atmospheric drag is relatively unimportant.

The use of this satellite has two major drawbacks. First, the eccentricity is very low ($\sim$ 0.01). This causes the line of apsides to be ill defined and therefore, the argument of perigee (ω) is both difficult to measure and to compute. This difficulty, in turn, is carried over into the mean motion (n)** and mean anomaly (M) (see Appendix III). Second, the satellite is a cylinder either spinning about its long axis or tumbling if spin-axis conversion has taken place. The angular motion about the center of mass is a function of time and must be considered an unknown because of gravitational torque, etc. This angular motion

---

* An example of such a satellite, consisting of a solid lead sphere surfaced with optical corner reflectors to provide a laser "radar" target has been proposed by H. M. Jones, I. I. Shapiro, and the author.

** The mean motion is simply the reciprocal of the orbit period for unperturbed satellite motion (see Appendix III for details).

can cause solar radiation pressure perturbations to be larger than with an equivalent spherical area-to-mass ratio (A/M) and to be unpredictable. [2.7]

To demonstrate the importance of the radiation pressure perturbations and to point out the danger in employing this type of data for improving geodetic constants, the results of three mathematical models for this perturbation (see Appendix II) are presented here. The first model (represented by a plus sign (+) in Figs. 2.1 through 2.6*) is an absorbing satellite with a constant area presented to the sun. (This model also represents the perturbations on the orbit of a specularly reflecting sphere.) The second model (represented by a Δ in Figs. 2.1 through 2.6) is a 100 percent specularly reflecting cylinder tumbling about an axis which both lies in the plane of the equator and is roughtly parallel to the initial spin axis at injection. The third model is the same as model two but with a tumbling axis rotated 90° in the equatorial plane from that tumbling axis. (This case is represented by a $\boxdot$ in Figs. 2.1 through 2.6) The importance of the radiation pressure perturbations and of the uncertainty of this effect for this satellite is demonstrated by the spread between these three cases.**

Despite the uncertainty in the radiation pressure perturbations, the second-order perturbations caused by the second harmonic of the gravitational field are dramatically emphasized by comparing the computed orbit parameters with and without the second-order theory included, to the experimental data. The theoretical second-order perturbation of the inclination contains only a linear and quadratic dependence on eccentricity (see Eq. 1.35) and is therefore small and somewhat masked by the approximations used in computing the lunar perturbations.***

---

*Time is reckoned in Modified Julian Days (MJD) for these data, (see Appendix IV.).

**The actual situation is probably more nearly represented by a diffusely reflecting cylinder, spinning or tumbling about a slowly processing axis.

***The present computation of lunar perturbations in the General Perturbation Program is in closed form. This computation uses overly simplified equations for the position of the moon and makes the approximation that $\frac{r}{r_{moon}} << 1$.

The computed values of eccentricity (see Fig. 2.1) for the three radiation pressure models bracket the observed data. The maximum discrepancy for the absorbing, constant area-to-mass ratio model is 2×10^{-5} and occurs approximately 60 days after the initial epoch. If the buildup of this discrepancy were linear to this point, the error would be approximately 3×10^{-8} per revolution compared with approximately 10^{-6} per revolution if the second-order second harmonic effects are neglected. The quoted one standard deviation (one sigma) error in the eccentricity data[2.1] averages approximately 5×10^{-6} or one-half of the smallest division of the figure.

The SAO mean motion for 1960 IOTA 2 (Fig. 2.2) contains a pseudo-sinusoidal oscillation of period ω and amplitude of approximately 5×10^{-4} revolutions per day. This oscillation is caused by the technique used at SAO to reduce the data (see Appendix III). An approximation to this oscillation was introduced into our numerical computations to facilitate comparisons of our results with the data. The secular drift of the computed – away from the observed – mean motion (10^{-7} (rev/day) per nodal period) may be fictitious and may be caused by the approximation (see Appendix III), or it may be the uncertainty of the radiation pressure model even though all three models presented here show some of this secular drift. The errors in the mean motion data (noise) are apparent from the amplitude ($\sim 1 \times 10^{-4}$ rev/day) of the frequent short-lived (two-day) slope reversals, the quoted one-sigma error,[2.1] however, averages only 2×10^{-5} rev/day or twice the smallest division of the figure.

The mean anomaly (Fig. 2.3) is the time integral of the mean motion. In the 208 days of data presented, the satellite (and therefore, the mean anomaly) makes 2,537 revolutions. The data is therefore plotted as a residual from a linear equation. Neglect of the second-order second harmonic effects causes the mean anomaly residual to drift off scale in only four days. The total error for the absorbing, constant A/M case is 0.01 revolution or 1.18 minutes of time in 208 days or 0.0004 percent of the total change. The average quoted one-sigma error in mean anomaly[2.1] is approximately 7.5×10^{-5} revolutions. The round-off error in the

output of time from the GPP is ± 4 sec corresponding to ± 5 x 10^{-4} rev. in mean anomaly. This round-off error is not cumulative during the computation because time is kept internally in double precision.

The argument of perigee (ω), (see Fig. 2.4)*, is the most difficult parameter to compute for 1961 IOTA 2 because of the low eccentricity of this satellite. Eccentricity appears in the denominator of expressions for the perturbations of this parameter which are caused by solar radiation pressure and the odd (i.e., 3rd and 5th) harmonics of the gravitational field of the earth[2.8] and in Eq. (1.30). This results in a perturbation of ω by the third harmonic that is one-tenth of the perturbation caused by the second harmonic. Therefore, terms of order J*K, which have been neglected, can be one-tenth of the second-order second-harmonic term.** The discrepancy in the comparison for ω (see Fig. 2.4) is of this order. The uncertainty of the radiation pressure effect is also of this order (see Fig. 2.4). The total error accumulated in ω (0.4°) is 0.07 percent of the total change in ω during the 208 days. The average quoted one-sigma error in the observational data is approximately 0.03°[2.1] or one-third the smallest division of the figure.

The comparison of computed inclination with observed inclination presented in Fig. 2.6 shows a general trend of correlation, but the details of this fit and the contributions of the second-order theory are completely masked by the errors in the lunar perturbation computation described earlier. The average quoted one-sigma error in the Smithsonian data for inclination is[2.1] approximately 5 x 10^{-4} degrees, or five of the smallest divisions of Fig. 2.6.

The right ascension of the ascending node (Ω) is presented as the residual from a linear function in Fig. 2.5. The discrepancy between the computed and observed Ω can be explained in part by the average errors in mean motion and inclination. The approximate effect of these

*Note that this data is plotted as a residual from a linear function.

**The importance of these terms has been borne out by Runge-Kutta integration tests similar to those described in Chapter I.

errors can be obtained by taking differentials of the first-order (in J) change in Ω given in Eq. (1.29) of Chapter I:

$$\delta(\Delta\Omega) \approx + \frac{2\pi J}{p^2} \left[2 \cos i \frac{\delta p}{p} + \sin i \cdot \delta i\right] \tag{2.1}$$

For small eccentricity:

$$p = a(1 - e^2) \approx a$$

$$\delta p \approx \delta a \approx -\frac{2}{3} \frac{a}{n} \delta n \tag{2.2}$$

therefore:

$$\delta(\Delta\Omega) \approx + \frac{2\pi J}{p^2} \left[-\frac{4}{3} \cos i \frac{\delta n}{n} + \sin i \, \delta i\right] \tag{2.3}$$

For the orbit parameters of 1961 IOTA 2:

$$\delta(\Delta\Omega) \approx -2.8 \times 10^{-2} \, \delta n + 4.8 \times 10^{-3} \, \delta i \quad \text{deg/rev}$$

where δn is in rev/day and δi expressed in degrees. The average error in the rate of change of Ω is approximately 1.2×10^{-5} deg/rev. Three sets of δi and δn which would explain this discrepancy are:

	δi (deg)	δn (rev/day)
SET 1	+ 0.0025	0.
SET 2	+ 0.0031	+ 0.0001
SET 3	0.	−0.0004

The uncertainty in the radiation pressure perturbation is a third of the discrepancy so that the above values may be one third too large. The total error in Ω during the 208-day period (0.03°) is 0.005 percent of the total change in Ω. The average quoted one-sigma error [2.1] is approximately $7.0^\circ \times 10^{-4}$, or 7/10 of the smallest division of the figure. Note that if the second-order effect is neglected, the residual in Ω drifts off scale in six days.

The comparisons of computed orbit parameters with the observed orbit of 1960 IOTA 2 have not "proved" the second-order theory, but the

theory is demonstrated to at least one significant figure of the J^2 term and is not disproved in any way. The study of the uncertainty caused by solar radiation pressure on this cylindrical satellite clearly indicates that care must be exercised when the orbital data of tumbling cylindrical satellites are employed for precise geodetic work.

2.3 1961 DELTA 1

The satellite 1961 Delta 1 (Explorer IX) is a twelve-foot-diameter, rigid balloon and was launched into orbit as an atmospheric density probe. This satellite is very sensitive to atmospheric drag and discussions of this effect and the perturbations of the mean motion which are a measure of this effect are given in Chapter III.

The solar radiation pressure perturbations of the orbit of 1961 Delta 1 are predictable because of the nearly spherical shape of the satellite. The eccentricity of its orbit is on the order of 0.1, [2.2*] a factor of ten greater than that of 1960 IOTA 2. Associated with this increase in eccentricity is a factor of ten increase in the accuracy of both the observed[2.2] and the computed argument of perigee (see Fig. 2.9). Otherwise, the accuracy of the observed and computed parameters is the same as for 1960 IOTA 2 (except for the mean motion, see Chapter III).

The geometry of the orbit of this satellite is such that solar radiation pressure produces a large secular decrease in eccentricity (see Fig. 2.7). This effect is known as "resonance". [2.10]

The mean anomaly residuals (Fig. 2.8) have the characteristic parabolic shape associated with a drag-sensitive satellite. The mean motion is rapidly changing in a more or less linear fashion; therefore, the mean anomaly, which is the integral of the mean motion, is a parabolic function of time.

The comparison of computed inclination with observation (Fig. 2.11) reflects once again the approximate lunar perturbations described earlier. Part of the secular portion of the discrepancy (approximately 1×10^{-3} deg in 208 days) is probably attributable to atmospheric rotation. [2.11]

---

*A similar set of 1961 Delta 1 observed orbital elements was later published in Ref. 2.1.

Predictions of the lifetime of 1961 Delta 1 were made with the GPP (Appendix II). These indicate that the demise of Explorer IX will occur on March 28, 1964 ± 10 days.* The uncertainty is introduced by the correlation of atmospheric density with the unpredictable 10.7-cm solar radio flux and with the geomagnetic planetary indices (see Chapter III). A similar technique was used to predict the lifetime of the Echo Balloon[2.12] and of the West Ford dipoles;[2.13 and 2.14] however, drag is unimportant in the lifetime computations for the latter.

2.4 A Heavy Satellite

A direct comparison of the theoretical time of nodal crossing perturbations given in Chapter I with measurement is shown in Fig. 2.12. The data are actually radar measurements of the time a heavy satellite (i.e., low A/M) crossed the 38° north latitude line.[2.15] The conversion to time of nodal crossing involves only a constant plus an oscillation of approximately ± 10 sec amplitude and with the period of ω (which was neglected). The time of nodal crossing residual in Fig. 2.12 is a straight, mean line plus a sinusoid of period ω (~ 300 days) and amplitude 100 seconds. This sinusoid cannot be explained on the basis of first order theory alone.

The GPP (Appendix II) will accept an equivalent two-body anomalistic period as input but not the nodal crossing period directly (see Table 4). This equivalent period converted from the Space Track data is:

$$P = 0.1061366 \text{ days}$$

The resulting mean line** (see Fig. 2.12) is represented by Δ's. An improved value of the initial orbit period was computed to account for the discrepancy; the result is:

$$P = 0.1063133 \text{ days}$$

---

* Based on SAO data for July 30, 1963.

** The oscillation in time of nodal crossing is of period ω and is sinusoidal. The mean line is defined by connecting points for which $\omega = n \cdot \pi$ ($n = 1, 2 \ldots$).

The result of this improvement is plotted as plus signs in Fig. 2.12.

Theoretically, the initial eccentricity could be improved by comparing the amplitude of the computed and observed sinusoidal oscillation. Any error in the eccentricity is smaller, however, than this method can detect in the time of nodal crossing data.

TABLE 1

Physical Constants

		Ref.
Equatorial Radius of Earth (E. R.)	RE = 6378.388 km	(2.18)
Gravitational Constant	GM = $1.53609904 \times 10^{-6}$ E. R.^{3}/sec^2	(2.16)
Coefficient of the Second Harmonic	J = 1.62327×10^{-3} E. R.^{2}	(2.18)
" " " Third "	K = 2.27×10^{-6} E. R.^{3}	(2.18)
" " " Fourth "	D = 9.2×10^{-6} E. R.^{4}	(2.18)
" " " Fifth "	= 2.6×10^{-7} E. R.^{5}	(2.18)
Radiation Pressure Constant	I/c = 4.65×10^{-5} gm/cm^2	(2.18)
Ratio of Sun Mass/Earth Mass	= 333432.	(2.18)
Ratio of Moon Mass/Earth Mass	= 0.01226	(2.18)

TABLE 2

Physical Parameters of 1961 IOTA 2

Average A/M	=	0.252 cm^2/gm	
Maximum A/M	=	0.310 cm^2/gm	
C_D	=	2.2	(2.17)

TABLE 3

Physical Parameters of 1961 DELTA 1

A/M	=	15.84 cm^2/gm	(2.17)
C_D	=	2.2	(2.17)

TABLE 4

Orbital Elements of a Heavy Satellite [2.19]*

$e = 0.03$

$\omega = 15°$

$\Omega = 125.60°$

$i = 86.5°$

Nodal Period = 0.10631422 days

Date = April 11, 1962

*The original source is USAF Space Track data.

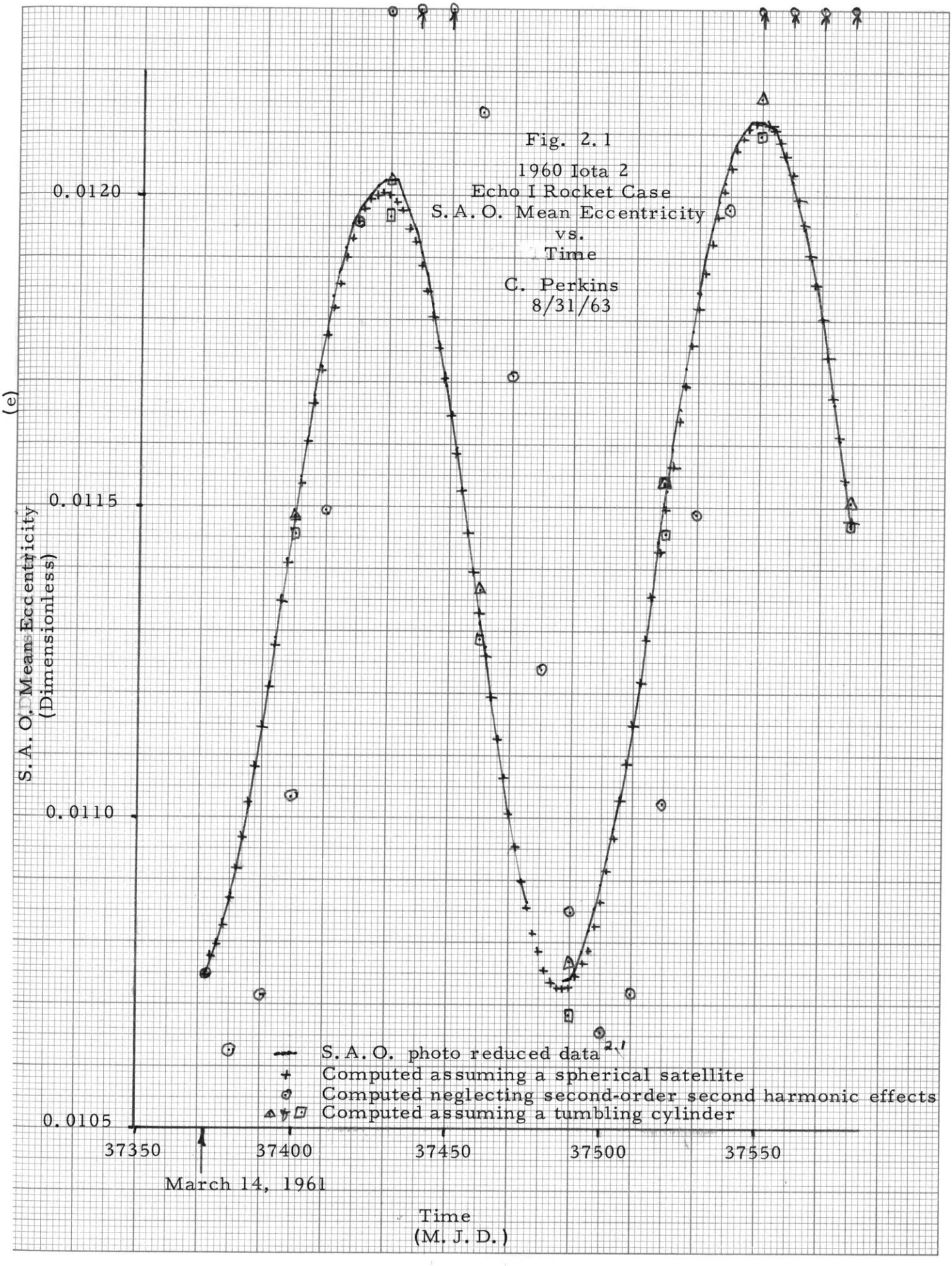
Fig. 2.1
1960 Iota 2
Echo I Rocket Case
S. A. O. Mean Eccentricity
vs.
Time
C. Perkins
8/31/63
0.0120
0.0115
0.0110
0.0105
(e)
S. A. O. Mean Eccentricity
(Dimensionless)
S. A. O. photo reduced data
Computed assuming a spherical satellite
Computed neglecting second-order second harmonic effects
Computed assuming a tumbling cylinder
37350
37400
37450
37500
37550
March 14, 1961
Time
(M. J. D.)

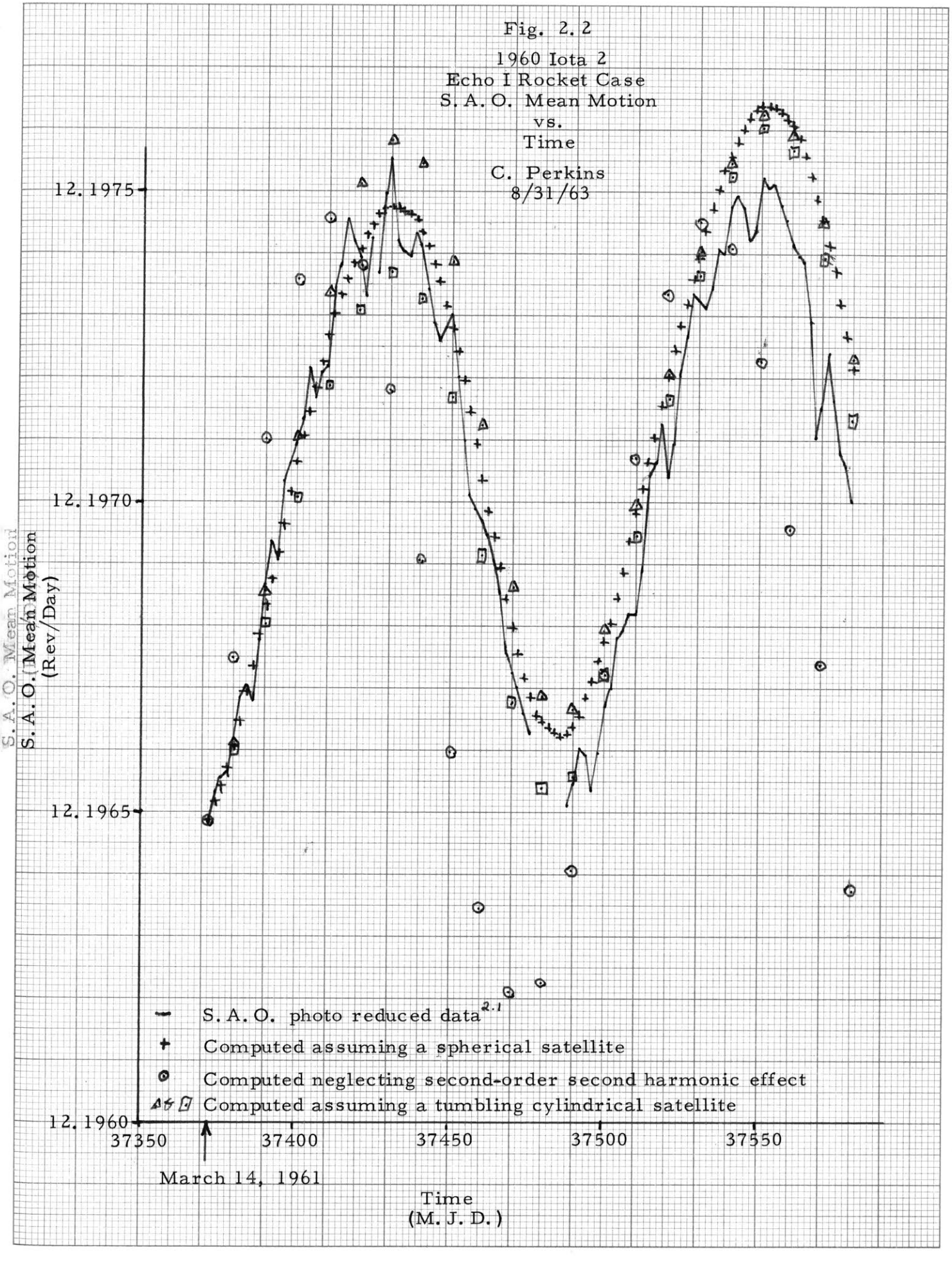
Fig. 2.2
1960 Iota 2
Echo I Rocket Case
S. A. O. Mean Motion
vs.
Time
C. Perkins
8/31/63
12.1975
12.1970
12.1965
12.1960
S. A. O. Mean Motion
(Rev/Day)
S. A. O. Mean Motion
S. A. O. photo reduced data 2.1
Computed assuming a spherical satellite
Computed neglecting second-order second harmonic effect
Computed assuming a tumbling cylindrical satellite
37350
37400
37450
37500
37550
March 14, 1961
Time
(M. J. D.)

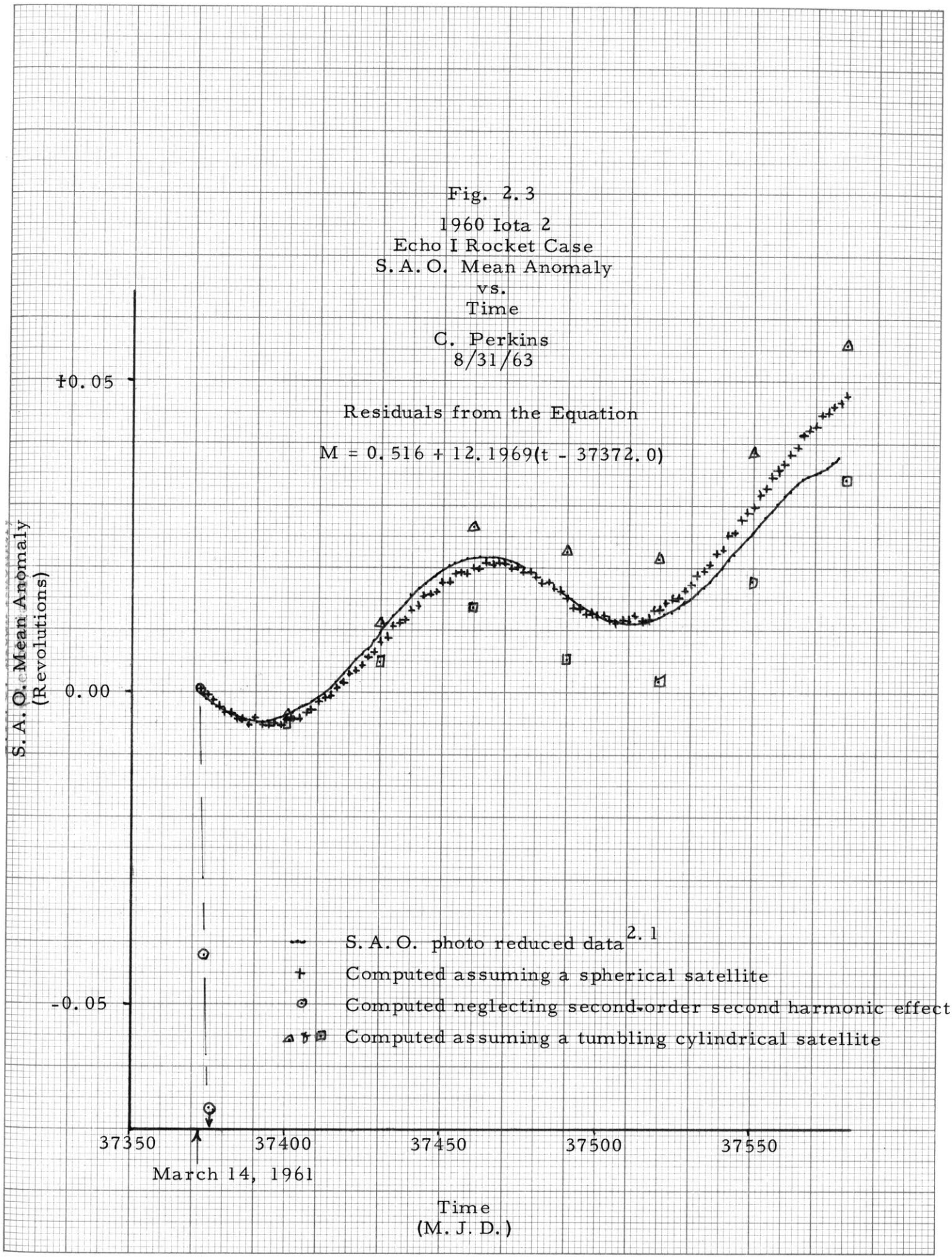
Fig. 2.3
1960 Iota 2
Echo I Rocket Case
S.A.O. Mean Anomaly
vs.
Time
C. Perkins
8/31/63
Residuals from the Equation
M = 0.516 + 12.1969(t - 37372.0)
+0.05
0.00
-0.05
S.A.O. Mean Anomaly
(Revolutions)
S.A.O. photo reduced data 2.1
Computed assuming a spherical satellite
Computed neglecting second-order second harmonic effects
Computed assuming a tumbling cylindrical satellite
37350
37400
37450
37500
37550
March 14, 1961
Time
(M.J.D.)

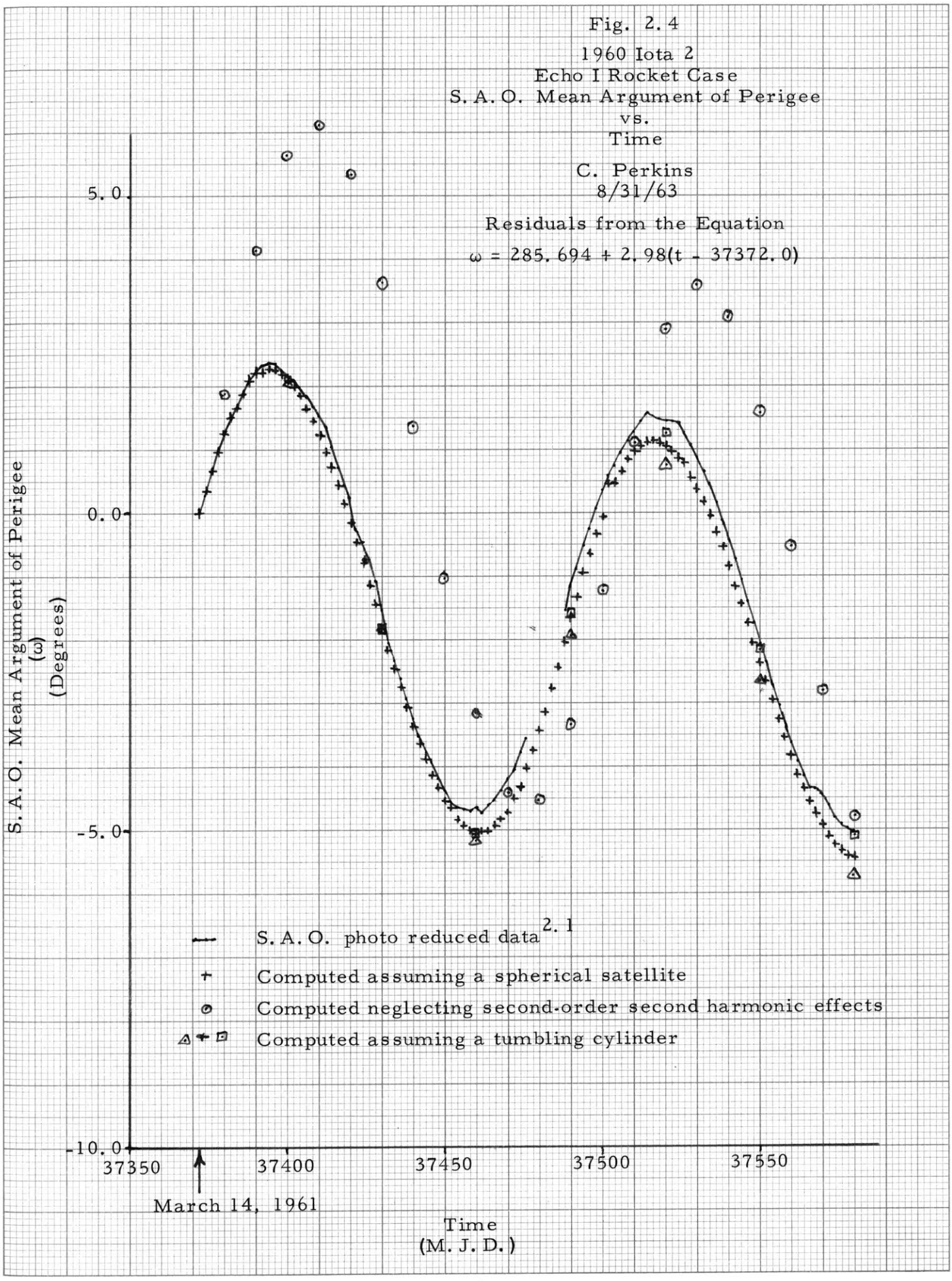
Fig. 2.4
1960 Iota 2
Echo I Rocket Case
S. A. O. Mean Argument of Perigee
vs.
Time
C. Perkins
8/31/63
Residuals from the Equation
ω = 285.694 + 2.98(t - 37372.0)
5.0
0.0
-5.0
-10.0
S.A.O. Mean Argument of Perigee (ω) (Degrees)
S. A. O. photo reduced data 2.1
Computed assuming a spherical satellite
Computed neglecting second-order second harmonic effects
Computed assuming a tumbling cylinder
37350
37400
37450
37500
37550
March 14, 1961
Time
(M. J. D.)

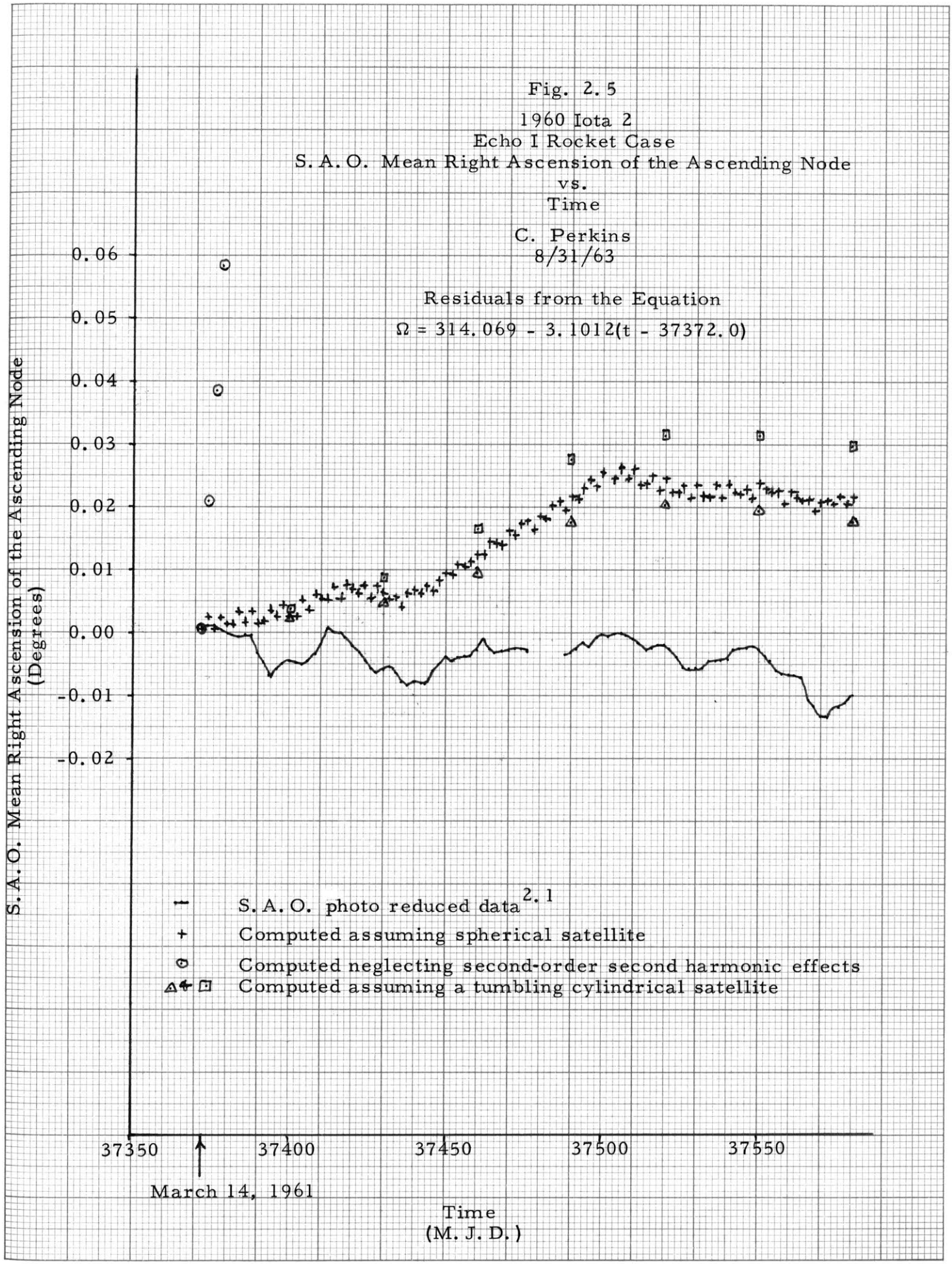
Fig. 2.5
1960 Iota 2
Echo I Rocket Case
S. A. O. Mean Right Ascension of the Ascending Node
vs.
Time
C. Perkins
8/31/63
Residuals from the Equation
Ω = 314.069 - 3.1012(t - 37372.0)
S. A. O. Mean Right Ascension of the Ascending Node
(Degrees)
0.06
0.05
0.04
0.03
0.02
0.01
0.00
-0.01
-0.02
S. A. O. photo reduced data 2.1
Computed assuming spherical satellite
Computed neglecting second-order second harmonic effects
Computed assuming a tumbling cylindrical satellite
37350
37400
37450
37500
37550
March 14, 1961
Time
(M. J. D.)

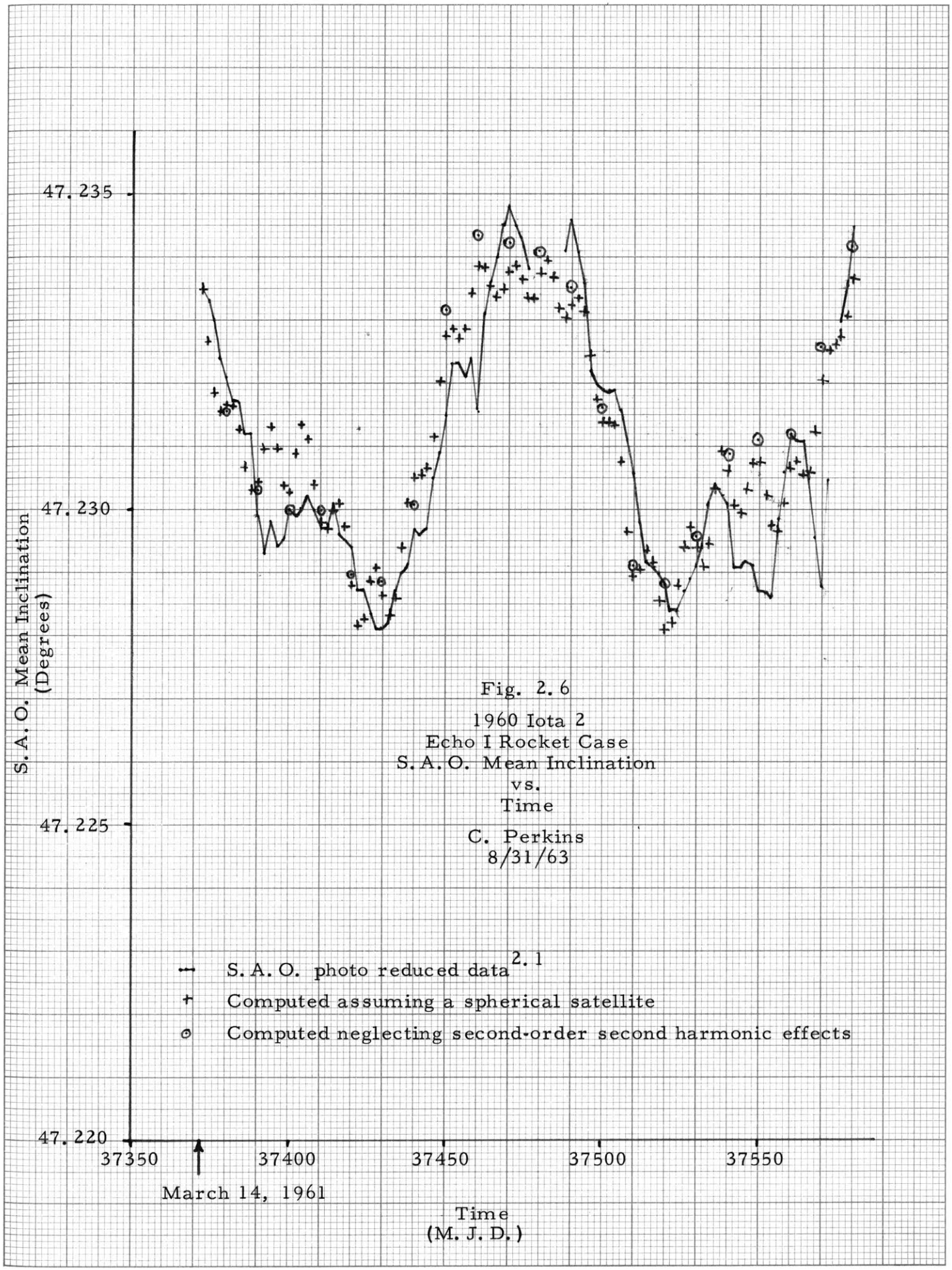

Fig. 2.6

1960 Iota 2
Echo I Rocket Case
S.A.O. Mean Inclination
vs.
Time

C. Perkins
8/31/63

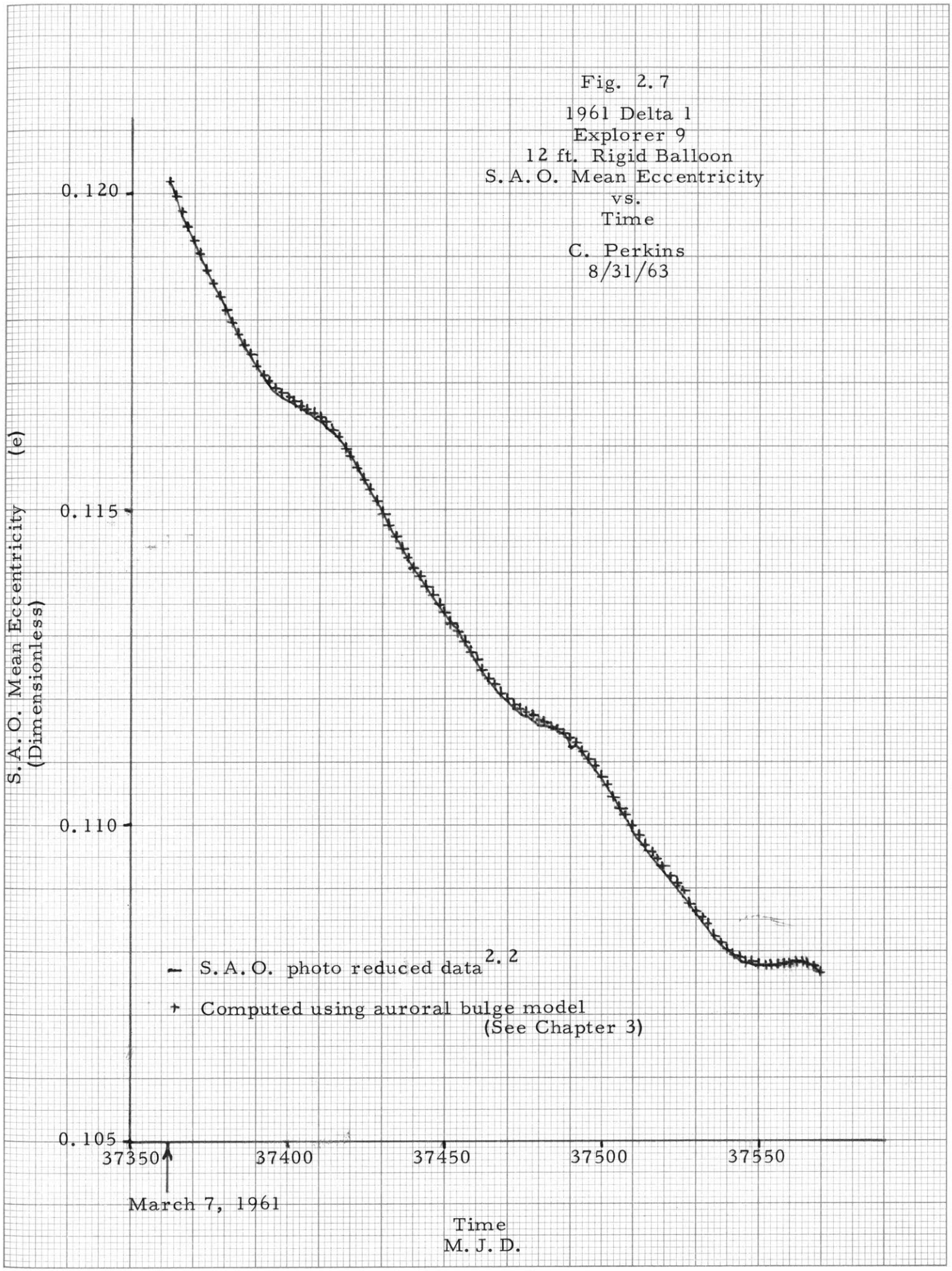
Fig. 2.7
1961 Delta 1
Explorer 9
12 ft. Rigid Balloon
S.A.O. Mean Eccentricity
vs.
Time
C. Perkins
8/31/63
0.120
0.115
0.110
0.105
S.A.O. Mean Eccentricity (e)
(Dimensionless)
S.A.O. photo reduced data 2.2
Computed using auroral bulge model
(See Chapter 3)
37350
37400
37450
37500
37550
March 7, 1961
Time
M.J.D.

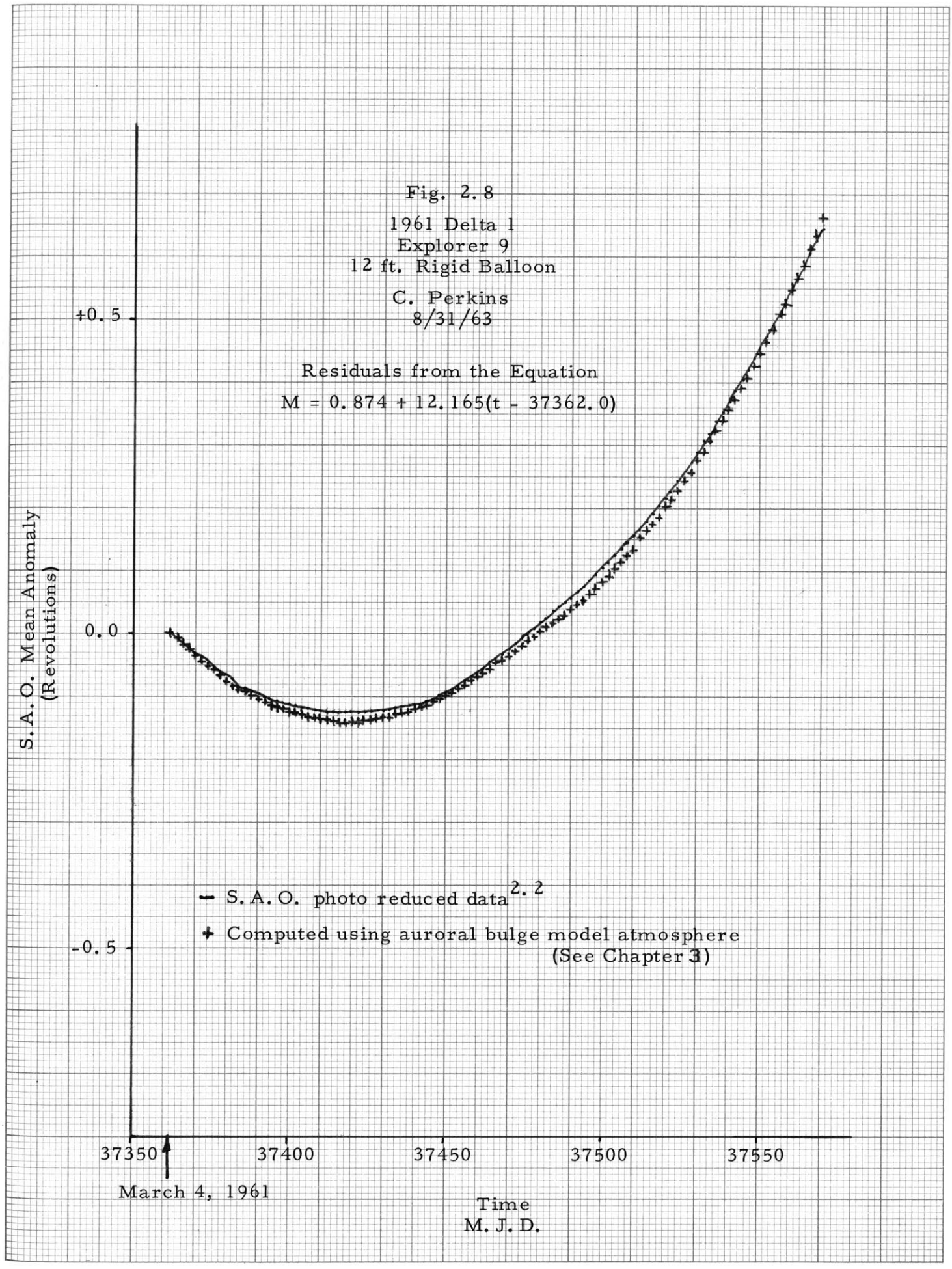
Fig. 2.8
1961 Delta 1
Explorer 9
12 ft. Rigid Balloon
C. Perkins
8/31/63
Residuals from the Equation
M = 0.874 + 12.165(t - 37362.0)
+0.5
0.0
-0.5
S.A.O. Mean Anomaly
(Revolutions)
S.A.O. photo reduced data 2.2
Computed using auroral bulge model atmosphere
(See Chapter 3)
37350
37400
37450
37500
37550
March 4, 1961
Time
M.J.D.

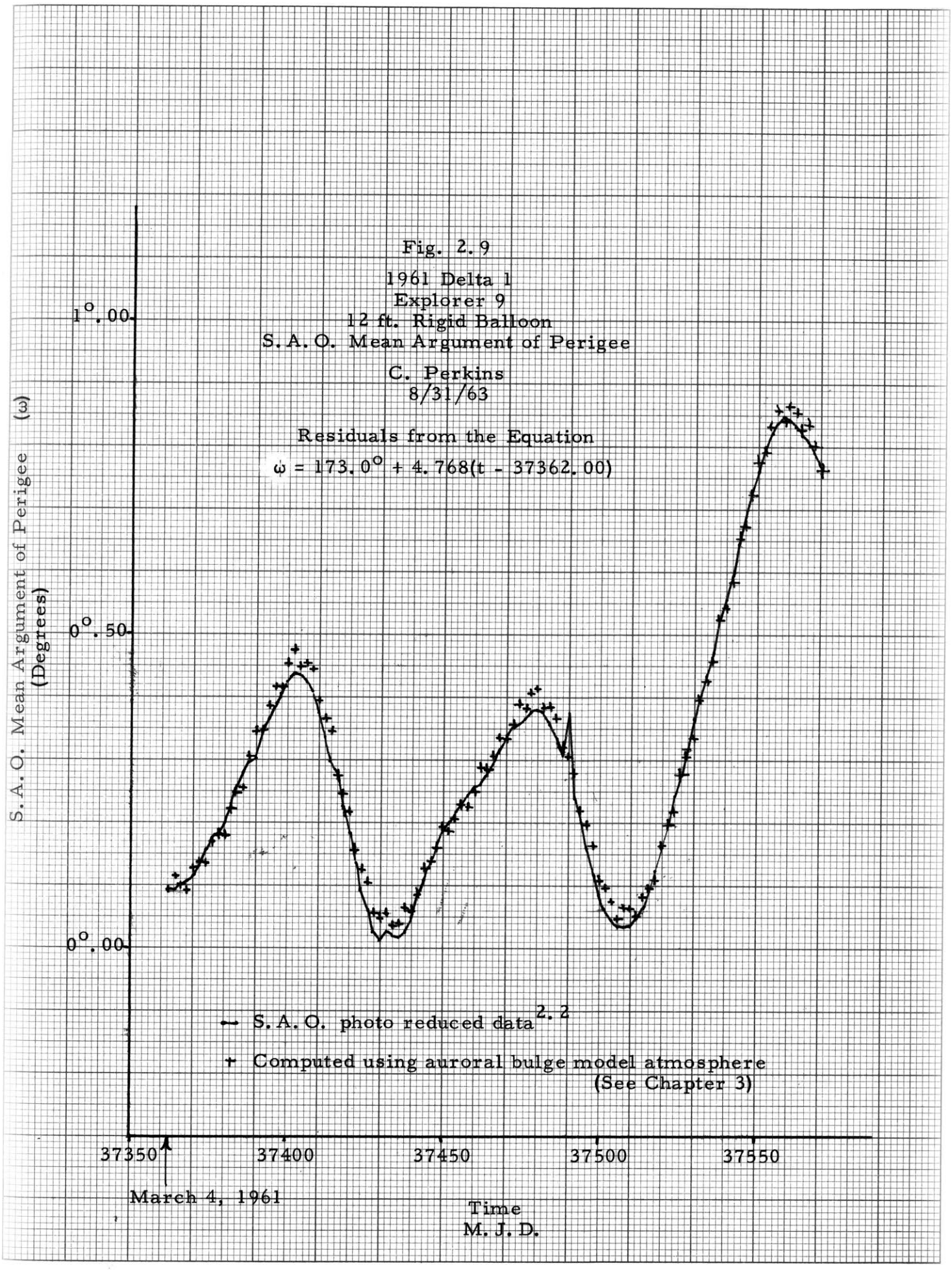
Fig. 2.9
1961 Delta 1
Explorer 9
12 ft. Rigid Balloon
S. A. O. Mean Argument of Perigee
C. Perkins
8/31/63
Residuals from the Equation
ω = 173.0° + 4.768(t - 37362.00)
1°.00
0°.50
0°.00
S. A. O. Mean Argument of Perigee (ω) (Degrees)
S. A. O. photo reduced data 2.2
Computed using auroral bulge model atmosphere
(See Chapter 3)
37350
37400
37450
37500
37550
March 4, 1961
Time
M. J. D.

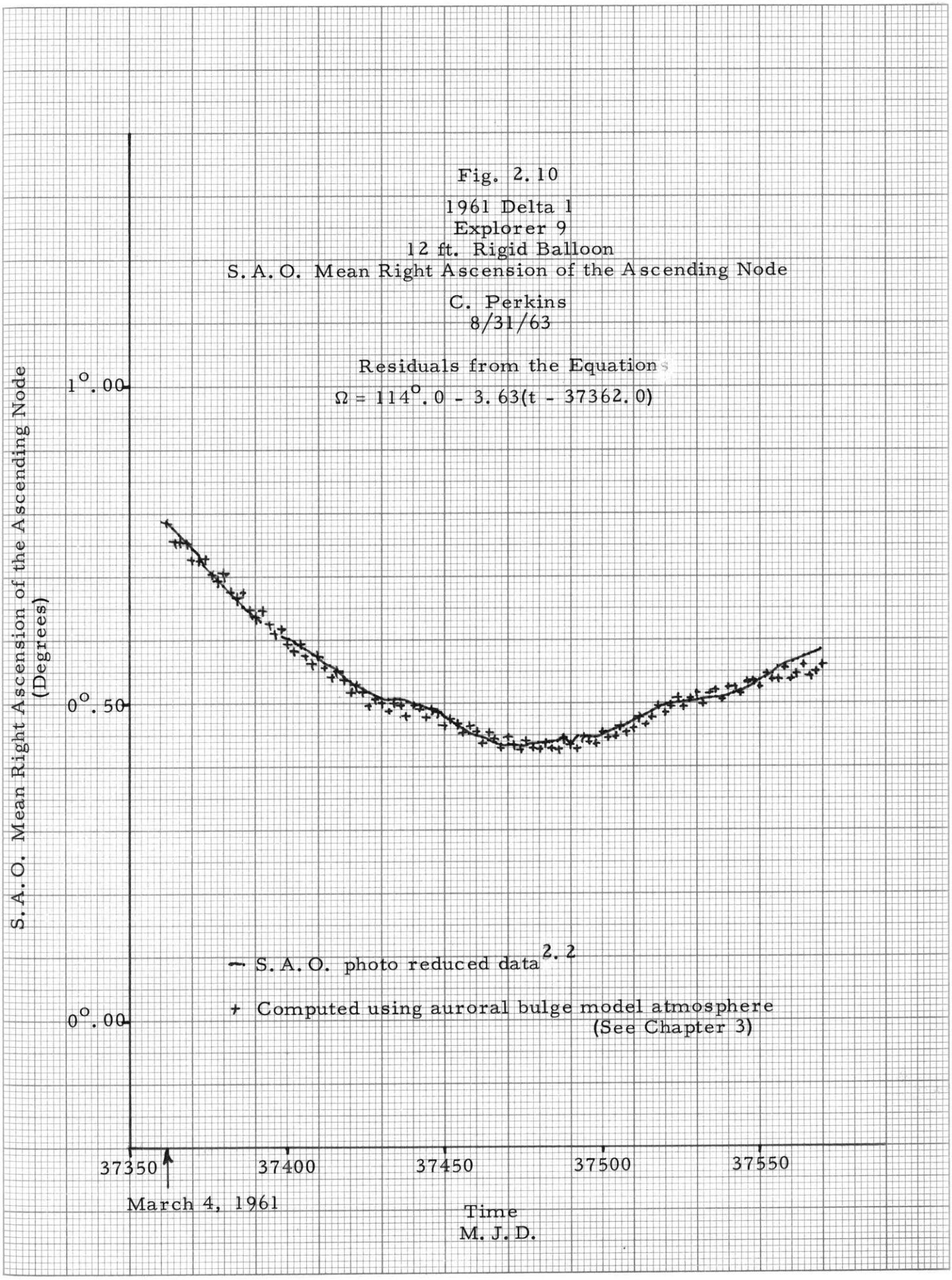
Fig. 2.10
1961 Delta 1
Explorer 9
12 ft. Rigid Balloon
S. A. O. Mean Right Ascension of the Ascending Node
C. Perkins
8/31/63
Residuals from the Equation
Ω = 114°.0 - 3.63(t - 37362.0)
S. A. O. Mean Right Ascension of the Ascending Node (Degrees)
1°.00
0°.50
0°.00
— S. A. O. photo reduced data 2.2
+ Computed using auroral bulge model atmosphere (See Chapter 3)
37350
37400
37450
37500
37550
March 4, 1961
Time
M. J. D.

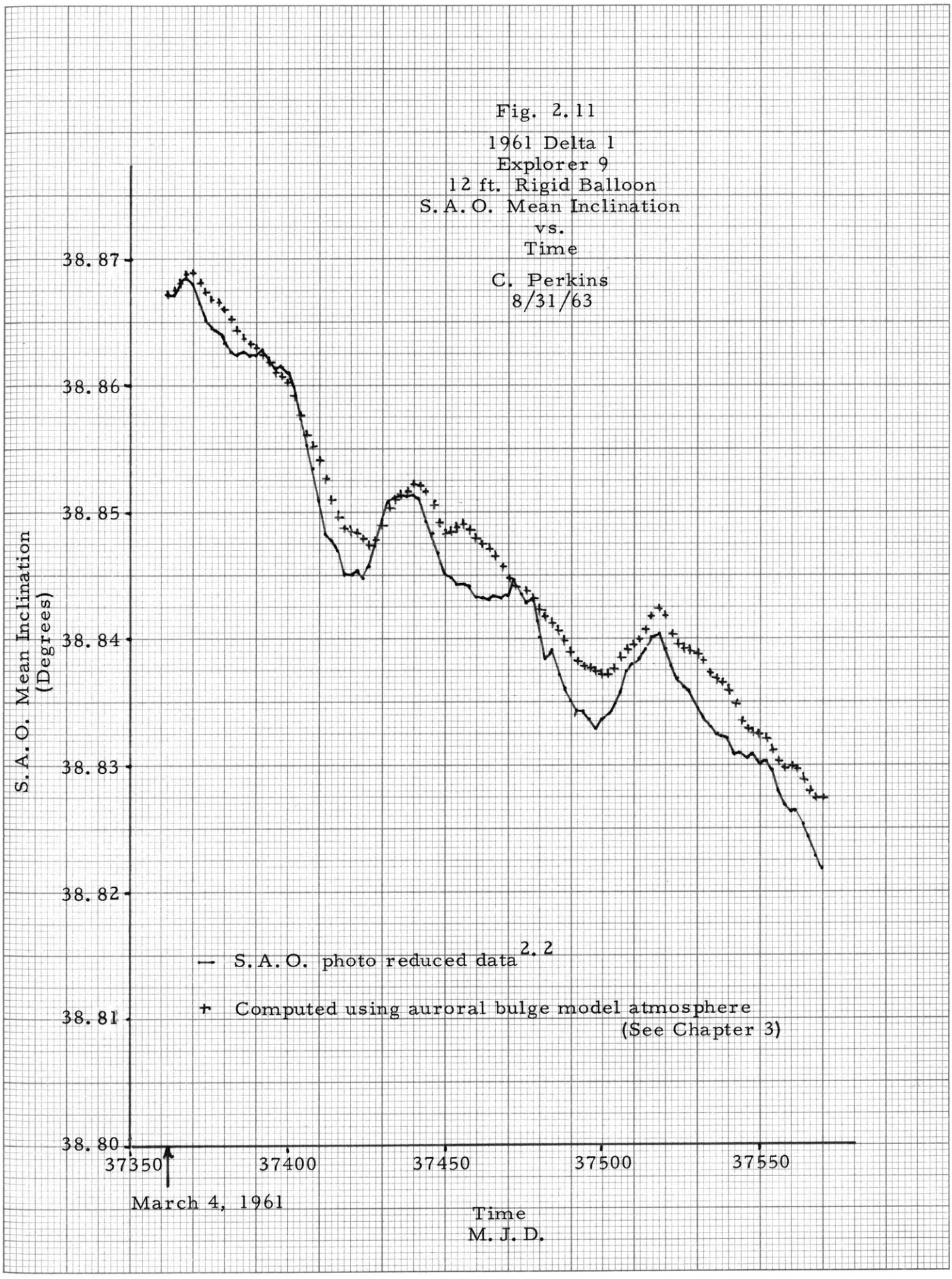
Fig. 2.11
1961 Delta 1
Explorer 9
12 ft. Rigid Balloon
S.A.O. Mean Inclination
vs.
Time
C. Perkins
8/31/63
38.87
38.86
38.85
38.84
38.83
38.82
38.81
38.80
S.A.O. Mean Inclination
(Degrees)
— S.A.O. photo reduced data 2.2
+ Computed using auroral bulge model atmosphere
(See Chapter 3)
37350
37400
37450
37500
37550
March 4, 1961
Time
M.J.D.

Fig. 2.12

A Heavy Satellite
Time of Nodal Crossing
vs.
Orbit Revolution Number

C. Perkins
9/10/63

Residuals from the Equation

$T_N = 37777.7516_{days} + 9181.18_{sec}(N-120)$

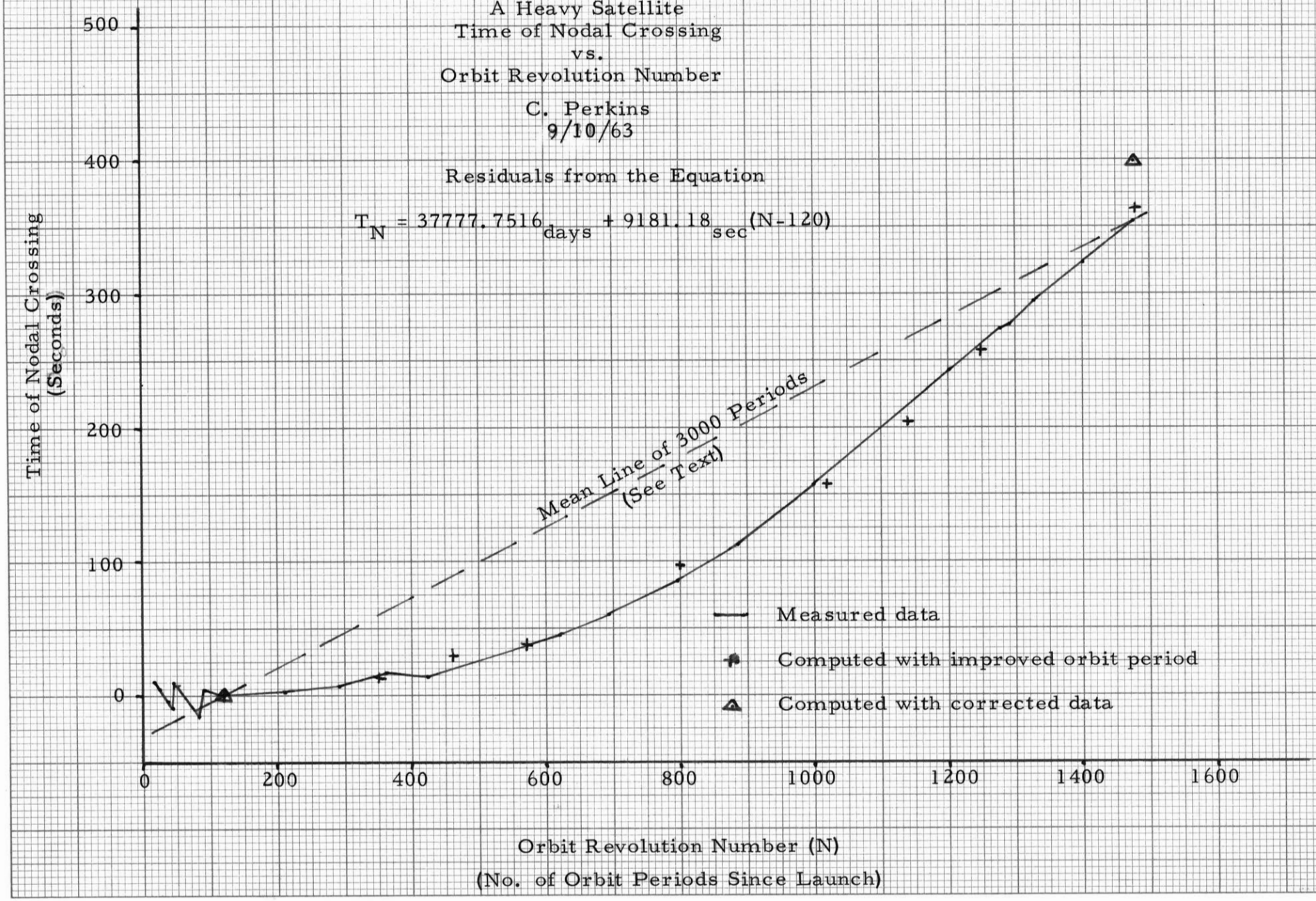

REFERENCES

2.1 I. G. Izsak, "Satellite Orbital Data," Special Report No. 119, Smithsonian Astrophysical Observatory (15 March 1963).

2.2 Private communications from L. Jacchia and B. Miller of the Smithsonian Astrophysical Observatory.

2.3 I. G. Izsak, "Satellite Orbital Data," Special Report No. 92, Smithsonian Astrophysical Observatory (23 April 1962).

2.4 P. Stern, "Catalog of Precisely Reduced Observations," No. P-8 Special Report No. 118, Smithsonian Astrophysical Observatory (14 February 1963).

2.5 D. V. Mechau, "Satellite Orbital Data," Special Report No. 51, Smithsonian Astrophysical Observatory (October 1960).

2.6 "Differential Orbit Improvement Program (DOI and DOI, II)," Smithsonian Astrophysical Observatory, unpublished.

2.7 I. I. Shapiro, "Effects of Sunlight Pressure on Air Density Determinations Involving Cylindrical Satellites," Journal of Geophysical Research 68, No. 19 (October 1, 1963).

2.8 I. I. Shapiro, "The Prediction of Satellite Orbits," ed. M. Roy, IUTAM Dynamics of Satellites Symposium, Paris, May 28-30, 1962 (Academic Press, 1963).

2.9 Y. Kozai, "Numerical Results from Orbits," Special Report No. 101, Smithsonian Astrophysical Observatory (31 July 1962).

2.10 R. W. Parkinson, H. M. Jones, I. I. Shapiro, "Effects of Solar Radiation Pressure on Earth Satellite Orbits," Science 131, No. 3404 (25 March 1960), pp. 920-921.

2.11 T. E. Sterne, An Introduction to Celestal Mechanics, Interscience Tracts on Physics and Astronomy, No. 9 (Interscience Publishers Inc., New York, 1960).

2.12 I. I. Shapiro, H. M. Jones, "Perturbation of the Orbit of the Echo Balloon," Science 132, No. 3438 (18 November 1960), p. 1984.

2.13 I. I. Shapiro, H. M. Jones, "Lifetimes of Orbiting Dipoles," Science 134 (October, 1961).

2.14 H. M. Jones, C. W. Perkins, I. I. Shapiro, "Orbital Lifetimes of the West Ford Dipoles," Letter to the Editor, Science 140 No. 3572 (14 June 1963), p. 1173.

2.15 I. I. Shapiro, I. Maron, L. Kraft, "Experimental Study of Charge Drag on Orbiting Dipoles," Journal of Geophysical Research 68, No. 7 (April 1, 1963).

2.16 Private communication from E. M. Gaposchkin of the Smithsonian Astrophysical Observatory.

2.17 L. Jacchia, J. Slowey, "Accurate Drag Determinations for Eight Artificial Satellites; Atmospheric Densities and Temperatures," Special Report No. 100, Smithsonian Astrophysical Observatory (30 July 1962).

2.18 Private communication from H. Jones of M. I. T. Lincoln Laboratory.

2.19 Private communication from I. Shapiro of M. I. T. Lincoln Laboratory.

CHAPTER III

Atmospheric Density Models

3.1 Introduction

The factors which presently limit the accuracy* which can be achieved in the computation of orbit perturbations caused by neutral** drag are inadequacies in current atmospheric density models, uncertainties about the interaction between the satellite and the impinging air molecules (i.e., uncertainty in the drag coefficient C_D) and possible uncertainty about the effective area-to-mass ratio because of unknown orientation. We apply accurate orbit perturbation computations to the study of semi-empirical atmospheric density models, with emphasis on systematic, long-period variations in density with time. The use of orbital data for 1961 Delta 1 minimizes the uncertainty in C_D*** and A/M since this satellite is nearly spherical.

Atmospheric density models have been improved as both the quality and quantity of satellite orbital data have increased. As early as February, 1958, variations were noted in the accelerations of the time of perigee passage of several satellites.[3.2, 3.3] Jacchia[3.4] later demonstrated these variations to be variations in atmospheric density, presumably caused by solar activity. Specifically, these variations in density were correlated, in part, to the decimeter solar radio flux+ by Priester[3.4] and later by Jacchia[3.4] and to the geocentric angular distance from the sub-solar point (the diurnal bulge) by Jacchia.[3.4] Jacchia also discovered a correlation between transient variations in density and geomagnetic disturbances.[3.6]

---

*In general, the care which must be exercised in drag perturbation computations depends, of course, on the accuracy required, the atmospheric density at perigee altitude and the area-to-mass ratio of the satellite.

**Coulomb interactions are excluded from the discussion of neutral drag.[3.1]

***The uncertainty in C_D is on the order of ± 5% for this satellite.[3.14]

+The decimeter solar fluxes (10.7 and 20 cm) are not the cause of the variations in density but merely an index to the solar effects which do cause the variations (probably atmospheric heating by solar radiation flux in the extreme-ultraviolet portion of the spectrum[3.5]).

In the late 50's, several naïve density models were compared with the available satellite data but did not account for the observed variations in density (for examples, see Refs. 3.3, 3.7, and 3.8). An empirical atmospheric density model* which attempted to account for the diurnal effect and for the correlation with the 20 cm solar flux was first presented by Jacchia in 1960. [3.9] The notable results were a pronounced lag, of between 25° and 30°, of the maximum point of the diurnal bulge from the sub-solar point, an almost linear dependence of the density on the 20 cm solar flux, and a $\cos^6(\psi/2)$ law for the shape of the bulge where ψ is the geocentric angular distance from the maximum point of the bulge.

Jacchia's 1960 model was improved by making use of a theoretical density model published by Nicolet [3.10] in 1961. Nicolet's model is based of diffusion equilibrium with assumed boundary conditions at 120 km altitude. Temperature is the most important parameter in Nicolet's model. The temperature asymptotically approaches a constant (the "top" temperature) at high altitudes (the thermopause), above which the atmosphere is essentially isothermal (this altitude is 300 km for a top temperature of 903°K and 650 km for a top temperature of 2131°K). Nicolet found that the vertical distribution of density depends on the top temperature of a vertical column and that the variations in density caused by the diurnal and solar effects can be represented by changes in the top temperature.

Using Nicolet's model, Jacchia demonstrated the correlation of the 10.7 cm solar flux with the top temperature and showed the maximum top temperature at the center of the bulge to be approximately a constant multiple (~ 1.35) of the night-time top temperature. [3.11]

Explorer IX (1961 Delta 1) provides an extremely sensitive instrument for the study of atmospheric density. Jacchia and Slowey used orbital data for this satellite to correlate a portion of the observed temperature variations with the daily geomagnetic planetary index**(A_p). [3.12]

---

*This density model is contained in the General Perturbation Program as an optional one for computing neutral drag perturbations (see Appendix II).

**The mechanism of atmospheric heating which correlates to the geomagnetic planetary index is not well understood, (see Ref. 3.5).

Later, by including additional orbital data for seven other satellites, Jacchia and Slowey [3.13] were able to confirm Paetzold's semiannual effect and to separate the solar flux effect into an "erratic" (or "27-day") effect which follows the daily 10.7* cm solar flux variations and a systematic effect which is correlated to the monthly average of the 10.7 cm flux and which closely parallels the trend of the decimetric solar flux over the 11-year solar cycle.

A complete density model that includes the above mentioned effects was published by Jacchia in 1962. [3.14] This model consists of empirical equations relating top temperature to the various physical effects. Density is then read from Nicolet's tables [3.10] using a computed top temperature and altitude as independent variables. The improved accuracy of photo-reduced data for 1961 Delta 1 (see Chapter II) allowed Jacchia to correlate the geomagnetic effect to the three hour geomagnetic planetary index (a_p) [3.14] instead of the daily average A_p. [3.12]

The observed variations in atmospheric density are presumably caused [3.5] by variations in atmospheric heating in the regions of 100 km to 200 km altitude. This heating is thought [3.5] to be caused by electromagnetic radiation (principally extreme-ultraviolet and soft x-ray) and possibly corpuscular streams from the sun. The various effects which are correlated to the variations in density are simply measures of the true causes.

3.2 Improvement of Density Models

The method used to compute orbit perturbations (in particular, mean motion perturbations) and the accuracy that can be achieved (see Chapter II) makes the General Perturbation Program (GPP) a useful instrument for the study of atmospheric densities. First, it can be used to test density models over long periods of time; second, it can be used to improve those constants in existing density models that cause systematic long-period and secular perturbations of satellite orbits; and third, it can be used to detect systematic, long period density variations.

Drag is, of course, a non-conservative perturbing force and its principal effect on an orbit is to reduce the orbital energy. The orbital

*The 20 cm solar flux data which originates in East Germany contained a slow drift, probably of instrument origin, and which masked the semi-annual effect. [3.13] The use of 20 cm solar flux data has been abandoned for this reason.

elements that depend on orbital energy include the semi-major axis (a), the mean motion (n), the anomalistic period, etc. The Smithsonian Astrophysical Observatory mean motion (see Appendix III) is used here because of the availability of high precision data for this quantity. A change in mean motion is a measure of drag and is therefore a measure of atmospheric density. Jacchia deduces density and temperature by determining the time rate of change of mean motion from satellite data at each epoch of interest and subtracting from $\dot{n}$, the theoretical contribution of radiation pressure, etc. [3.13] The resulting corrected derivative of mean motion parallels the daily variations of density (and therefore top temperature) at perigee. The fine structure of these variations is therefore readily apparent.

The mean motion, derived from satellite observations, reflects the integral of all the variations in density over the history of the satellite. The small "spikes" in the time history of $\dot{n}$ are essentially smoothed in the time history of n. The GPP computes the time history of the mean motion (indirectly from p, e, and i, see Appendix III) from a single set of initial orbital elements (see Chapter II). Thus, small long-period and secular discrepancies of the density model from the actual density will build up and be visible in this time history (see Fig. 3.1).

The result of computing the mean motion of 1961 Delta 1* using Jacchia's 1960 density model (described above) is presented in Fig. 3.1** (symbol Δ). The comparison of this result with the experimentally determined [3.15] mean motion in Fig. 3.1 shows that the drag perturbation computed with this model is approximately four times too great.

Drag perturbations are computed in the GPP by numerical quadratures. Density if computed with the model desired for each argument

---

*1961 Delta 1 is a 12-ft-diameter, rigid, spherical balloon with an area-to-mass ratio of 15.84 cm^2/gm [3.13] which makes it particularly sensitive to neutral drag. A drag coefficient of 2.2 is assumed.

**Time is reckoned in Modified Julian days (MJD) for these data (see Appendix IV).

of each quadrature. In Jacchia's density model, based on top temperatures, [3.14, 3.16] the night-time temperature is used in the following form:

$$T_N = a_1 + a_2\bar{F}_{10.7} + a_3 \cdot \cos\left(\frac{4\pi}{a_4}(t - a_5)\right) \cdot \bar{F}_{10.7} + a_6 \cdot \bar{F}_{10.7}^{\,2} \qquad (3.1)^*$$

where a_m, $m = 1, \ldots, 6$, are constants; $\bar{F}_{10.7}$ is the monthly average of the 10.7 cm solar flux** (see Figs. 3.4 and 3.5); and t is time.

The top temperature for a given point is:

$$T = T_N[1 + b_1\cos^{\ell}(\psi/2)] + b_2 a_p + b_3(F_{10.7} - \bar{F}_{10.7}) \qquad (3.2)$$

where b_m, $m = 1, 2, 3$ are constants; $F_{10.7}$ is the daily average of the 10.7 cm solar flux**(see Figs. 3.4 and 3.5); a_p is the three-hour geomagnetic planetary index delayed, in time, up to six hours (see Figs. 3.4 and 3.5); ℓ is a constant exponent; and ψ is the geocentric angular distance from the given point to the maximum point of the bulge. The bulge maximum is assumed to be at the same latitude as the sun and lagging λ degrees behind. [3.9] The altitude at a given point is computed above the International Ellipsoid of Reference. [3.17] Density is then determined from T and altitude by two-dimensional, linear interpolation from Nicolet's tables. [3.10] ***

Table 3.1 contains a list of Jacchia's constants for this density model. The curve of mean motion vs. time presented in Fig. 3.1 (represented by the symbols ⊡) is the result of using these constants. The table also contains a revised list of constants used to compute the mean motion vs. time represented by the symbols ⊙ in Fig. 3.1 and continued through Fig. 3.3. This latter list is the result of an effort to improve the agreement between the computed mean motion and the data using various combinations of constants. The most significant new values

---

*The third term on the right represents the semi-annual effect.

**$F_{10.7}$ and $\bar{F}_{10.7}$ are measured in "flux units" where one flux unit equals 10^{-22} watts/m^2/cycle/sec bandwidth. [3.11]

***These tables were extended to lower top temperatures with data kindly furnished by Dr. Jacchia.

are those for the lag angle (λ), the amplitude of the bulge (b_1), and possibly the amplitude of the semi-annual effect (a_3). The new value of b_3 (the amplitude of the "27-day" effect) is probably erroneous; Jacchia's value is probably better because his method is more sensitive for measuring short-term variations in density. In addition, the values of λ and b_1 (the amplitude of the bulge) are difficult to separate using just one satellite. 1961 Delta 1 is especially unsuitable in this respect because of the slow change in the geocentric angle between the bulge maximum and perigee (i.e., the orbit is resonant, see Chapter II). Figure 3.1 definitely demonstrates however that a significant improvement can be made in the constants of atmospheric density models using this method.

3.3 An Auroral Bulge Model

Figures 3.4 and 3.5 present in residual form, the discrepancy between the observed mean motion and the mean motion computed using the improved constants described above (labeled: without auroral bulge). Here, residual is defined to mean the computed mean motion minus the observed mean motion. A positive slope of this residual curve indicates the density computed by the program is too high, etc.

A comparison of the residual curve with the approximate curves of the latitude of the sun vs. time and the latitude of perigee* vs. time shows that when the sun is in the northern hemisphere, the computed density is too low if perigee is in the southern hemisphere and too high when perigee is in the northern hemisphere. When the sun is in the southern hemisphere, the opposite is true: computed density is too high when perigee is in the southern hemisphere, etc. The oscillation in the computed density error changes phase when the sun is over the equator.

This discrepancy can be explained by assuming that the diurnal bulge is extended in the north-south direction. To account for this extension and also the possibility that it is caused by atmospheric heating in the auroral zones,** an ad hoc density model was programmed

*Most of the drag perturbation of 1961 Delta 1 occurs within a few degrees of perigee and for purposes of this discussion it is assumed to occur entirely at perigee.

**Jacchia and Slowey have independently postulated auroral heating[3.18] from a study of the orbit of 1962 Beta Tau 2 (INJUN III) for which $e = 0.16$, $i. = 70.4°$, and perigee height $\sim$ 250 km.

that included two additional bulges located approximately in the regions of diurnal auroral activity.[3.19, 3.20, 3.21] This model is the same as Jacchia's top temperature model described above except that the top temperature for a given point is:

$$T = T_N(1 + b_1 \cos^{\ell} \psi/2) + b_2 a_p + b_3(F_{10.7} - \overline{F}_{10.7})$$
$$+ (c_1 + c_2 \cdot T_N + c_3 \cdot a_p + c_4 \cdot A_p) \cdot (c_5 \cos^{\ell_N} \psi_N/2 + c_6 \cos^{\ell_S} \psi_S/2) \qquad (3.3)$$

where c_m, $m = 1,\ldots, 6$ are constants; A_p is the daily average geomagnetic planetary index (see Figs. 3.4 and 3.5); ℓ_N and ℓ_S are constant exponents; and ψ_N and ψ_S are the geocentric angular distances from the given point to the points at which the north and south bulges reach their respective maxima. The points of bulge maxima are assumed to be at constant latitudes (δ_N and δ_S) and to lag behind the sun at constant angles (λ_N and λ_S).

Table 3.2 contains a list of constants used to obtain the curve of mean motion vs. time presented in Fig. 3.1 (symbol +). The values of the constants λ_N, λ_S, δ_N, δ_S, ℓ_N, ℓ_S, c_5 and c_6 were assumed, and the constants b_1, c_2, and c_4 were determined from a comparison of computed mean motion of 1961 Delta 1 with observation over the period from MJD 37362 to MJD 37526. The fit is approximate and only valid for this particular satellite in a limited region (see Fig. 3.2) but a definite improvement can be noted in the residual curve in Fig. 3.4.

The separation and measurement of the individual effects implicit in the model are extremely difficult for the satellite considered (and the orbital data available) and further refinement is not worthwhile at the present time because two additional balloon satellites (ECHO II and another 12-ft balloon) will be launched in the near future into near-polar orbits[3.16] and will provide much better data for this type of study (and for the improvement of Jacchia's constants, described above).

TABLE 3.1

Density Model Constants

Jacchia's Top Temperature Model

(Eqs. 3.1 and 3.2)

Constant	Jacchia's Values	Improved Values	Units	Ref.
a_1	647	647**	°K	*
a_2	0.01	0.01**	°K/flux unit	*
a_3	0.5	0.37	°K/flux unit	(3.15)
a_4	365.25	365.25**	days	(3.15)
a_5	April 7	April 7**		(3.15)
a_6	0.01318	0.01318**	°K/(flux unit)^2	*
λ	30°	25°	deg	(3.16)
ℓ	4	4	dimensionless	(3.15)
b_1	0.35	0.4	dimensionless	(3.16)
b_2	1.2	1.2	°K/a_p unit	(3.15)
b_3	2.2	3.2	°K/flux unit	(3.15)

*This quadratic was fit to data kindly supplied by Dr. Jacchia (also see Fig. 5 of Ref. 3.5).

**No improvement attempted.

TABLE 3.2

Density Model Constants
Auroral Bulge Model
(Eq. (3.3))

Constant	Value	Units
b_1	0.18	dimensionless
b_2	1.2	°K/a_p unit
b_3	2.2	°K/flux unit
c_1	0.0	°K
c_2	1.5	dimensionless
c_3	0.0	°K/a_p unit
c_4	1.0	°K/A_p unit
c_5	0.35	dimensionless
c_6	0.35	dimensionless
ℓ	4	dimensionless
λ	25°	deg.
ℓ_N	8.0	dimensionless
δ_N	60°	deg.
λ_N	60°	deg.
ℓ_S	8.0	dimensionless
δ_S	− 60°	deg.
λ_S	60°	deg.

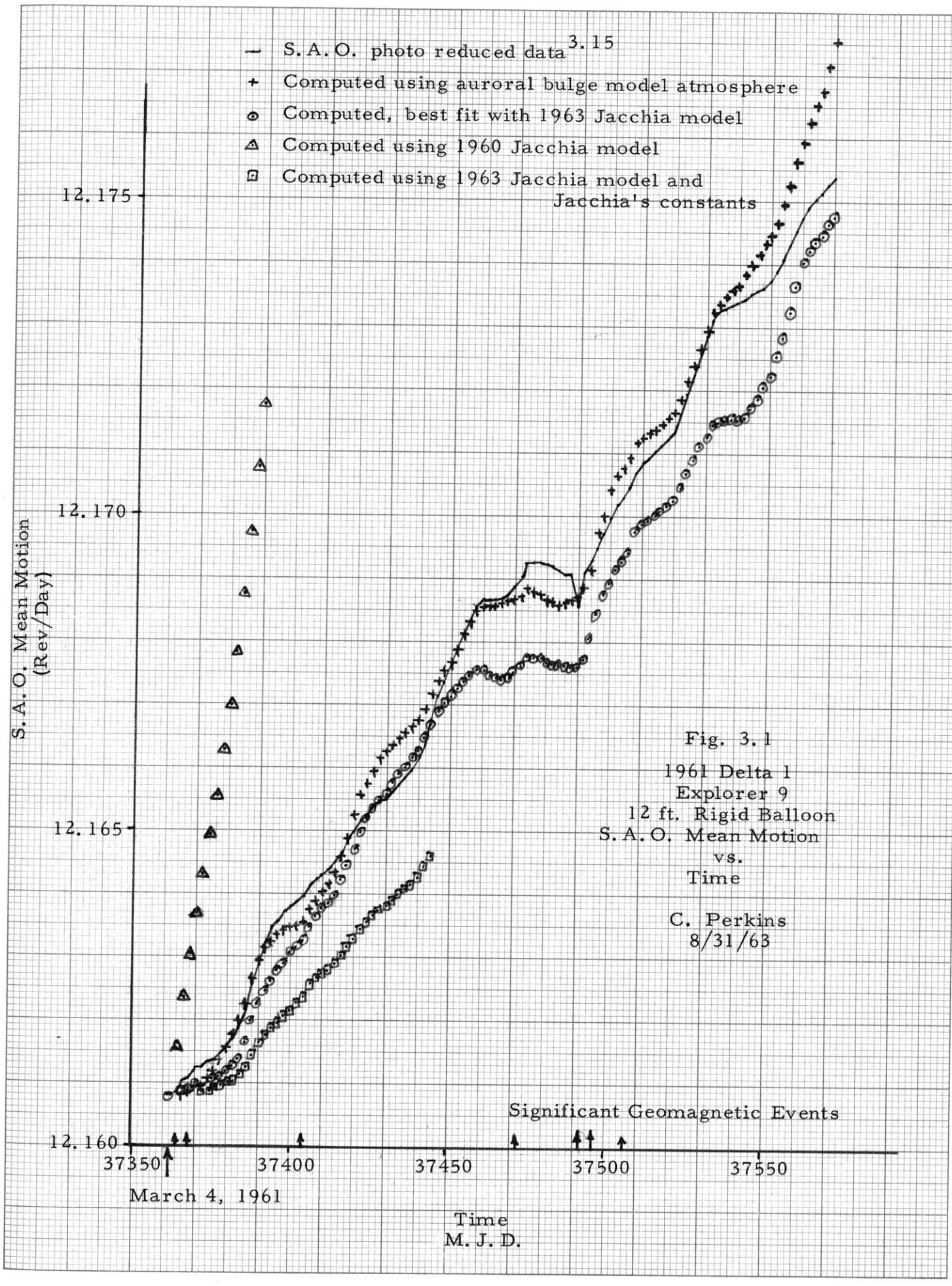

Fig. 3.1

1961 Delta 1
Explorer 9
12 ft. Rigid Balloon
S. A. O. Mean Motion
vs.
Time

C. Perkins
8/31/63

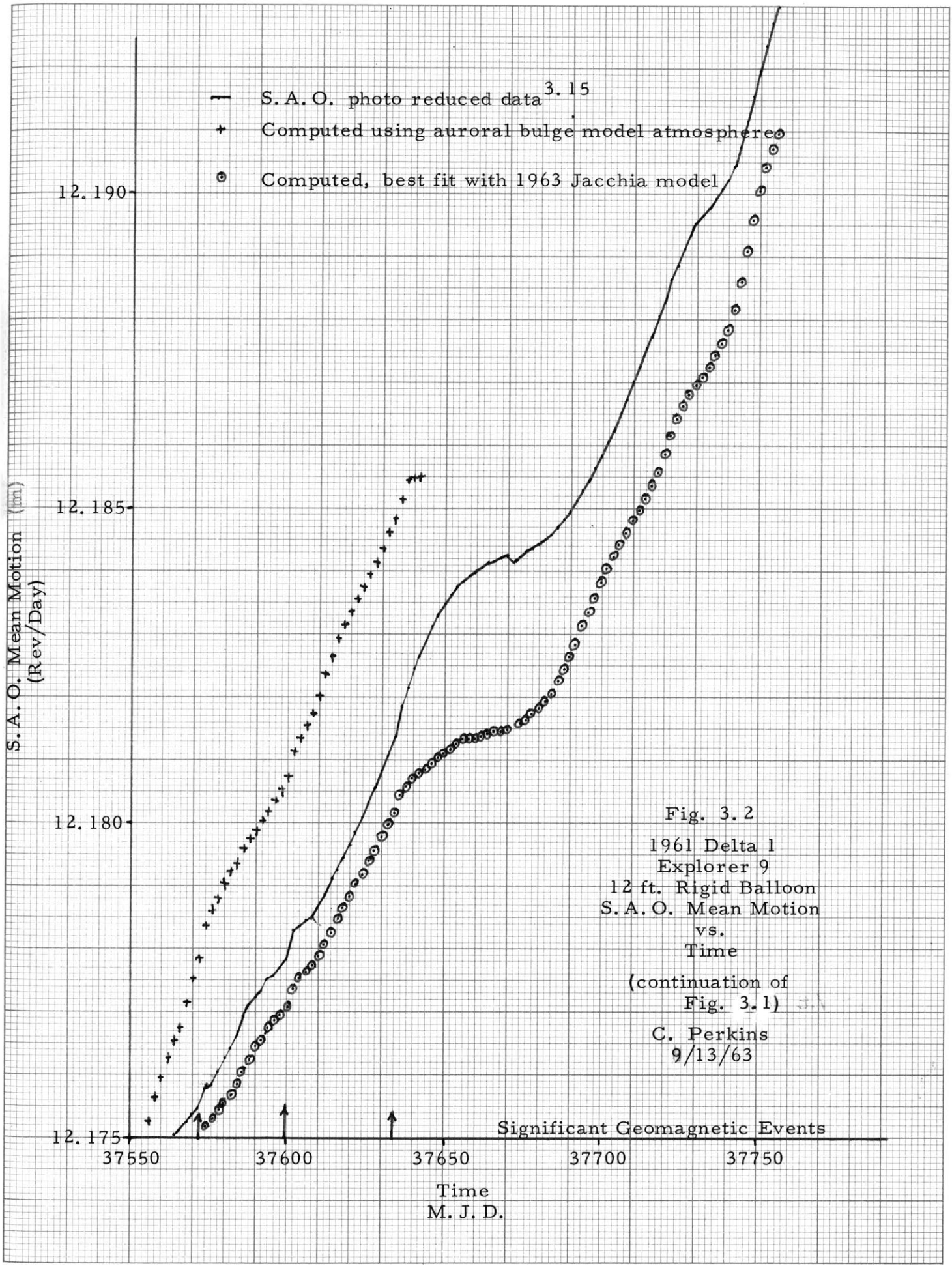

Fig. 3.2

1961 Delta 1
Explorer 9
12 ft. Rigid Balloon
S.A.O. Mean Motion
vs.
Time

(continuation of
Fig. 3.1)

C. Perkins
9/13/63

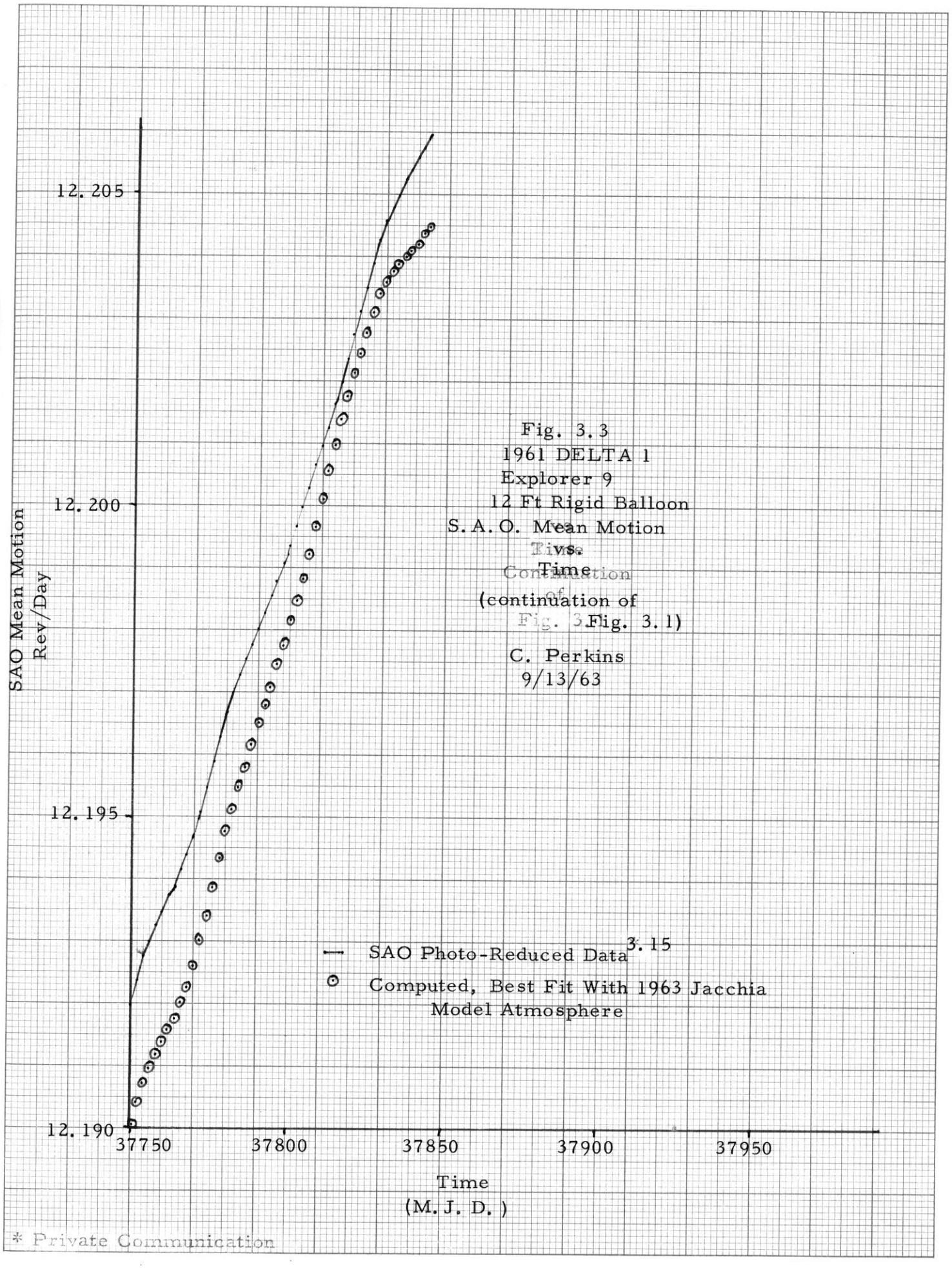

Fig. 3.3
1961 DELTA 1
Explorer 9
12 Ft Rigid Balloon
S.A.O. Mean Motion
vs.
Time
(continuation of
Fig. 3.1)

C. Perkins
9/13/63

* Private Communication

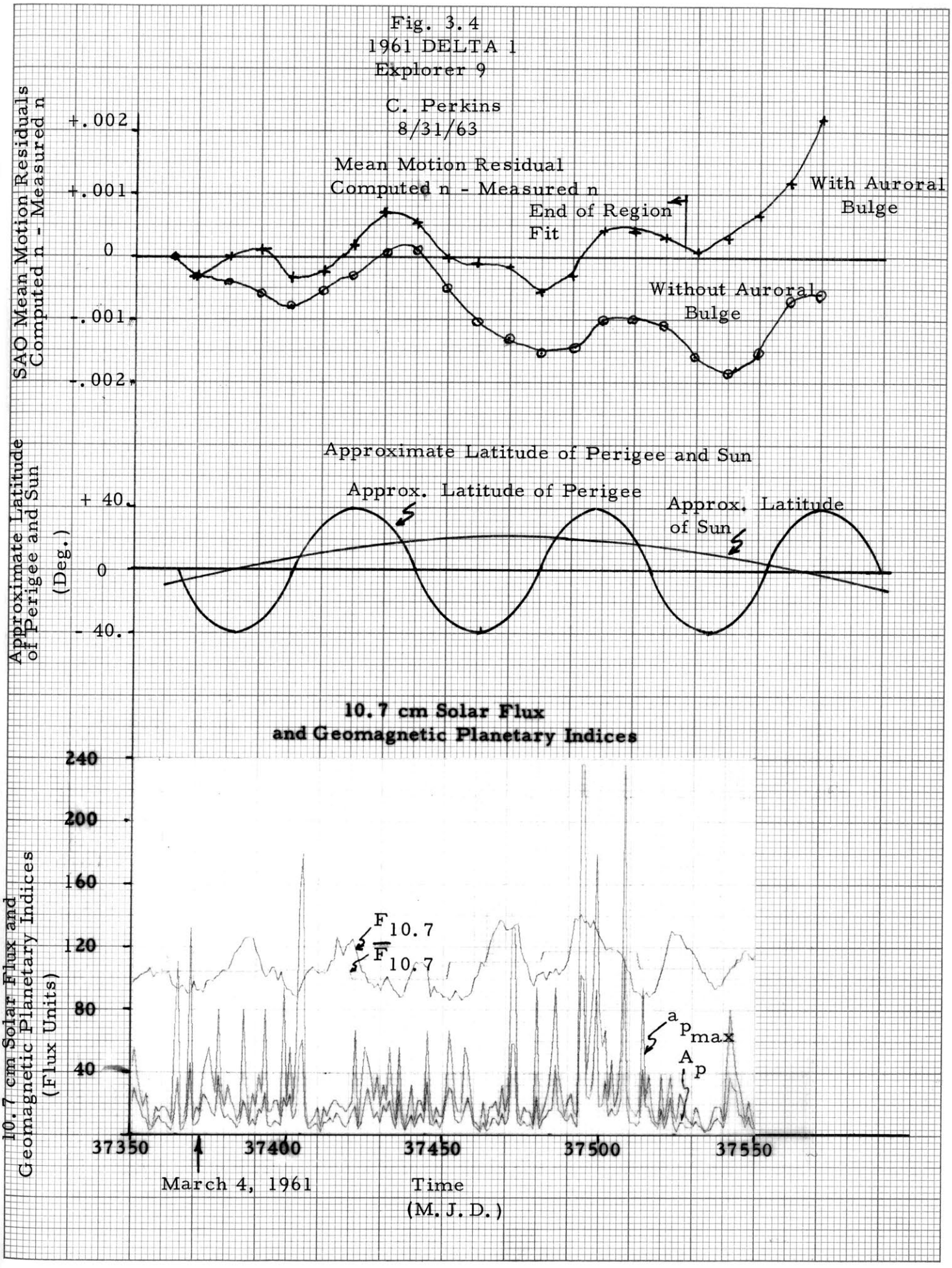
Fig. 3.4
1961 DELTA 1
Explorer 9
C. Perkins
8/31/63
SAO Mean Motion Residuals
Computed n - Measured n
+.002
+.001
0
-.001
-.002
Mean Motion Residual
Computed n - Measured n
End of Region
Fit
With Auroral
Bulge
Without Auroral
Bulge
Approximate Latitude
of Perigee and Sun
(Deg.)
+ 40.
0
- 40.
Approximate Latitude of Perigee and Sun
Approx. Latitude of Perigee
Approx. Latitude
of Sun
10.7 cm Solar Flux
and Geomagnetic Planetary Indices
10.7 cm Solar Flux and
Geomagnetic Planetary Indices
(Flux Units)
240
200
160
120
80
40
$F_{10.7}$
$\overline{F}_{10.7}$
$a_{p_{max}}$
A_p
37350
37400
37450
37500
37550
March 4, 1961
Time
(M. J. D.)

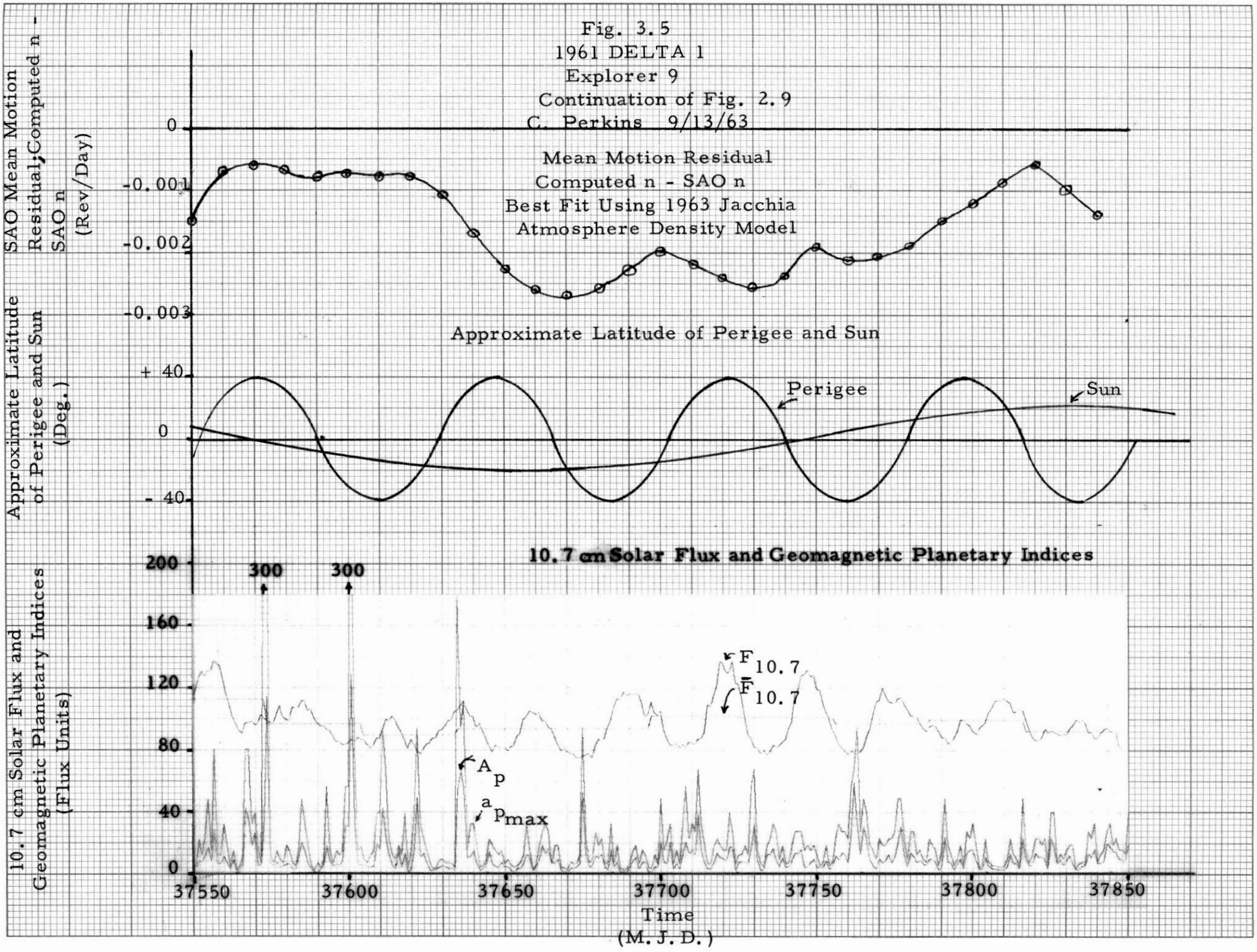
Fig. 3.5
1961 DELTA 1
Explorer 9
Continuation of Fig. 2.9
C. Perkins 9/13/63
SAO Mean Motion Residual; Computed n - SAO n (Rev/Day)
0
-0.001
-0.002
-0.003
Mean Motion Residual
Computed n - SAO n
Best Fit Using 1963 Jacchia
Atmosphere Density Model
Approximate Latitude of Perigee and Sun (Deg.)
+ 40
0
- 40
Approximate Latitude of Perigee and Sun
Perigee
Sun
10.7 cm Solar Flux and Geomagnetic Planetary Indices (Flux Units)
200
160
120
80
40
0
300
300
10.7 cm Solar Flux and Geomagnetic Planetary Indices
$F_{10.7}$
$\bar{F}_{10.7}$
A_p
$a_{p_{max}}$
37550
37600
37650
37700
37750
37800
37850
Time
(M.J.D.)

REFERENCES

3.1 I. I. Shapiro, "The Prediction of Satellite Orbits," ed. M. Roy, IUTAM Dynamics of Satellites Symposium, Paris, May 28-30, 1962, (Academic Press, 1963).

3.2 L. G. Jacchia, "Solar Effects on the Acceleration of Artificial Satellites," Special Report No. 29, Smithsonian Astrophysical Observatory (21 September 1959).

3.3 C. A. Whitney, "The Structure of the High Atmosphere," Special Report No. 21, Smithsonian Astrophysical Observatory (27 February 1959).

3.4 L. Jacchia, "Two Atmospheric Effects in the Orbital Acceleration of Artificial Satellites," Nature 183 (21 February 1959), pp. 526-527.

3.5 L. G. Jacchia, "Atmospheric Structure and its Variations at Heights above 200 km," Report to Working Group IV (International Reference Atmosphere) presented at the Fourth International Space Science Symposium, Warsaw, Poland, 1963, Smithsonian Astrophysical Observatory.

3.6 L. Jacchia, "Corpuscular Radiation and the Acceleration of Artificial Satellites," Nature 183 (13 June 1959), pp. 1662-1663.

3.7 C. A. Whitney, "The Structure of the High Atmosphere-II-A Conduction Model," Special Report No. 25, Smithsonian Astrophysical Observatory (20 April 1959).

3.8 L. Berkner, editor, Annals of the International Geophysical Year, Vol. VI, "Rochets and Satellites," (Pergamon Press, N. Y., 1958).

3.9 L. G. Jacchia, "A Variable Atmospheric Density Model from Satellite Accelerations," Journal of Geophysical Research 65 No. 9 (September, 1960), p. 2775.

3.10 M. Nicolet, "Density of the Heterosphere Related to Temperature," Special Report No. 75, Smithsonian Astrophysical Observatory (September, 1961).

3.11 L. G. Jacchia, "A Working Model for the Upper Atmosphere," Nature 192, No. 4808 (December 23, 1961).

3.12 L. G. Jacchia and J. Slowey, "Preliminary Analysis of the Atmospheric Drag of the Twelve-foot Balloon Satellite (1961)," Special Report No. 84, Smithsonian Astrophysical Observatory (February, 1962).

3.13 L. G. Jacchia and J. Slowey, "Accurate Drag Determinations for Eight Artificial Satellites; Atmospheric Densities and Temperatures," Special Report No. 100, Smithsonian Astrophysical Observatory (July, 1962).

3.14 L. G. Jacchia, "Variations in the Earth's Upper Atmosphere as Revealed by Satellite Drag," Smithsonian Astrophysical Observatory (December, 1962).

3.15 Private communication from L. Jacchia and B. Miller, Smithsonian Astrophysical Observatory.

3.16 Private communication from L. Jacchia, Smithsonian Astrophysical Observatory.

3.17 K. Ehricke, Space Flight, Vol. I, "Environment and Celestial Mechanics," (D. Van Nostrand Co., Inc., N. J., 1960).

3.18 L. G. Jacchia and J. Slowey, "Atmospheric Heating in the Auroral Zones," Special Report No. 136, Smithsonian Astrophysical Observatory (17 September 1963).

3.19 Private communication from L. Martin, M. I. T. Lincoln Laboratory.

3.20 C. Stormer, The Polar Aurora, (Oxford Press, London, England, 1955).

3.21 J. Chamberlain, Physics of Aurora and Airglow (Academic Press, New York, 1961).

CHAPTER IV

Distributions of Orbiting Particles

4.1 Introduction

The project West Ford dipoles, placed in orbit in May, 1963, [4.1] provide a unique opportunity to study a large ensemble of particles in nearly identical orbits. In particular, one can study the distribution of particles caused by the dipole dispensing process.

The techniques developed here for this study can easily be applied to other applications (e.g., other dispensing techniques, explosions of orbiting vehicles, etc.).

4.2 The West Ford Dipole Dispenser

The West Ford dipoles were packaged in five* cylindrical dispensers. [4.2] They were aligned with the common axis of these cylinders and bound together with naphthalene. As these cylinders were ejected from the parent vehicle, they were set spinning (at ~ 480 rpm) about their cylindrical axes.** The spin axis was very nearly in the plane of the orbit. [4.2] Dipoles were then gradually released from the surfaces of these spinning cylinders as the naphthalene sublimed. According to laboratory experiments, [4.3] about a day was required to dispense all of the dipoles.

The distribution of velocity increments imparted to the dipoles by the dispensers can be closely approximated by assuming that (1) the number of dipoles released at any dispenser radius is proportional to the surface area of the cylindrical shell at that radius; (2) each dipole is released tangentially with the circumferential speed of its shell; and (3) the directions of release in the plane perpendicular to the angular velocity vector of the dispenser are uniformly distributed. The dispensers are further approximated by neglecting the relatively small hollow core, i.e., by assuming the final dispensing radius to be zero.

---

*One was only half size and was attached to a telemetry system (see Ref. 4.2).

**Because of the possibility of spin axis conversion, the individual dispensers are separated[4.2] to prevent possible conversion to a tumbling motion but their spin axes remain parallel.

The probability density function (p_V) of the dispensing speed increment (i.e., the speed of dipole release relative to the dispenser) is proportional to the number of dipoles released with speed V. Let m equal the number of dipoles in a cylindrical shell of radius r_d and let ω_s equal the angular velocity of the dispenser. Clearly,

$$m \propto V$$

Thus, since $p_V \propto m$;

$$p_V \propto V$$

Normalizing p_V gives (see Fig. 4.1):

$$p_V = \begin{cases} 0 & V < 0 \\ \dfrac{2V}{V_{max}^2} & 0 \leq V \leq V_{max} \\ 0 & V_{max} < V \end{cases} \qquad (4.1)$$

where V_{max} is the maximum dispensing speed increment (the circumferential speed of the outermost shell).

Let Θ be the angle between the orbit plane of the dispenser and the direction of release. Theta has been approximated as a random variable with a uniform probability density (see above). It is also assumed to be statistically independent of V. A useful form of the density function of theta (p_Θ) is (see Fig. 4.1):

$$p_\Theta = \begin{cases} 0 & \Theta < -\pi \\ \dfrac{1}{2\pi} & -\pi \leq \Theta \leq \pi \\ 0 & \pi < \Theta \end{cases} \qquad (4.2)$$

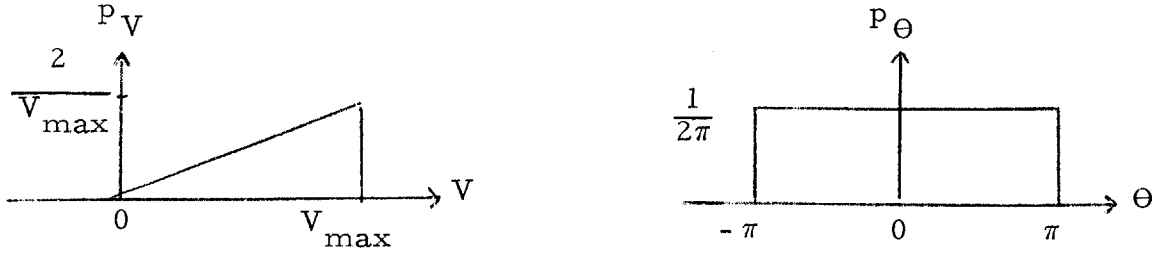

Fig. 4.1
Probability Density Functions of the Speed
and Direction of Dispensed Dipoles

The distribution of the component of the velocity increment that lies in the plane of the dispenser orbit and of the component that is perpendicular to this plane can be derived from Eqs. (4.1) and (4.2). The component of V which lies in the orbit plane (μ) is:

$$\mu = V \cdot \cos \Theta \tag{4.3}$$

Let:

$$\alpha = \cos \Theta \tag{4.4}$$

Then:

$$p_\alpha = \frac{1}{\pi} \quad \frac{1}{\sqrt{1-\alpha^2}} \quad \text{for } -1 \leq \alpha \leq 1 \tag{4.5}$$

And:

$$\mu = V \cdot \alpha \tag{4.6}$$

The probability density function of $\mu(p_\mu)$ is:

$$p_\mu = \int_{-\infty}^{\infty} \frac{1}{|\alpha|} \; p_V \left(\frac{\mu}{\alpha}\right) p_\alpha \, d\alpha \; *$$

---

*This relation is simply derived from the principles of conditional probability

$$p_\mu = \int_{-\infty}^{\infty} p_{\mu,\alpha} \, d\alpha = \int_{-\infty}^{\infty} p_{\mu/\alpha} \cdot p_\alpha \, d\alpha$$

where $p_{\mu/\alpha} = \frac{1}{|\alpha|} \; p_V \left(\frac{\mu}{\alpha}\right)$

Thus:

$$p_\mu = \int_{-\infty}^{\infty} \frac{1}{|\alpha|} \; p_{V,\alpha} \left(\frac{\mu}{\alpha}, \alpha\right) d\alpha$$

Since V and α are statistically independent:

$$p_\mu = \int_{-\infty}^{\infty} \frac{1}{|\alpha|} \; p_V \left(\frac{\mu}{\alpha}\right) \cdot p_\alpha \, d\alpha$$

From Eqs. (4.1), (4.5), and (4.6):

$$p_\mu = \frac{2\mu}{\pi V_{max}^2} \int_{-\infty}^{\infty} \frac{1}{|\alpha|} \cdot \frac{1}{\alpha} \cdot \frac{d\alpha}{\sqrt{1-\alpha^2}}$$

$$\text{for: } 0 < \frac{\mu}{\alpha} \leq V_{max}$$

$$\text{and: } -1 \leq \alpha \leq +1 \qquad (4.7)$$

Integrating:

$$p_\mu = \begin{cases} 0 & \mu < -V_{max} \\ \frac{2}{\pi V_{max}} \sqrt{1-\left(\frac{\mu}{V_{max}}\right)^2} & -V_{max} \leq \mu \leq V_{max} \\ 0 & V_{max} < \mu \end{cases} \qquad (4.8)$$

The probability density function of velocity increments perpendicular to the orbit plane (p_η) can be derived from a similar analysis:

$$p_\eta = \begin{cases} 0 & \eta < -V_{max} \\ \frac{2}{\pi V_{max}} \sqrt{1-\left(\frac{\eta}{V_{max}}\right)^2} & -V_{max} \leq \eta \leq V_{max} \\ 0 & V_{max} < \eta \end{cases} \qquad (4.9)$$

4.3 Spatial Distributions

The spatial distribution of dipoles in the West Ford cloud caused by the dispensing process can be derived from the distribution of velocity increments (Eqs. (4.8) and (4.9)). The release of a dipole has an effect on its orbital motion like that of an impulsive perturbing acceleration. Since the maximum dispensing velocity increment is small compared with the orbital velocity ($V_{max} \approx 9.5$ ft/sec), the resulting perturbations will be small.

The analysis of the spatial distribution is simplified by making the valid approximation that the duration of dispensing (t_D) is long compared

with an orbital period P_o (actually $t_D \approx 9 \cdot P_o$). Further, we only consider epochs considerably after the completion of dispensing but before the cloud closes on itself to form a completed belt.* The duration of dispensing and the restriction on the epoch of interest allows the dipoles released during the second orbit period to be essentially indistinguishable from those released in the first period, and so on, so that the dispensing speed (V), which is dependent on the instantaneous radius of the dispenser, is essentially statistically independent of the time of dipole release. The time of dipole release can therefore be ignored. Two additional approximations are made to further simplify the analysis. One, the orbit of the dispenser is assumed to be circular (the actual eccentricity was about 0.004 [4.1]); two, during the time period of interest, the changes in the spatial distribution caused by differential perturbations other than those resulting from dispensing, are neglected.

Figure 4.2 depicts a coordinate system which is especially useful for the analysis of the spatial distributions and which closely simulates a "mode of operation" frequently used in radar observations of the West Ford ensemble. In this mode of operation, the radar scans a fixed plane perpendicular to the orbit as the cloud passes through this plane.** The plane labeled "Intersection Plane" (defined by the X, Z axes) depicts this scanned plane. This plane is inclined by ϕ degrees to the dispenser spin axis (which lies approximately in the plane of the dispenser orbit). The distributions represented in this coordinate system are distributions in the two dimensions of the intersection plane and a dimension along the dispenser orbit which is a measure of the time that a given section of the dipole ensemble passes through this plane.

4.4 Distribution along the Orbit

The coordinate σ (see Fig. 4.2) of a dipole is the distance along the dispenser (or reference) orbit from the empty dispenser (or a dipole released with zero velocity) to the dipole at the time the dipole crosses the intersection plane. Since the dispenser orbit is assumed to be circular,

*Our results can be applied to later times by proper folding of the appropriate distributions (i.e., by merging the leading and trailing extremes of the cloud).

**Since the actual orbit is near polar (inclination $\approx 87.4°$), the radar actually scans at a constant colatitude.

the orbital velocity of the dispenser (V_o) will be constant. The coordinate σ is therefore proportional to the time a dipole crosses the intersection plane measured from the time the dispenser crosses this plane. The spreading of dipoles along the orbit is mainly caused by the small differences intheir orbital periods.

Since the orbit of each dipole will be nearly circular, the separation between a dipole and the dispenser will be:

$$\sigma(t) \approx \left(\frac{2\pi r_o}{P} - \frac{2\pi r_o}{P_o}\right) \cdot t \qquad (4.10)$$

where P and P_o are the orbital periods of the dipole and dispenser, respectively, and r_o is the radius of the dispenser's orbit (see Fig. 4.3). Since:

$$\frac{P - P_o}{P_o} = \frac{\delta P}{P_o} << 1$$

the separation along the orbit is:

$$\sigma \approx -V_o \cdot \frac{\delta P}{P_o} \cdot t \qquad (4.11)$$

where V_o is the orbital velocity of the dispenser.

$$V_o = \sqrt{\frac{GM}{a_o}} \qquad (4.12)$$

Since:

$$P = \frac{2\pi}{\sqrt{GM}} a^{3/2}$$

then:

$$\frac{\delta P}{P_o} = \frac{3}{2} \frac{\delta a}{a_o} \qquad (4.13)$$

The equation for the perturbation of the semi-major axis (a) is[4.4] (see Chapter I):

$$\frac{da}{dt} = \frac{2a^2}{\sqrt{GMp}} \left[e \sin v \cdot \tilde{R} + (1 + e \cos v) \tilde{S} \right] \tag{4.14}$$

For nearly circular orbits:

$$\frac{da}{dt} \approx \frac{2a}{V_o} \tilde{S} \tag{4.15}$$

We approximate the sudden release of a dipole from the dispenser by

$$V_S = \tilde{S} \, \delta t$$

where V_S is the component of the dispensing velocity increment which lies along the direction $\vec{S}$ (see Fig. 4.3). Therefore:

$$\frac{\delta a}{a_o} = \frac{2V_S}{V_o} \tag{4.16}$$

and

$$\sigma = -3 \cdot V_S \cdot t \tag{4.17}$$

Since the spin axis of the dipole dispenser remains fixed in direction as the dispenser moves along its orbit, the component of the dispensing velocity along the reference orbit ($\vec{S}$ direction) is (see Fig. 4.3):

$$V_S = \mu \cdot \cos \gamma \tag{4.18}$$

and

$$\gamma = \Omega + \phi \tag{4.19}$$

The approximation that the velocity of release is statistically independent of the position of the dispenser along the orbit (i.e. time) implies that the angular position Ω (see Fig. 4.3) is a uniformly distributed random variable that is statistically independent of the velocity of release.

In addition, the angle ϕ is a constant for any particular location of the intersection plane. Therefore, γ is also a uniformly distributed random variable. Let:

$$p_\gamma = \begin{cases} 0 & \gamma < -\pi \\ \frac{1}{2\pi} & -\pi \leq \gamma \leq \pi \\ 0 & \pi < \gamma \end{cases} \tag{4.20}$$

Letting:

$$\beta = \cos \gamma \tag{4.21}$$

we find:

$$p_\beta = \frac{1}{\pi} \frac{1}{\sqrt{1-\beta^2}} \quad \text{for} \quad -1 \leq \beta \leq 1 \tag{4.22}$$

and from Eqs. (4.17) and (4.18)

$$\sigma = -3 \cdot V_S \cdot t = -3 \cdot \mu \cdot \beta \cdot t \tag{4.23}$$

where μ and β are statistically independent random variables.

The probability density function of σ is:

$$p_\sigma = \frac{1}{3t} \int_{-\infty}^{\infty} \frac{1}{|\mu|} p_\beta \left(\frac{\sigma/-3t}{\mu} \right) p_\mu(\mu)\, d\mu \tag{4.24}$$

Substituting Eqs. (4.8) and (4.22) into Eq. (4.24) gives:

$$p_\sigma = \frac{2}{\pi^2 3t V_{max}} \int_{-\infty}^{\infty} \frac{1}{|\mu|} \frac{\sqrt{1-(\mu/V_{max})^2}}{\sqrt{1-(\frac{-\sigma/3t}{\mu})^2}}\, d\mu$$

$$\text{for} \quad -1 \le \frac{-\sigma/3t}{\mu} \le +1 \quad \text{and} \quad -V_{max} \le \mu \le +V_{max} \tag{4.25}$$

Let $\sigma_m = 3tV_{max}$, then for $\sigma > 0$:

$$p_\sigma = \frac{2}{\pi^2 \sigma_m} \left[\int_{\frac{\sigma}{\sigma_m}V_{max}}^{V_{max}} \frac{1}{\mu} \frac{\sqrt{1-(\frac{\mu}{V_{max}})^2}}{\sqrt{1-(\frac{\sigma}{\sigma_m}\cdot\frac{V_{max}}{\mu})^2}}\, d\mu \right.$$

$$\left. - \int_{-V_{max}}^{-\frac{\sigma}{\sigma_m}\cdot V_{max}} \frac{1}{\mu} \frac{\sqrt{1-(\frac{\mu}{V_{max}})^2}}{\sqrt{1-(\frac{\sigma}{\sigma_m}\cdot\frac{V_{max}}{\mu})^2}}\, d\mu \right] \tag{4.26}$$

and by symmetry

$$p_\sigma(+\sigma) = p_\sigma(-\sigma)$$

Let:

$$\xi = \frac{\mu/V_{max}}{\sigma/\sigma_m}$$

and

$$k = \frac{\sigma}{\sigma_m} \tag{4.27}$$

Then:

$$p_\sigma = \frac{4}{\pi^2 \sigma_m} \int_1^{1/k} \frac{\sqrt{1-k^2\xi^2}}{\sqrt{\xi^2-1}}\, d\xi \qquad (4.28)$$

Integrating:[4.5]

$$p_\sigma = \frac{4}{\pi^2 \sigma_m} \left[K(\sqrt{1-k^2}) - E(\sqrt{1-k^2}) \right] \qquad (4.29)$$

where K and E are complete elliptic integrals of the first and second kinds, respectively.

Since the density of dipoles ($n(\sigma)$) along the orbit* is proportional to p_σ, we have: **

$$n(\sigma) = \frac{4N}{\pi^2 \sigma_m} \left[K(\sqrt{1-(\frac{\sigma}{\sigma_m})^2}) - E(\sqrt{1-(\frac{\sigma}{\sigma_m})^2}) \right] \qquad (4.30)$$

where N is the total number of dipoles released.

The theoretical distribution of dipoles along the orbit is compared in Fig. 4.5 with experimental data *** from a radar observation of the West Ford dipole cloud. A comparison of the absolute values of the ordinates of theory and experiment is not meaningful, but a comparison of the shapes is. The experimental points are proportional to a five second average of the radar cross section of dipoles that are in the radar beam,[4.7] which happens to be smaller than the transverse dimensions of the belt. The measurements were made on 20 May 1963 or about nine days after release.

---

*For a dispenser spin axis perpendicular to the orbit plane, the density of dipoles along the orbit follows from Eqs. (4.8) and (4.17) when one considers Θ to be the angle between the dispensing velocity and the $\vec{S}$ direction (see Fig. (4.3)). The result is:

$$n_\perp(\sigma) = \frac{2N}{\pi \sigma_m} \sqrt{1-(\frac{\sigma}{\sigma_m})^2}$$

**This confirms the earlier work of Jones and Shapiro.[4.6]

***These data were kindly supplied by F. Nagy of M.I.T. Lincoln Laboratory.

The standard deviation depicted in Fig. 4.5 for these measurements are approximately 10% of the measured cross section. The base line of these measurements contains an additional uncertainty.

4.5 Distribution Out of Plane

The coordinate τ in Figs. 4.2 and 4.4 is the perpendicular distance from the orbit plane of the dispenser to a dipole lying in the intersection plane. The angle ψ (see Fig. 4.4) is the earth-centered angle in the intersection plane between the dispenser orbit and a dipole orbit. Since the perturbations caused by dispensing are small, ψ is small and:

$$\tau = r \sin \psi \approx r_o \cdot \psi \tag{4.31}$$

Using the spherical triangle formed by the radial projection onto a unit sphere of the origin of the Intersection Plane, the dipole intersection point and the dipole release point (see Fig. 4.2), we find that

$$\psi \approx -i \cdot \sin \Omega \tag{4.32}$$

The inclination (i) of the dipole orbit to the dispenser orbit is simply:

$$i \approx \frac{V_W}{V_o} \tag{4.33}$$

which is apparent from the vector diagram:

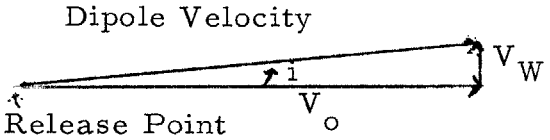

But $V_W = \eta$ (see Eq. (4.9)) since the spin axis of the dispenser lies in the orbit plane. Also, V_W is independent of ϕ. Therefore:

$$\tau = - r_o \frac{\eta}{V_o} \sin \Omega \tag{4.34}$$

Let:

$$\delta = \sin \Omega \tag{4.35}$$

then:

$$\tau = -\frac{r_o}{V_o}\,\eta \cdot \delta$$

Since Ω is a uniformly distributed random variable

$$p_\delta = \frac{1}{\pi}\,\frac{1}{\sqrt{1-\delta^2}} \qquad \text{for} \quad -1 \le \delta \le 1$$

$$= 0 \qquad \text{elsewhere} \tag{4.36}$$

Whereas the density of dipoles as a function of τ and σ could be found, it is of interest (for comparison with the data available) to find the "total" out of plane distribution of dipoles as the complete cloud passes through the intersection plane, i.e., the distribution of intersection points of the orbits of the dipoles with the intersection plane.

The total probability density function of τ is:

$$p_\tau = \frac{V_o}{r_o}\int_{-\infty}^{\infty} \frac{1}{|\eta|}\, p_\delta\left(\frac{\tau/(-r_o/V_o)}{\eta}\right) p_\eta(\eta)\, d\eta$$

$$\text{for} \quad -1 \le \frac{\tau/(-r_o/V_o)}{\eta} \le 1$$

$$\text{and} \quad -V_{max} \le \eta \le +V_{max} \tag{4.37}$$

From the similarity between Eqs. (4.37) and (4.24), Eqs. (4.9) and (4.8), and Eqs. (4.36) and (4.22), the number of dipoles ($n(\tau)$) per unit length of τ is directly:

$$n(\tau) = \frac{4N}{\pi^2 \tau_m}\left[K\left(\sqrt{1-(\tau/\tau_m)^2}\right) - E\left(\sqrt{1-(\tau/\tau_m)^2}\right)\right] \tag{4.38}$$

where τ_m is defined as

$$\tau_m = r_o\,\frac{V_{max}}{V_o}$$

$$= \frac{P_o}{2\pi}\,V_{max} \tag{4.39}$$

The density of the intersection points of the orbits of the dipoles is independent of time.

Figure 4.6 presents a comparison of the theoretical out of plane distribution with an experimental observation. The theoretical curves are similar to those in Fig. 4.5. The experimental data (taken from Fig. 1 of Ref. 4.8) is the result of a photometric density reduction of a Baker-Nunn photograph. The abscissa scale of the experimental data in Fig. 4.6 assumes that the photograph was taken when the West Ford cloud was at near minimum range (near zenith)* and that the angular units in Fig. 1 of Ref. 4.8 are measured from the camera (i.e., 1' of arc $\approx$ 1.0 km in the cloud and corresponds to $\tau/\tau_m = .22$). The ordinate of the experimental data is some measure of relative photographic density ΔD (see Ref. 4.8). The base line is the average local night sky brightness. (The maximum measured optical brightness of the West Ford cloud was less than 10% of the night sky.)[4.8] As in Fig. 4.5, only the relative shapes of the experimental and theoretical curves can be compared.

4.6 Distribution in the Orbit Plane

The coordinate ρ in Fig. 4.2 is the radial distance to a dipole in the intersection plane relative to the reference orbit. Let r equal the earth-centered radius of a dipole's orbit at the intersection plane, then:

$$\rho = r \cos \psi - r_o \tag{4.40}$$

Since ψ is small:

$$\rho \approx r - r_o \tag{4.41}$$

From Fig. 4.3, the radius r is:**

$$r = \frac{p}{1 + e \cos (\omega + \Omega)} \tag{4.42}$$

*The photograph is actually a composite of several photographs and is blurred by transverse motion of the cloud relative to the camera.[4.6] In addition, the observations were made at approximately 35° from the zenith which means that the experimental distribution is not truly out-of-plane. The shape of the distribution for this viewing angle will not differ much from the true out-of-plane distribution however.

**One must consider ω to be the argument of perigee measured from the release point.

Let:

$$W = \Omega + \omega$$

and let:

$$b = e \cos W$$

Then:

$$r = \frac{p}{1 + b} \tag{4.43}$$

but:

$$b << 1$$
$$b_o = 0$$

and

$$p_o = r_o$$

Therefore:

$$r \approx (r_o + \delta p)(1 + \delta b) \tag{4.44}$$

and:

$$\rho = \delta p - r_o \delta b \tag{4.45}$$

Where δp and δb are the changes in the orbit parameters p and b caused by dispensing. The perturbation equation of p gives (see Eq. (4.16))

$$\delta p = \frac{2r_o}{V_o} V_S \tag{4.46}$$

The perturbation equation of b gives:[4.9]

$$\delta b = \frac{2}{V_o} \cos (W + v) V_S + \frac{1}{V_o} \sin (W + v) V_R \tag{4.47}$$

The angle $W + v$ is the location along the dispenser orbit (from the X axis) where the dipole is released and V_R is the radial component of the dispensing velocity. Therefore (see Fig. 4.2):

$$W + v = \Omega$$

Equation (4.47) becomes:

$$\delta b = \frac{2}{V_o} \cos \Omega V_S + \frac{1}{V_o} \sin \Omega V_R \tag{4.48}$$

where the velocity increments V_S and V_R are (see Eq. (4.18)):

$$V_S = \mu \cos (\Omega + \phi)$$
$$V_R = \mu \sin (\Omega + \phi) \tag{4.49}$$

Substituting Eqs. (4.46), (4.48), and (4.49) into Eq. (4.45) gives:

$$\rho = - \frac{r_o}{V_o} \mu \left[(1 - \cos \Omega)^2 \cos \phi + (2 - \cos \Omega) \sin \Omega \sin \phi \right] \tag{4.50}$$

It is of particular interest here to find the distribution of dipoles as a function of both ρ and position along the orbit σ (i.e., the joint probability density function $p_{\rho, \sigma}$). From Eq. (4.23):

$$\sigma = - \sigma_m \cdot \frac{\mu}{V_{max}} \cdot \cos (\Omega + \phi) \tag{4.51}$$

To nondimensionalize and simplify Eqs. (4.50) and (4.51), let:

$$\rho_m = \frac{4 r_o V_{max}}{V_o} \tag{4.52}$$

and let:

$$u = \frac{\mu}{V_{max}} \tag{4.53}$$

$$y = \frac{\rho}{\rho_m} \tag{4.54}$$

and

$$x = \frac{\sigma}{\sigma_m} \tag{4.55}$$

Then:

$$x = - u \cos (\Omega + \phi) \tag{4.56}$$

and

$$y = -\tfrac{1}{4} u \left[(1 - \cos\Omega)^2 \cos\phi + (2 - \cos\Omega) \sin\Omega \sin\phi \right] \tag{4.57}$$

where

$$p_u = \frac{2}{\pi} \sqrt{1 - u^2} \qquad \text{for} \quad -1 \le u \le 1$$

$$p_u = 0 \qquad \text{elsewhere} \tag{4.58}$$

The random variables u and Ω are statistically independent, therefore:

$$p_{u,\Omega} = p_u \cdot p_\Omega$$

The general derivation of $p_{\rho,\sigma}$ or $p_{x,y}$ involves a mapping from the u, Ω space to the x, y space. The mathematical details are, however, quite complicated. Two special cases ($\phi = 0°$ and $\phi = 90°$) of this mapping demonstrate the general nature of the West Ford cloud.

For $\phi = 0°$, let:

$$\lambda = \cos\Omega$$

Then:

$$y = -\tfrac{1}{4} u (1 - \lambda)^2$$

$$x = -u\lambda \tag{4.59}$$

and

$$p_\lambda = \frac{1}{\pi} \frac{1}{\sqrt{1 - \lambda^2}} \qquad \text{for} \quad -1 \le \lambda \le 1 \tag{4.60}$$

Inverting Eqs. (4.59) gives

$$u = -(2y + x) \pm \sqrt{(2y + x)^2 - x^2}$$

$$\lambda = \frac{-x}{-(2y + x) \pm \sqrt{(2y + x)^2 - x^2}} \tag{4.61}$$

The upper sign holds for $y < 0$ and the lower for $y > 0$.

The region in the u, λ space bounded by $-1 \leq u \leq 1$ and $-1 \leq \lambda \leq 1$ maps one-to-one onto the regions in the x, y space shown in Fig. 4.7. These regions are bounded by:

$$\begin{aligned} y &= -x && [\lambda = -1] \\ y &= 0 && [\lambda = +1] \\ y &= -\tfrac{1}{4}(1+x)^2 && [u = +1] \\ y &= +\tfrac{1}{4}(1-x)^2 && [u = -1] \end{aligned} \tag{4.62}$$

The joint density function $p_{x,y}$ is simply:

$$p_{x,y} = p_{u,\lambda} \cdot \left| \frac{\partial(u,\lambda)}{\partial(x,y)} \right| \tag{4.63}$$

where u and λ are given as functions of x and y in Eq. (4.61) and where the Jacobian reduces to:

$$\frac{\partial(u,\lambda)}{\partial(x,y)} = \frac{1}{u}\frac{\partial u}{\partial y} \tag{4.64}$$

The Jacobian further reduces to

$$\frac{\partial(u,\lambda)}{\partial(x,y)} = \mp \frac{2}{\sqrt{(2y+x)^2 - x^2}} \tag{4.65}$$

Substituting Eqs. (4.58), (4.60), (4.61), and (4.65) into Eq. (4.63) gives for the joint probability density function of x and y:

$$p_{x,y} = \frac{8}{\pi^2} \frac{\sqrt{\frac{1}{u^2} - 1}}{\left(1 - \left(\frac{x}{u}\right)^2\right)^{3/2}} \tag{4.66}$$

where, from Eq. (4.61):

$$u = -(2y + x) - 2\sqrt{y(y+x)} \qquad \text{for} \quad y > 0 \tag{4.67}$$

$$u = -(2y + x) + 2\sqrt{y(y+x)} \qquad \text{for} \quad y < 0 \tag{4.68}$$

The number density of dipoles is simply:

$$n(x, y) = \frac{8N}{\pi^2} \frac{\sqrt{\frac{1}{u^2} - 1}}{(1 - (\frac{x}{u})^2)^{3/2}} \tag{4.69}$$

This distribution is singular along the straight line boundaries of the region and zero along the hyperbola boundaries (see Eq. (4.62)). In addition, the equidensity lines for $p_{x, y} = 1$ and $p_{x, y} = 2$ are plotted in Fig. 4.7 as dashed lines.

For the special case of $\phi = 90°$, Eqs. (4.56) and (4.57) become

$$\begin{aligned} x &= u \sin \Omega \\ y &= -\tfrac{1}{4} u [(2 - \cos \Omega) \sin \Omega] \end{aligned} \tag{4.70}$$

Inverting Eqs. (4.70) gives:

$$\begin{aligned} u &= \frac{\pm x^2}{\sqrt{x^2 - (2x + 4y)^2}} \\ \Omega &= \sin^{-1} \frac{x}{u} \end{aligned} \tag{4.71}$$

where:

$$0 < |\Omega| < \pi/2 \qquad \text{for} \qquad |y| > |\tfrac{1}{2}x|$$

and where:

$$\pi/2 < |\Omega| < \pi \qquad \text{for} \qquad |y| < |\tfrac{1}{2}x|$$

The plus and minus signs result from a double mapping from the u,Ω space onto the x, y space (i.e., the regions $(u > 0, \Omega > 0)$ and $(u < 0, \Omega < 0)$ both map onto the region $(x < 0, y < 0)$ etc.). However, if u is restricted to positive values, the probability density function $p_{x, y}$ is:

$$p_{x, y} = 2 \cdot p_{u, \Omega} \left| \frac{\partial(u,\Omega)}{\partial(x, y)} \right| \tag{4.72}$$

because of the symmetries involved.

The populated region in the x, y space (see Fig. 4.8) is bounded by the curve (in parametric form):

$$y = -\tfrac{1}{4}(2 - \cos\Omega)\,\sin\Omega$$

$$x = \sin\Omega \tag{4.73}$$

for

$$-\pi \leq \Omega \leq \pi$$

The maximum value of $|y|$ is 0.55 and occurs at $\sin\Omega = \pm\,(\frac{3}{4})^{\frac{1}{4}}$ (i.e., $x = \pm\,0.93$).

The probability density function for the case $\phi = 90°$ reduces to:

$$p_{x,\,y} = \frac{8}{\pi^2}\,\frac{u^2}{|x^3|}\,\sqrt{1-u^2} \tag{4.74}$$

where

$$u = \frac{x^2}{\sqrt{x^2 - (2x + 4y)^2}}$$

The number density of dipoles is simply

$$n(x, y) = \frac{8N}{\pi^2}\,\frac{u^2}{|x^3|}\,\sqrt{1-u^2} \tag{4.75}$$

Contours of equal probability density are plotted in Fig. 4.8. The density at the boundary (Eq. (4.73)) is zero and the density at the origin is singular. The equidensity contours fall into two classes. For $p_{x,\,y} \leq 0.576$ the sign of the curvature of the contour is constant and for $p_{x,\,y} > 0.576$ the contours have reversals in curvature (see Fig. 4.8).

In general, as the dipole cloud moves around its orbit, a double set of "jaws" open and close. The jaws are open at $\phi = 0°$, $180°$ and closed at $\phi = 90°$, $270°$. In the transition from $\phi = 0°$ to $\phi = 180°$, the dipoles which were in the $y > 0$ region for $\phi = 0°$, all migrate* to the $y < 0$ region for $\phi = 180°$ and vice versa.

*For a description of the motion of a single dipole, see Ref. 4.10.

4.7 Monte Carlo Numerical Procedure

The General Perturbation Program (see Appendix II) was used as the basis for a Monte Carlo procedure for estimating numerically the spacial distribution of the West Ford dipoles. This procedure requires fewer restrictions than the analytical analysis. In particular, both the dispersion of dipoles over long periods of time, caused by differential perturbations and the effect of the dispensing process can be studied in detail. This procedure is limited however to a relatively small statistical sample (present maximum is 500 dipoles) by the computation time required and the capacity of the computer memory.

The orbital elements of a dipole are computed by the GPP over a period of time (see Chapters II and III) and this time history is stored on magnetic tape. Each of the statistically distributed quantities involved in the perturbations of the orbit of a dipole is generated by using a pseudo-random number subroutine available in the Fortran library. This procedure is repeated for each new dipole until the desired sample size is attained.

The West Ford dipole dispenser is specified for the GPP by (1) its angular velocity vector relative to its center of mass, (2) the time that dispensing starts, (3) the duration of dispensing, (4) the initial dispenser radius, and (5) the final dispenser radius. The orbit of the dispenser is also specified. The radius of the dispenser is assumed to decrease linearly with time and the dispensing rate is assumed proportional to the radius (as described above). The resulting probability density for time of release is therefore similar to Eq. (4.1). In addition to the pure tangential dipole release described above, provision is made to allow the velocity of dipole release an additional increment in magnitude and a component along the dispenser spin axis (both are uniformly distributed random variables within a given percentage of V). This is an attempt to simulate the "hinge-like" release of a long, thin dipole when one end separates before the other (a phenomenon observed in vacuum chamber experiments).

An important contribution to the long-term dispersion of the dipole belt is the differential radiation pressure perturbations caused by the different orientation of each tumbling cylindrical dipole relative to the earth-sun line. The angular velocity vector of a dipole about its center of mass is therefore an important quantity. The angular velocity of tumbling

of a dipole at release is taken to be the angular velocity of the dispenser plus an additional vector increment with random components, each uniformly distributed within a chosen percentage of ω_s. Because of the dependence of dispersion on the tumbling axes of the dipoles, changes of these axes by meteoroid collisions become important.[4.11] To simulate meteor collision effects in the GPP (see Appendix II) use is made of the random number generator.

The magnetic tape containing the orbit histories of the sample dipoles is used as input to a second computer program called the Data Reduction Program (DRP) which computes the spatial relationships between the dipoles at some given epoch of interest.

The simplified dispensing process used in the analytic analysis was simulated with the Monte Carlo procedure by deleting all orbit perturbations other than those caused by dispensing. A sample of 500 dipoles was used and all parameters were approximately those of the West Ford experiment.

The histograms in Figs. 4.5 and 4.6 were constructed by computing σ and τ for each dipole at a particular epoch and counting the number of dipoles in each quantization cell. The histograms are plotted to the same scale as the analytic theory by dividing the number of dipoles in each cell by

$$\frac{4N}{\pi^2}\frac{\ell}{\sigma_m} \quad \text{and} \quad \frac{4N}{\pi^2}\frac{\ell}{\tau_m}$$

for Figs. 4.5 and 4.6, respectively. In particular $\frac{\ell}{\sigma_m} = \frac{1}{20}$, and $\frac{\ell}{\tau_m} = \frac{1}{5}$ are the lengths of the quantization cells relative to that of the maximum in-plane (along the orbit) and maximum out-of-plane extension of the dipole cloud, respectively and N = 500.

Figures 4.9 and 4.11 are diagrams of the population of dipoles in the orbit plane for $\phi = 0°$ and $\phi = 90°$, respectively. The photographs were generated by the DRP on a cathode ray tube display device. A comparison between the numerical and analytical figures shows that the Monte Carlo procedure can demonstrate the analytic results, which lends credibility to the extension of the Monte Carlo procedure to include additional perturbations. Figures 4.10 and 4.12 are population diagrams in

the intersection planes at $\phi = 0$ and $\phi = 90°$, respectively. The scales of Figs. 4.9 through 4.12 are in earth radii except for σ which is in degrees of arc along the orbit.

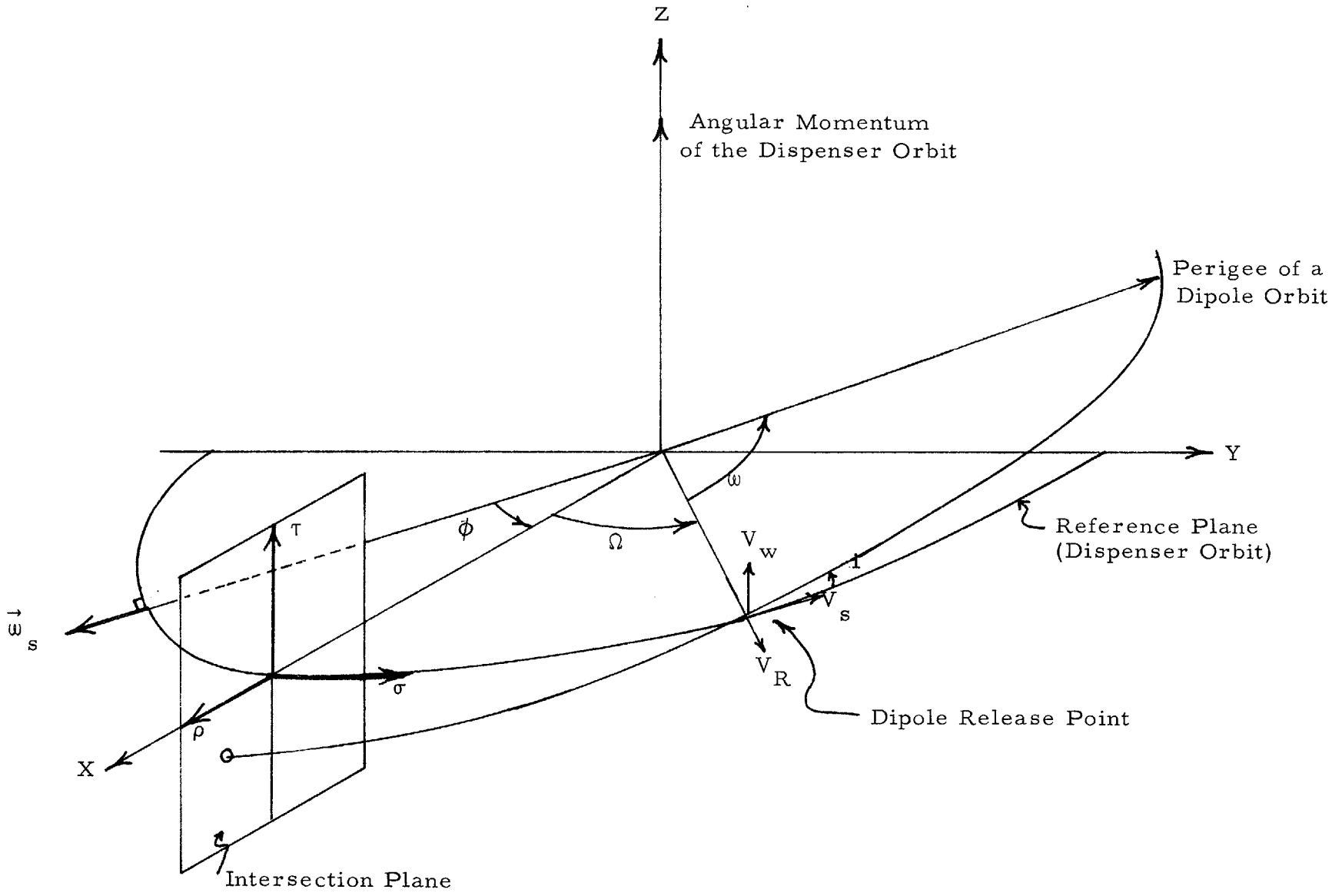

Fig. 4.2

Geocentric Coordinate System for Dipole Dispenser

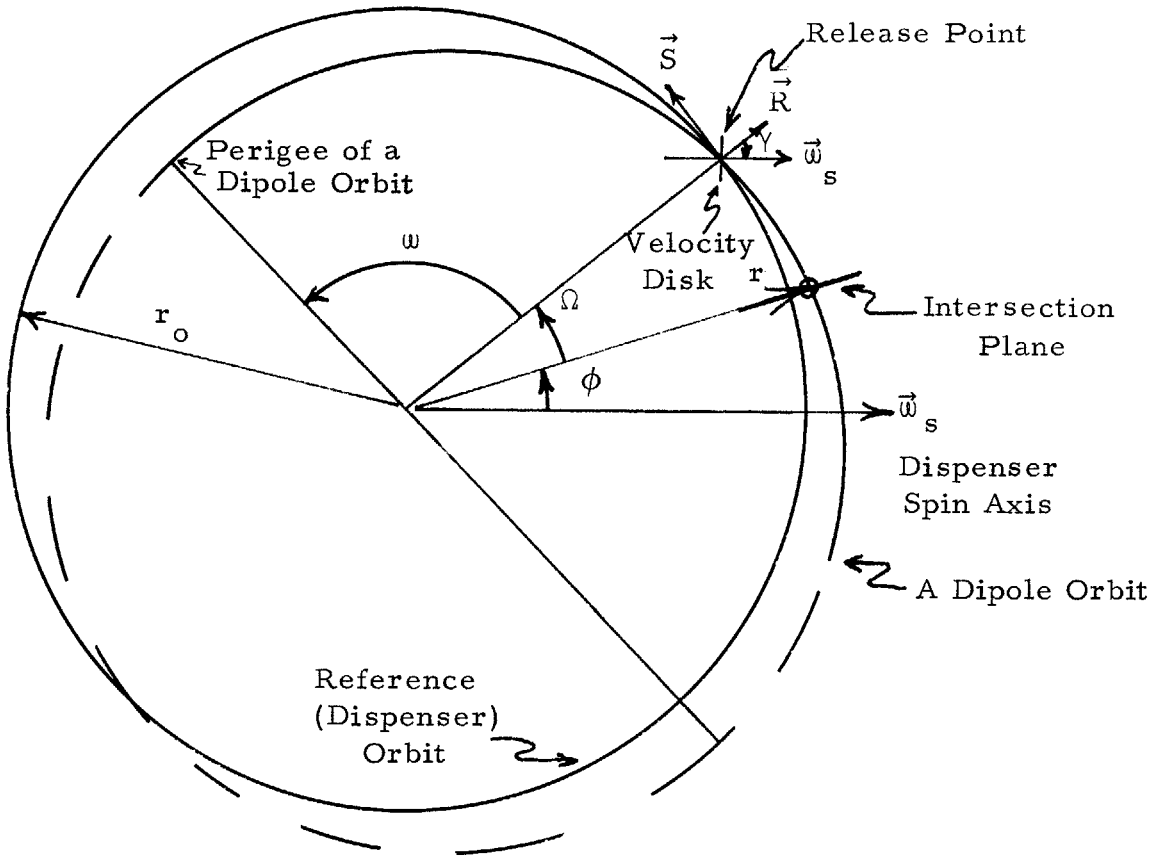

Fig. 4.3

Orbit Plane of the Dispenser

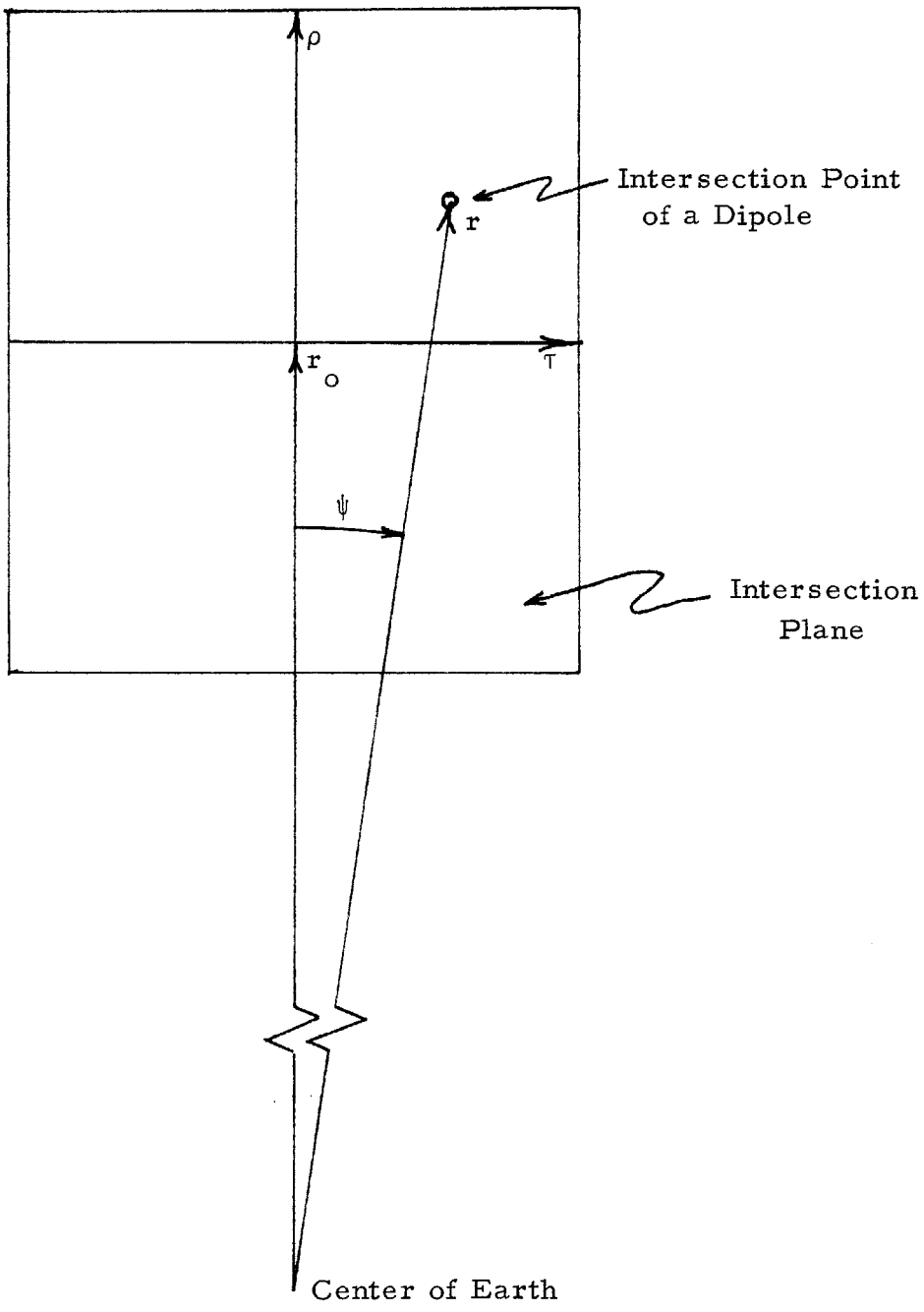

Fig. 4.4

Intersection Plane

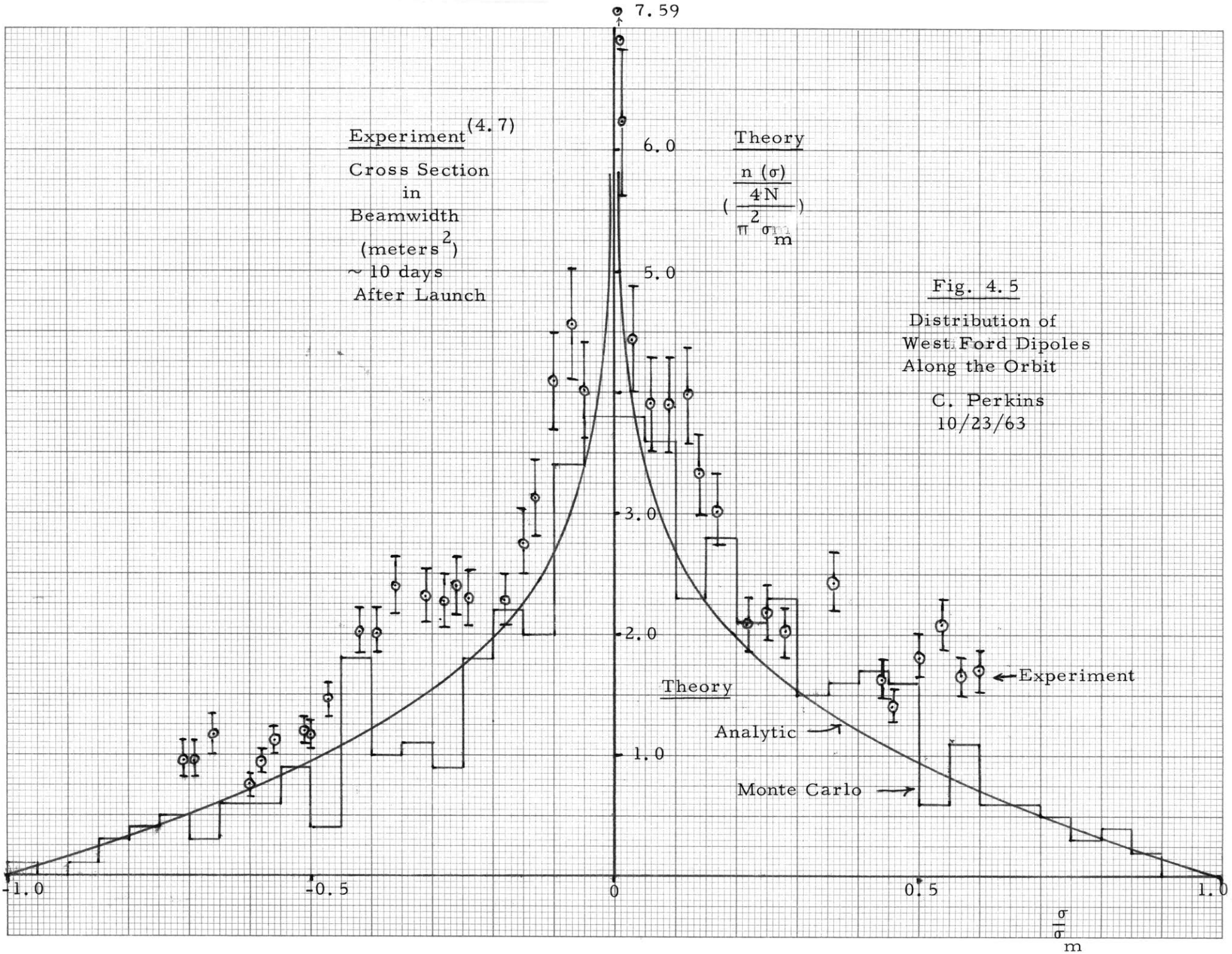

Fig. 4.5

Distribution of
West Ford Dipoles
Along the Orbit

C. Perkins
10/23/63

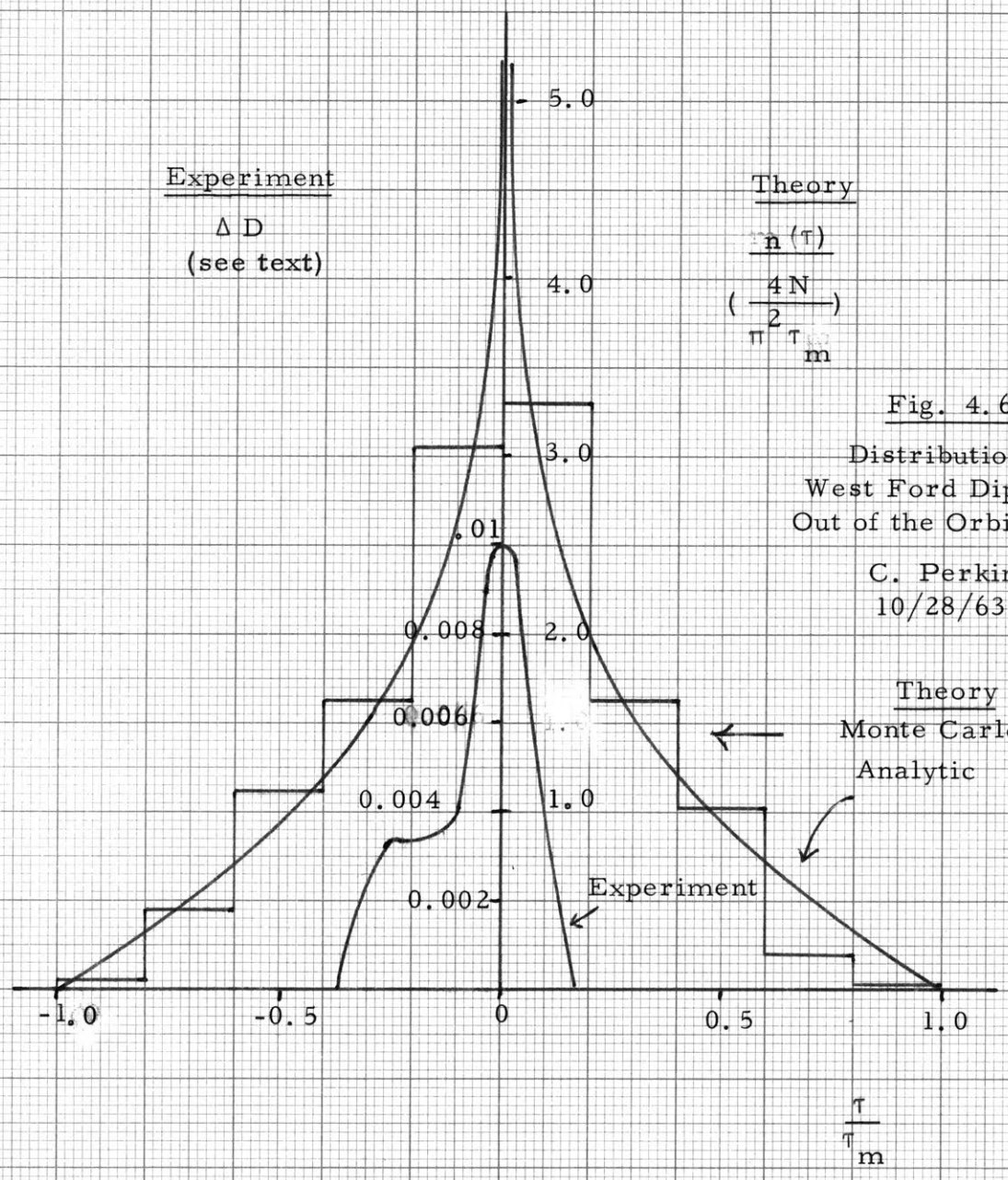

Fig. 4.6

Distribution of
West Ford Dipoles
Out of the Orbit Plane

C. Perkins
10/28/63

Fig. 4.6

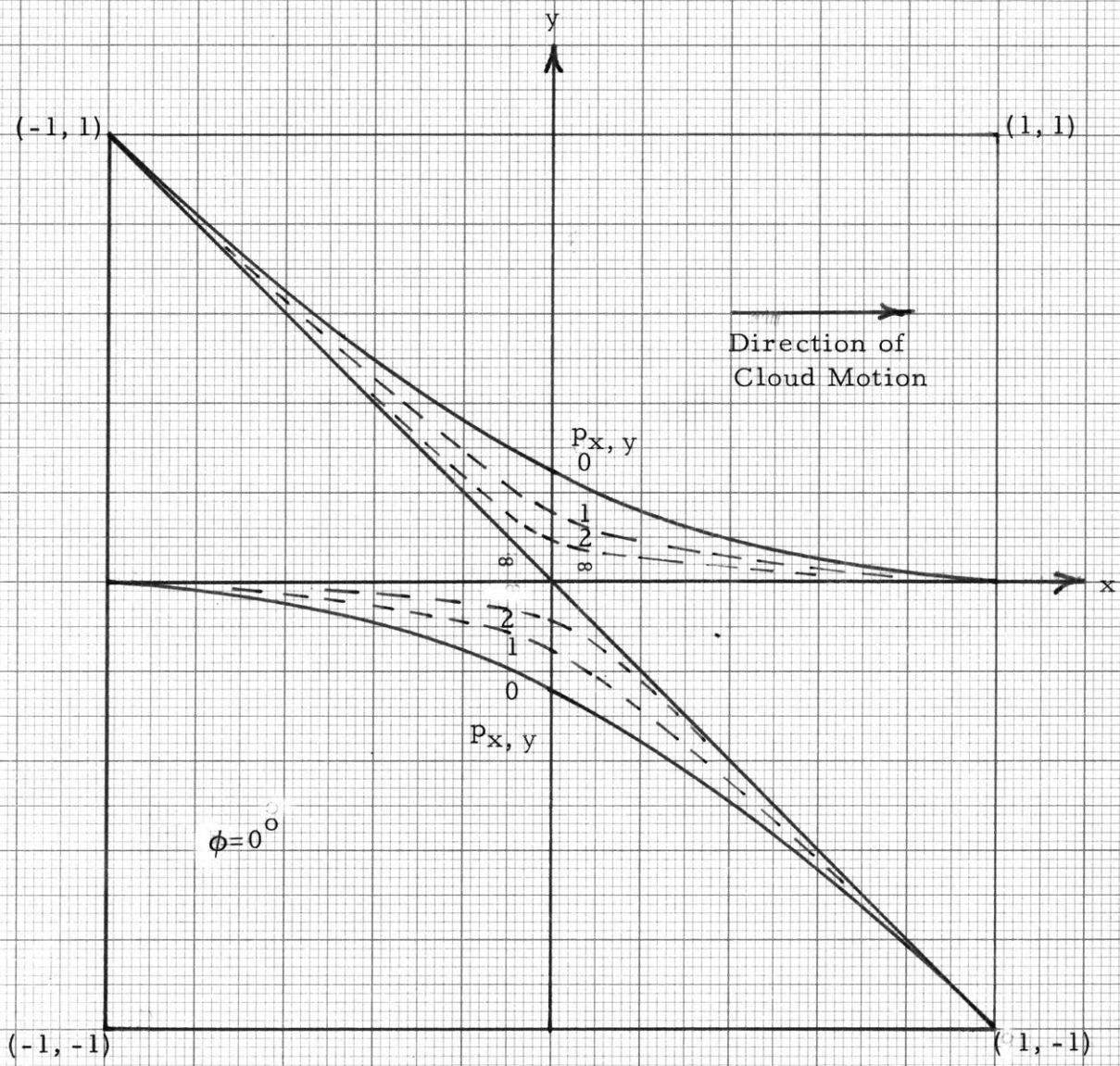

Fig. 4.7

Population Region
of
West Ford Dipoles
in the Orbit Plane

C. Perkins
10/29/63

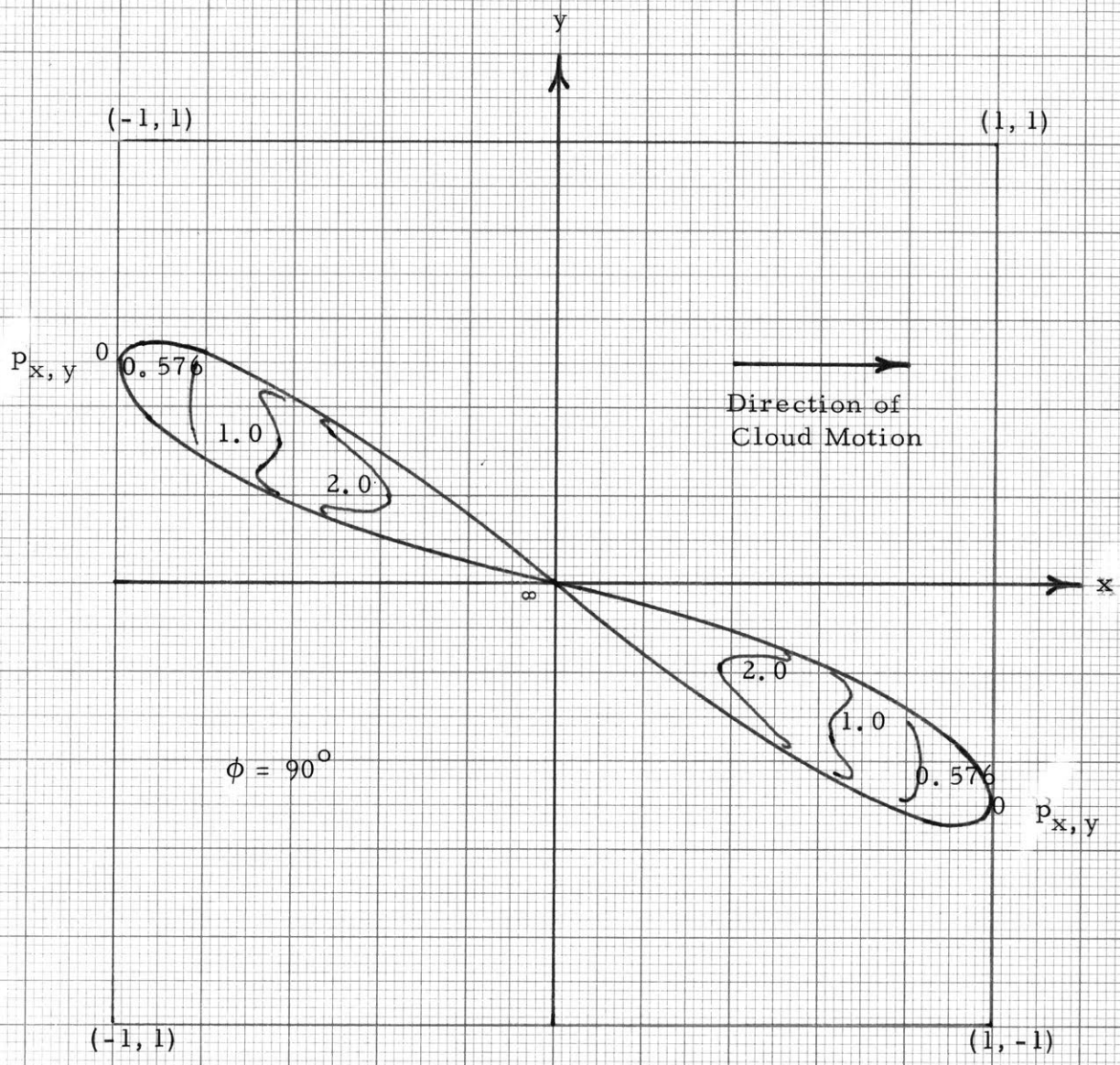

Fig. 4.8

Population Region
of
West Ford Dipoles
in the
Orbit Plane

C. Perkins
10/30/63

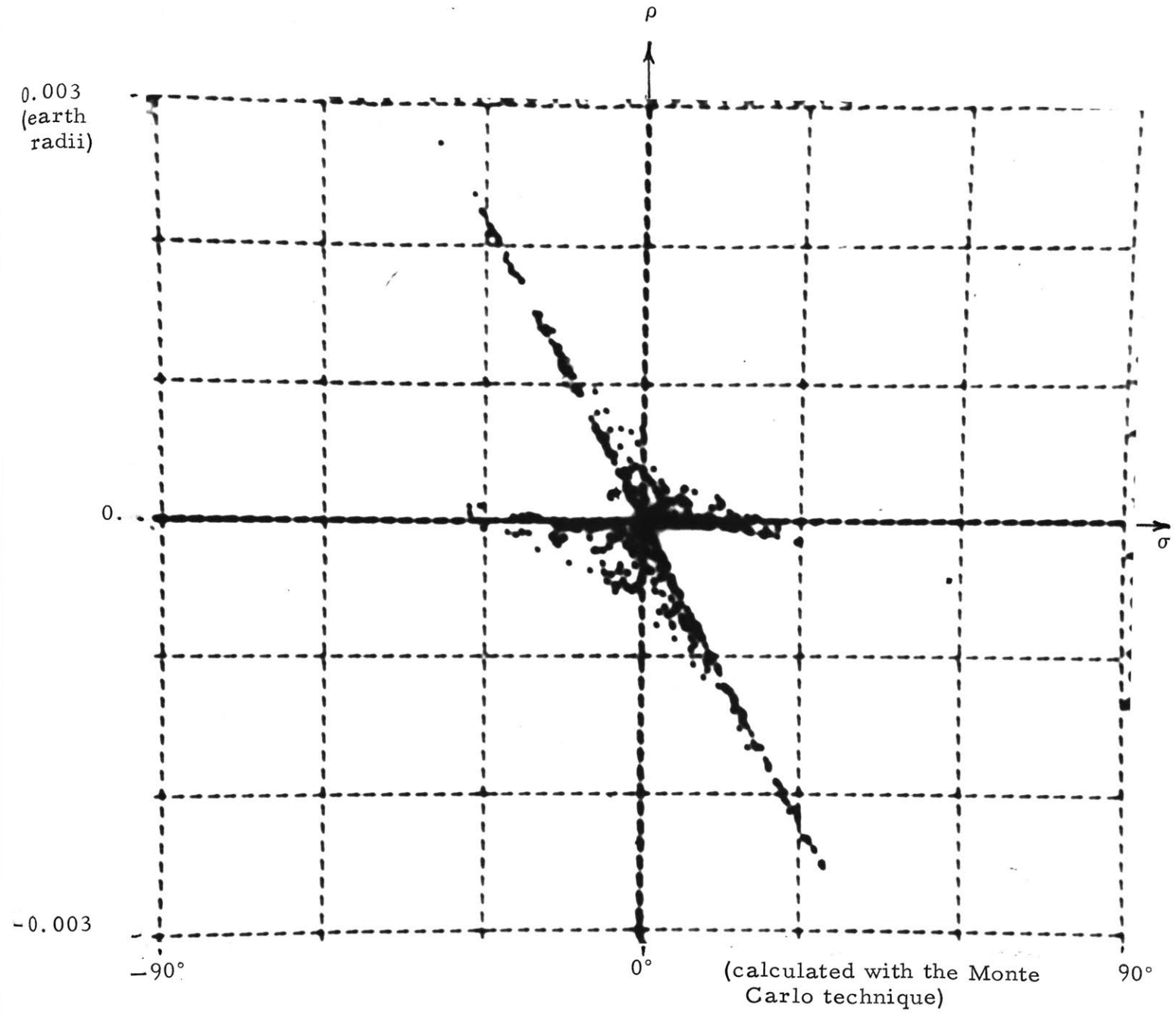

Fig. 4.9

Population Diagram

of

West Ford Dipoles
in the

Orbit Plane

N = 500 , $\phi = 0°$

Approximately 10 days

After Launch

C. Perkins
10/20/63

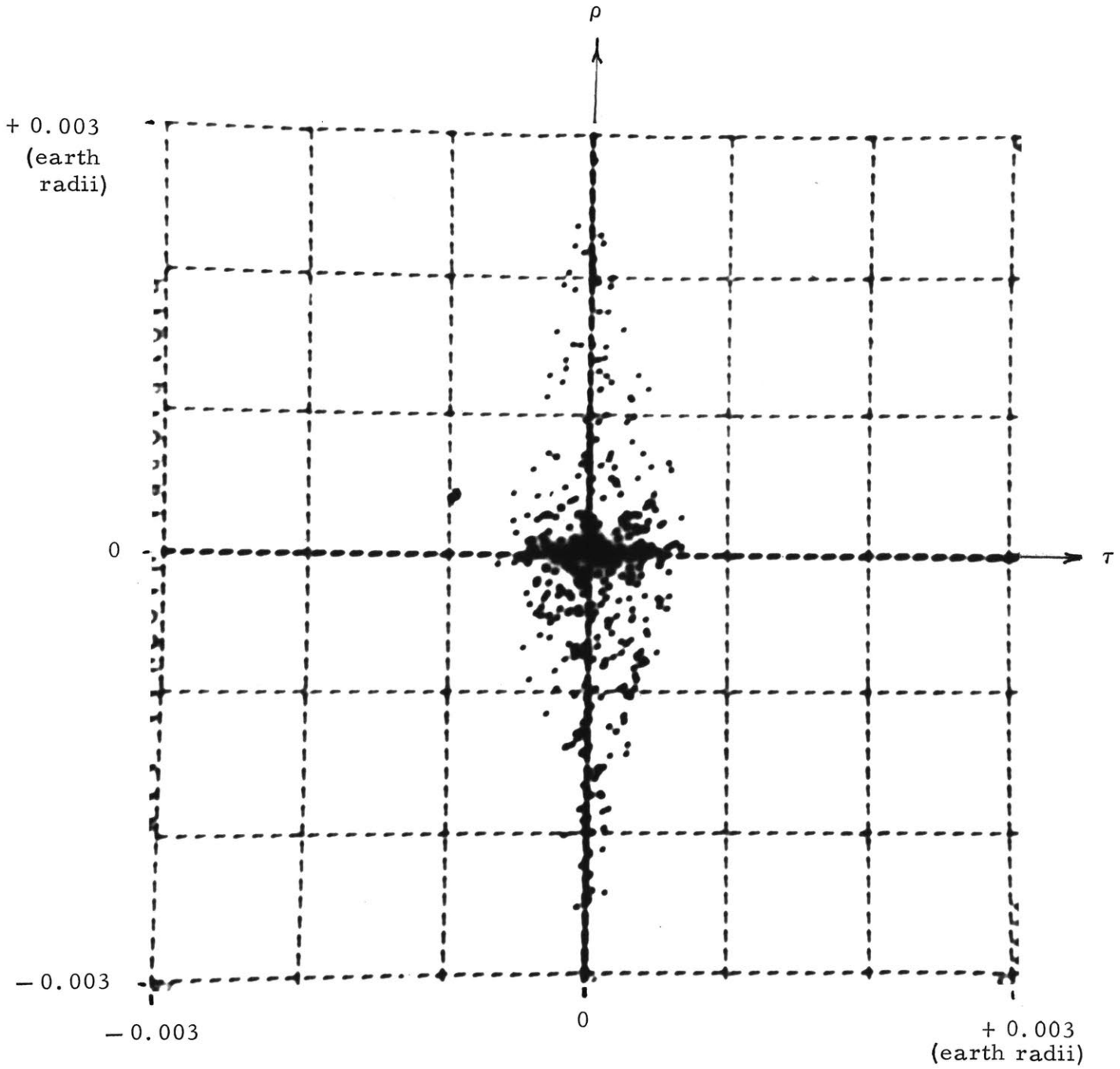

Fig. 4.10

Intersection Plane

for

West Ford Dipoles
(calculated with the Monte
Carlo technique)

N = 500 $\phi = 0°$
Approximately 10 days
After Launch

C. Perkins

10/20/63

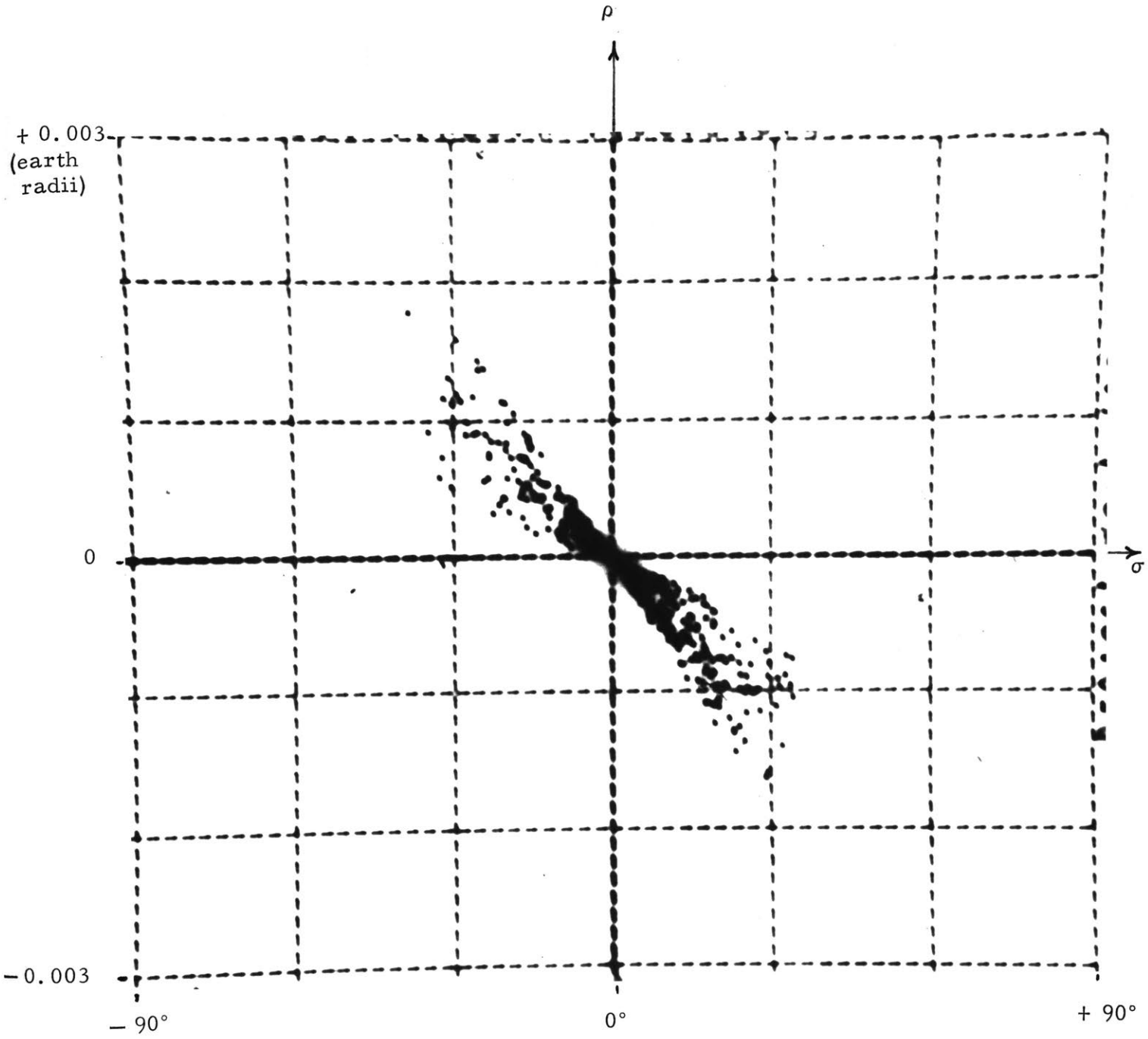

Fig. 4.11

Population Diagram
of
West Ford Dipoles
in
The Orbit Plane
(calculated with the Monte
Carlo technique)

N = 500 , ϕ = 90°
Approximately 10 days
After Launch

C. Perkins

10/20/63

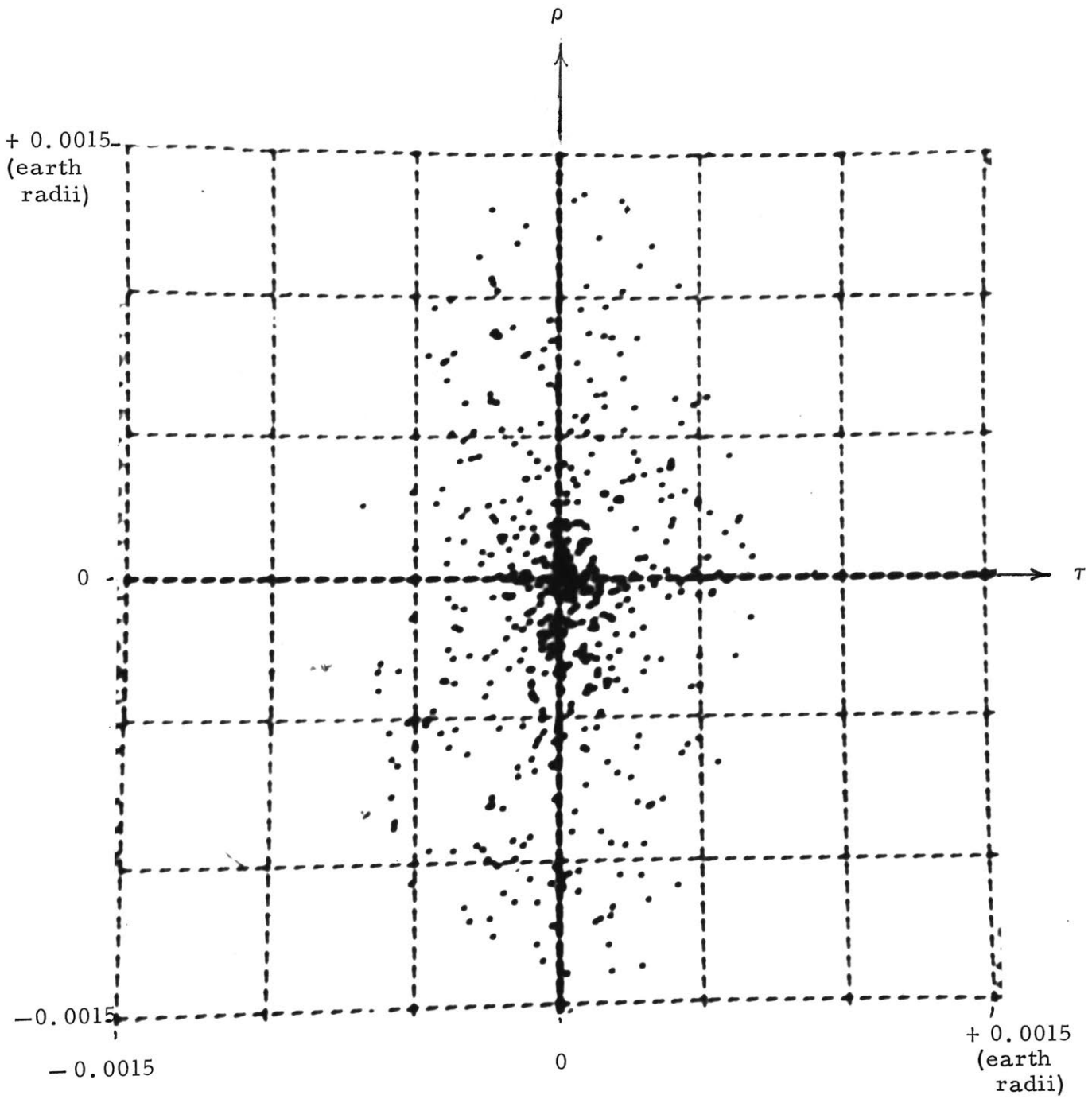

Fig. 4.12

Intersection Plane
for
West Ford Dipoles
(calculated with the Monte
Carlo technique)

N = 500, $\phi = 90°$

Approximately 10 days
After Launch

C. Perkins
10/20/63

REFERENCES

4.1 H.M. Jones, C.W. Perkins, I.I. Shapiro, "Orbital Lifetime of the West Ford Dipoles," Science 140, No. 3572 (14 June 1963), p. 1173.

4.2 W.E. Morrow, Jr., "Long Range Communication by Orbiting Dipole Belts (Project West Ford)," presented at the XIV General assembly of the International Scientific Radio Union, Tokyo, Japan (September 9-20, 1963).

4.3 Private communication from C.M. Crocker of M.I.T. Lincoln Laboratory.

4.4 F.R. Moulton, An Introduction to Celestial Mechanics, 2nd edition, (MacMillan Company, 1914).

4.5 W. Grobner, N. Hofreiter, Integraltafel, Zweiter Teil, Bestimmte Integrale, Zweite, verbesserto Auflage, Wien und Innsbruck, Springer-Verlag, 1958.

4.6 Private communication from H.M. Jones and I.I. Shapiro of M.I.T. Lincoln Laboratory.

4.7 Private communication from F. Nagy and D. Karp of M.I.T. Lincoln Laboratory.

4.8 W. Liller, "The Optical Effects of the 1963 Project West Ford Experiment," Science, to be published.

4.9 C. Perkins, "Low Thrust Propulsion Requirements for Maneuvering Satellites in Near Circular, Low Inclination Orbits," United Aircraft Company, unpublished (13 September 1960).

4.10 S. Ross, "The Orbital Motion of Pellet Clouds," Journal of the Astronautical Sciences VIII , No. 3 (Fall, 1961) p. 79.

4.11 I.I. Shapiro and H.M. Jones, "Lifetimes of Orbiting Dipoles," Science 134, No. 3484 (October 6, 1961), pp. 973-979.

4.12 Private communication from H.M. Jones of M.I.T. Lincoln Laboratory.

CONCLUDING REMARKS

The orbit perturbation computations presented in Chapters II and III are, to the best of our knowledge, the most accurate theoretical computations (short of prohibitively time consuming numerical integrations) of near-earth satellite orbits in existence. The General Perturbation Program (GPP), which includes the second order theory derived in Chapter I and the detailed atmospheric density models described in Chapter III, is nearly as accurate as a straight forward numerical integration of the exact perturbation equations and nearly as economical of time and far more accurate than a computer program of a closed form analytic solution. The accuracy attained by the GPP approaches the accuracy to which orbits can presently be determined from observation.

The importance of the second order perturbations derived in Chapter I is clearly demonstrated in the comparison of computed orbital elements with the observed orbital elements of 1960 Iota 2 (see Chapter II). For example, the residuals between observed and computed eccentricity are reduced by a factor of about 40 for 1960 Iota 2 when the second order effects are included. This comparison also demonstrates that the observational accuracy warrants the inclusion, theoretically, of crossproduct perturbations of the second and third harmonics (i. e., J*K terms). The surprisingly large (but small compared with J^2 terms) and uncertain effect of solar radiation pressure on this satellite is also demonstrated.

In Chapter III, the GPP is employed as a new and important technique in the study of atmospheric density. An existing atmospheric density model is improved upon, and the existence of a north-south extension of the atmospheric "bulge" is deduced. The same technique used in Chapter III can be used to improve other geophysical parameters (such as the coefficients of the zonal harmonics of the gravitational field of the earth).

Once the accuracy of the GPP was verified by comparison with existing orbital data, the program was used to predict the orbit of the drag sensitive satellite 1961 Delta 1 (a 12 ft diameter balloon). The prediction of orbital lifetime for 1961 Delta 1 (to be down on March 28, 1964 ± 10 days) was based on orbital data for July 30, 1963. In December, 1963, the predicted perigee height (an important parameter in the lifetime computation) was within 1 km of the observed value (the perigee height

decreased 100 km during this interval). This prediction was relied upon in the planning of the launch of the new 12 ft balloon satellite (Explorer 19). A similar prediction for the orbit of the West Ford dipole belt based on May, 1963 data is still being used to acquire the belt with one-tenth degree beam radars. It can be concluded that this method of orbit perturbation computation is a general and accurate method for predicting satellite orbits.

The theoretical distributions of dipoles in the West Ford dipole belt derived in Chapter IV are in accord with the observed distributions to within the experimental uncertainties. A Monte Carlo technique for predicting the behavior of the West Ford dipole ensemble was also developed and its capability verified. This technique is being used to study the long term dispersion of the dipole belt caused by differential orbit perturbations.

APPENDIX I

Integration of the Perturbation Equations for the Second Harmonic of the Gravitational Field of the Earth

I.1 First-Order Perturbations

The first-order perturbations of the orbital elements are derived by integrating the respective perturbation equations (see Eq. (1.2) of Chapter I).

The perturbation equation for the semi-latus rectum (p) (Eq. 1.17a), to first-order in J, is:

$$\frac{dp}{du} = -\frac{2J}{r}\sin^2 i_o \sin 2u$$

where to first-order:

$$r = \frac{p_o}{1 + e_o \cos v} \tag{I.1}$$

and

$$v = \nu$$

Substituting $u = \nu + \omega_o$ and using Eq. (I.1) gives:

$$\frac{dp}{du} = -\frac{2J}{p_o}\sin^2 i_o \left[\sin (2\nu + 2\omega_o)(1 + e_o \cos \nu)\right] \tag{I.2}$$

Hence:

$$\delta p = \int_{-\omega_o}^{\nu} \frac{dp}{du}\, d\nu = -\frac{2J \sin^2 i_o}{p_o} \int_{-\omega_o}^{\nu} [\cos 2\omega_o \sin 2\nu + \sin 2\omega_o \cos 2\nu$$

$$+ \tfrac{1}{2} e_o \cos 2\omega_o \sin \nu + \tfrac{1}{2} e_o \cos 2\omega_o \sin 3\nu$$

$$+ \tfrac{1}{2} e_o \sin 2\omega_o \cos \nu + \tfrac{1}{2} e_o \sin 2\omega_o \cos 3\nu] d\nu$$

Integration yields Eq. (1.20):

$$\delta p = -\frac{2}{3}\frac{J}{p_o}\sin^2 i\,[P_1 + P_2 \sin\nu + P_3 \sin 2\nu + P_4 \sin 3\nu + P_5 \cos\nu + P_6 \cos 2\nu + P_7 \cos 3\nu]$$

where:

$$\begin{aligned} P_1 &= \frac{3}{2} + 2e_o \cos\omega_o \\ P_2 &= \frac{3}{2} e_o \sin 2\omega_o \\ P_3 &= \frac{3}{2} \sin 2\omega_o \\ P_4 &= \frac{1}{2} e_o \sin 2\omega_o \\ P_5 &= -\frac{3}{2} e_o \cos 2\omega_o \\ P_6 &= -\frac{3}{2} \cos 2\omega_o \\ P_7 &= -\frac{1}{2} e_o \cos 2\omega_o \end{aligned} \qquad (1.20)$$

To first order in J, the equation for the change in eccentricity (e) (Eq. (1.17b)) is:

$$\frac{de}{du} = -J\left[\frac{\sin v}{r^2} + \sin^2 i_o\left(-\frac{3}{2}\frac{\sin v}{r^2} + \frac{3}{2}\frac{\sin v \cos 2u}{r^2} + \frac{\cos v \sin 2u}{r^2} + \frac{\cos v \sin 2u}{rp_o} + \frac{e_o \sin 2u}{rp_o}\right)\right] \qquad (I.3)$$

Substituting for r (Eq. (I.1)) and rearranging terms in a power series in e yields:

$$\frac{de}{du} = -\frac{J}{p_o^2}\Big[\sin\nu + \sin^2 i_o(-3\sin\nu\sin^2 u + 4\cos\nu\cos u\sin u)$$

$$+ e_o(2\sin\nu\cos\nu + 2\sin^2 i_o(-3\sin\nu\cos\nu\sin^2 u + (1+3\cos^2\nu)\sin u\cos u))$$

$$+ e_o^2(\cos^2\nu\sin\nu + \sin^2 i_o(-3\sin\nu\cos^2\nu\sin^2 u + 2(1+\cos^2\nu)\cos\nu\sin u\cos u))\Big]$$

(I. 4)

Hence:

$$\delta e = -\frac{J}{p_o^2}\Big[\cos\omega_o - \cos\nu + \sin^2 i_o(-\frac{2}{3}\cos\omega_o + (\frac{3}{2} - \frac{1}{4}\cos 2\omega_o)\cos\nu$$

$$+\frac{1}{4}\sin 2\omega_o\sin\nu - \frac{7}{12}\cos 2\omega_o\cos 3\nu$$

$$+ \frac{7}{12}\sin 2\omega_o\sin 3\nu)$$

$$+ e_o(\frac{1}{2}\cos 2\omega_o - \frac{1}{2}\cos 2\nu + 2\sin^2 i_o((\frac{5}{8} - \frac{3}{16}\cos 2\omega_o) + (\frac{3}{8} - \frac{5}{8}\cos 2\omega_o)\cos 2\nu$$

$$+ \frac{5}{8}\sin 2\omega_o\sin 2\nu - \frac{3}{16}\cos 2\omega_o\cos 4\nu$$

$$+ \frac{3}{16}\sin 2\omega_o\sin 4\nu))$$

$$+ e_o^2(\frac{1}{3}\cos^3\omega_o - \frac{1}{4}\cos\nu - \frac{1}{12}\cos 3\nu + \sin^2 i_o(\frac{1}{8}\cos 2\omega_o\cos\omega_o + \frac{29}{48}\cos\omega_o$$

$$- \frac{1}{16}\cos 3\omega_o + \frac{3}{8}(1 - 2\cos 2\omega_o)\cos\nu$$

$$+ \frac{5}{8}\sin 2\omega_o\sin\nu + \frac{1}{48}(6 - 17\cos 2\omega_o)\cos 3\nu$$

$$+ \frac{17}{48}\sin 2\omega_o\sin 3\nu - \frac{1}{16}\cos 2\omega_o\cos 5\nu$$

$$+ \frac{1}{16}\sin 2\omega_o\sin 5\nu))\Big]$$

(I. 5)

Rearranging terms gives Eq. (1.21)

$$\delta e = -\frac{J}{p_o^2}[E_1 + E_2 \sin\nu + E_3 \sin 2\nu + E_4 \sin 3\nu + E_5 \sin 4\nu + E_6 \sin 5\nu + E_7 \cos\nu + E_8 \cos 2\nu + E_9 \cos 3\nu + E_{10} \cos 4\nu + E_{11} \cos 5\nu]$$

where

$$E_1 = \cos\omega_o - \frac{2}{3}\sin^2 i_o \cos\omega_o + e_o(\frac{1}{2}\cos 2\omega_o + \sin^2 i_o(\frac{5}{4} - \frac{3}{8}\cos 2\omega_o)) + e_o^2(\frac{1}{3}\cos^3\omega_o + \sin^2 i_o(\frac{2}{3}\cos\omega_o))$$

$$E_2 = \frac{1}{4}\sin^2 i_o \sin 2\omega_o + \frac{5}{8} e_o^2 \sin^2 i_o \sin 2\omega_o$$

$$E_3 = \frac{5}{4} e_o \sin^2 i_o \sin 2\omega_o$$

$$E_4 = \frac{7}{12}\sin^2 i_o \sin 2\omega_o + \frac{17}{48} e_o^2 \sin^2 i_o \sin 2\omega_o$$

$$E_5 = \frac{3}{8} e_o \sin^2 i_o \sin 2\omega_o$$

$$E_6 = \frac{1}{16} e_o^2 \sin^2 i_o \sin 2\omega_o$$

$$E_7 = -1 + \sin^2 i_o(\frac{3}{2} - \frac{1}{4}\cos 2\omega_o) + e_o^2(-\frac{1}{4} + \frac{3}{8}\sin^2 i_o(1 - 2\cos 2\omega_o))$$

$$E_8 = -\frac{1}{2} e_o + e_o \sin^2 i_o(\frac{3}{4} - \frac{5}{4}\cos 2\omega_o)$$

$$E_9 = -\frac{7}{12}\sin^2 i_o \cos 2\omega_o + e_o^2(-\frac{1}{12} + \sin^2 i_o(\frac{1}{8} - \frac{17}{48}\cos 2\omega_o))$$

$$E_{10} = -\frac{3}{8} e_o \sin^2 i_o \cos 2\omega_o$$

$$E_{11} = -\frac{1}{16} e_o^2 \sin^2 i_o \cos 2\omega_o$$

(1.21)

The equation for the behavior of the argument of perigee (ω), Eq. (1.17c), to first order in J, is:

$$\frac{d\omega}{du} = -\frac{J}{e_o}\left[-\frac{\cos v}{r^2} + \sin^2 i\left(\frac{3}{2}\frac{\cos v}{r^2} - \frac{3}{2}\frac{\cos v \cos 2u}{r^2} + \frac{\sin v \sin 2u}{r^2} + \frac{\sin v \sin 2u}{p_o r}\right) - \frac{2e_o}{p_o r}\cos^2 i_o \sin^2 u\right] \tag{I.6}$$

Substituting for r (Eq. (I.1)), and rearranging terms gives:

$$\begin{aligned}\frac{d\omega}{du} = -\frac{J}{e_o p_o^2}\Big[&-\cos\nu + \sin^2 i_o\,(3\cos\nu\sin^2 u + 4\sin\nu\cos u\sin u)\\ &+ e_o(-2\cos^2\nu + 6\sin^2 i_o(\cos^2\nu\sin^2 u + \cos\nu\sin\nu\sin u\cos u) - 2\cos^2 i_o\sin^2 u)\\ &+ e_o^2(-\cos^3\nu + \sin^2 i_o\,(3\cos^3\nu\sin^2 u + 2\cos^2\nu\sin\nu\sin u\cos u)\\ &\qquad - 2\cos^2 i\cos\nu\sin^2 u)\Big]\end{aligned} \tag{I.7}$$

Integration yields:

$$\begin{aligned}\delta\omega = -\frac{J}{e_o p_o^2}\Big[&-\sin\omega_o - \sin\nu + \sin^2 i_o\left(\frac{2}{3}\sin\omega_o + \left(\frac{3}{2} + \frac{1}{4}\cos 2\omega_o\right)\sin\nu\right.\\ &\qquad - \frac{7}{12}\cos 2\omega_o\sin 3\nu + \frac{1}{4}\sin 2\omega_o\cos\nu\\ &\qquad \left. - \frac{7}{12}\sin 2\omega_o\cos 3\nu\right)\\ &+ e_o\left(-2(\nu+\omega_o) - \frac{1}{2}\sin 2\omega_o - \frac{1}{2}\sin 2\nu + \frac{1}{2}\cos 2\omega_o\sin 2\nu + \frac{1}{2}\sin 2\omega_o\cos 2\nu\right.\\ &\quad + \sin^2 i_o\left(\frac{5}{2}(\nu+\omega) + \frac{3}{8}\sin 2\omega_o + \left(\frac{3}{4} - \frac{5}{4}\cos 2\omega_o\right)\sin 2\nu\right.\\ &\quad \left.\left. - \frac{3}{8}\cos 2\omega_o\sin 4\nu - \frac{5}{4}\sin 2\omega_o\cos 2\nu - \frac{3}{8}\sin 2\omega_o\cos 4\nu\right)\right.\\ &+ e_o^2\left(-\frac{25}{12}\sin\omega_o - \frac{1}{12}\sin 3\omega_o + \left(-\frac{7}{4} + \frac{1}{2}\cos 2\omega_o\right)\sin\nu + \left(-\frac{1}{12} + \frac{1}{6}\cos 2\omega_o\right)\sin 3\nu\right.\end{aligned}$$

(continued)

$$+\frac{1}{2}\sin 2\omega_o \cos\nu + \frac{1}{6}\sin 2\omega_o \cos 3\nu$$

$$+ \sin^2 i_o \left(\left(\frac{125}{48}\sin\omega_o + \frac{1}{16}\sin 3\omega_o - \frac{1}{8}\cos 2\omega_o \sin\omega_o\right)\right.$$

$$+ \left(\frac{17}{8} - \cos 2\omega_o\right)\sin\nu + \left(\frac{1}{8} - \frac{19}{48}\cos 2\omega_o\right)\sin 3\nu$$

$$-\frac{1}{16}\cos 2\omega_o \sin 5\nu - \frac{7}{8}\sin 2\omega_o \cos\nu$$

$$\left.\left. - \frac{19}{48}\sin 2\omega_o \cos 3\nu - \frac{1}{16}\sin 2\omega_o \cos 5\nu\right)\right] \qquad \text{(I. 8)}$$

Rearranging terms gives Eq. (1. 22):

$$\delta\omega = -\frac{J}{e_o p_o^2}\left[W_1 + W_2\nu + W_3 \sin\nu + W_4 \sin 2\nu + W_5 \sin 3\nu\right.$$

$$+ W_6 \sin 4\nu + W_7 \sin 5\nu + W_8 \cos\nu + W_9 \cos 2\nu + W_{10} \cos 3\nu$$

$$\left. + W_{11} \cos 4\nu + W_{12} \cos 5\nu\right]$$

where

$$W_1 = -\sin\omega_o + \frac{2}{3}\sin^2 i_o \sin\omega_o + e_o\left(-2\omega_o - \frac{1}{2}\sin 2\omega_o + \sin^2 i_o \cdot\right.$$

$$\left. \cdot \left(\frac{5}{2}\omega_o + \frac{3}{8}\sin 2\omega_o\right)\right) + e_o^2\left(-2\sin\omega_o - \frac{1}{3}\cos^2\omega_o \sin\omega_o\right.$$

$$\left. + \sin^2 i_o \left(\frac{8}{3}\sin\omega_o\right)\right)$$

$$W_2 = e_o\left(-2 + \frac{5}{2}\sin^2 i_o\right)$$

$$W_3 = -1 + \sin^2 i_o \left(\frac{3}{2} + \frac{1}{4}\cos 2\omega_o\right) + e_o^2\left(-\frac{7}{4} + \frac{1}{2}\cos 2\omega_o\right.$$

$$\left. + \sin^2 i_o \left(\frac{17}{8} - \cos 2\omega_o\right)\right)$$

$$W_4 = e_o\left(-\frac{1}{2} + \frac{1}{2}\cos 2\omega_o + \sin^2 i_o \left(\frac{3}{4} - \frac{5}{4}\cos 2\omega_o\right)\right)$$

(continued)

$$W_5 = -\frac{7}{12}\sin^2 i_o \cos 2\omega_o + e_o^2\left(-\frac{1}{12} + \frac{1}{6}\cos 2\omega_o + \sin^2 i_o\left(\frac{1}{8} - \frac{19}{48}\cos 2\omega_o\right)\right)$$

$$W_6 = -\frac{3}{8} e_o \sin^2 i_o \cos 2\omega_o$$

$$W_7 = -\frac{1}{16} e_o^2 \sin^2 i_o \cos 2\omega_o$$

$$W_8 = \frac{1}{4}\sin^2 i_o \sin 2\omega_o + e_o^2\left(\frac{1}{2}\sin 2\omega_o - \frac{7}{8}\sin^2 i_o \sin 2\omega_o\right)$$

$$W_9 = e_o\left(\frac{1}{2}\sin 2\omega_o - \frac{5}{4}\sin^2 i_o \sin 2\omega_o\right)$$

$$W_{10} = -\frac{7}{12}\sin^2 i_o \sin 2\omega_o + e_o^2\left(\frac{1}{6}\sin 2\omega_o - \frac{19}{48}\sin^2 i_o \sin 2\omega_o\right)$$

$$W_{11} = -\frac{3}{8} e_o \sin^2 i_o \sin 2\omega_o$$

$$W_{12} = -\frac{1}{16} e_o^2 \sin^2 i_o \sin 2\omega_o$$

(1.22)

The first order perturbation of the inclination angle was derived in the text. The result (Eq. (1.24)) was:

$$\delta i = \frac{1}{2p_o}\cot i_o \, \delta p \qquad (1.24)$$

The first order perturbation of the semi-major axis (a) is simply derived from the relation $p = a(1 - e^2)$.

$$\delta a = \frac{1}{(1 - e_o^2)}\,\delta p + \frac{2e_o p_o}{(1 - e_o^2)^2}\,\delta e \qquad (I.9)$$

This perturbation was not required in determining the second-order perturbations, but is stated here for reference.

The first order perturbation of the right ascension of the ascending node was also not required to obtain the second-order perturbations. For completeness this perturbation is given here (as a function of the argument of latitude):

$$\delta\Omega = -\frac{J\cos i_o}{p_o^2}\left[\frac{4}{3}e_o\sin\omega_o + u + \frac{1}{2}e_o\cos\omega_o\sin u\right.$$

$$-\frac{1}{2}\sin 2u - \frac{1}{6}e_o\cos\omega_o\sin 3u - \frac{3}{2}e_o\sin\omega_o\cos u$$

$$\left.+\frac{1}{6}e_o\sin\omega_o\cos 3u\right] \qquad \text{(I. 10)}$$

The time at which a satellite is at a given argument of latitude, calculated to zero order in J, is simply the time of nodal crossing plus the time required for the satellite to travel from nodal crossing to perigee plus the time for the satellite to travel to the true anomaly $v = u - \omega_o$, which may be negative. The intermediate step of including time at perigee is included because of the particular symmetry of an orbit about the line of apsides. This relation is:

$$t = T_o + \frac{a_o^{3/2}}{\sqrt{GM}}\left[E(\omega_o) + E(u-\omega_o) - e_o\left(\sin E(\omega_o) + \sin E(u-\omega_o)\right)\right] \qquad \text{(I. 11)}$$

where

$$E(x) = 2\tan^{-1}\left(\sqrt{\frac{1-e_o}{1+e_o}}\tan\frac{x}{2}\right) \qquad \text{(I. 12)}$$

I. 2 Second-Order Perturbations

The net second-order perturbations after one nodal cycle are defined by Eq. (1. 3) in the text.

To evaluate these changes, we need the expansion of the instantaneous orbital radius to include the first-order variation of the elements.

$$r^{-1} = \frac{1}{p_o}\left(1 - \frac{\delta p}{p_o}\right)\left(1 + e_o\cos\nu + \cos\nu\,\delta e + e_o\sin\nu\,\delta\omega\right)$$

$$+ \text{Higher Order Terms} \qquad \text{(I. 13)}$$

Similarly,

$$\sin v = \sin \nu - \cos \nu \, \delta\omega + \text{Higher order terms} \qquad \text{(I. 14)}$$

$$\cos v = \cos \nu + \sin \nu \, \delta\omega + \text{Higher order terms} \qquad \text{(I. 15)}$$

Substituting Eqs. (I. 13), (I. 14), (I. 15), and (1. 24) into Eq. (1. 17a), yields

$$\frac{dp}{du} = -\frac{2J}{p_o}\left[\left(\sin^2 i_o + \cos 2i_o \frac{\delta p}{p_o}\right)(1 + e_o \cos \nu + \cos \nu \, \delta e + e_o \sin \nu \, \delta\omega)\cdot\right.$$

$$\cdot(\cos 2\omega_o \sin 2\nu + \sin 2\omega_o \cos 2\nu)] + \frac{8J^2 \cos^2 i_o \sin^2 i_o}{p_o^3}$$

$$[(\sin^3 u \cos u)(1 + 2e_o \cos\omega_o \cos u + 2e_o \sin\omega_o \sin u$$

$$+ 2e_o^2 \cos\omega_o \sin\omega_o \cos u \sin u + e_o^2 \cos^2\omega_o \cos^2 u$$

$$\left. + e_o^2 \sin^2\omega_o \sin^2 u)\right] \qquad \text{(I. 16)}$$

Expanding Eq. (I. 16) gives Eq. (1. 26) in the text:

$$\frac{dp}{du} = -\frac{2J}{p_o}[\sin^2 i_o(\cos 2\omega_o \sin 2\nu \cos \nu + \sin 2\omega_o \cos 2\nu \cos \nu)\delta e$$

$$+ \sin^2 i_o (e_o \cos 2\omega_o \sin 2\nu \sin \nu + e_o \sin 2\omega_o \cos 2\nu \sin \nu)\delta\omega$$

$$+ \cos 2i_o(\cos 2\omega_o \sin 2\nu + \sin 2\omega_o \cos 2\nu + e_o \cos 2\omega_o \sin 2\nu \cos \nu$$

$$+ e_o \sin 2\omega_o \cos 2\nu \cos \nu) \frac{\delta p}{p_o} + \text{Higher order terms}$$

$$+ \text{terms that will vanish upon integration}]$$

$$+ \frac{8J^2 \cos^2 i_o \sin^2 i_o}{p_o^3}[2e_o^2 \cos\omega_o \sin\omega_o \sin^4 u \cos^2 u$$

$$+ \text{terms that will vanish upon integration}]$$

(1. 26)

Integration of Eq. (1. 26) gives Eq. (1. 27) in the text. This reduces to the final form of the perturbation of p accurate to second-order, (Eq. (1. 28)).

$$\Delta p = \frac{\pi J^2}{p_o^3} \sin^2 i_o \left[e_o \sin \omega_o \left(-\frac{16}{3} + \frac{20}{3} \sin^2 i_o \right) + e_o^2 \sin 2\omega_o \left(\frac{7}{3} - \frac{5}{2} \sin^2 i_o \right) \right] \tag{1. 28}$$

Substituting Eqs. (I. 13), (I. 14), (I. 15), and (1. 24) into the perturbation equation for Ω yields:

$$\begin{aligned} \frac{d\Omega}{du} = & -\frac{J}{p_o^2} \cos i_o \left[\left(1 - \frac{5}{2} \frac{\delta p}{p_o}\right) (1 + e_o \cos \nu + \cos \nu \, \delta e + e_o \sin \nu \, \delta \omega)(1 \right. \\ & \left. - \cos 2\omega_o \cos 2\nu + \sin 2\omega_o \sin 2\nu) \right] \\ & + \frac{4J^2}{p_o^4} \cos^3 i_o \left[\sin^4 u (1 + 2e_o \cos \omega_o \cos u + 2e_o \sin \omega_o \sin u \right. \\ & \left. + e_o^2 \cos^2 \omega_o \cos^2 u + 2e_o^2 \cos \omega_o \sin \omega_o \cos u \sin u + e_o^2 \sin^2 \omega_o \sin^2 u) \right] \end{aligned} \tag{I. 17}$$

Expansion gives:

$$\begin{aligned} \frac{d\Omega}{du} = & -\frac{J \cos i_o}{p_o^2} \left[1 + (\cos \nu - \cos 2\omega_o \cos 2\nu \cos \nu + \sin 2\omega_o \sin 2\nu \cos \nu) \delta e \right. \\ & + (e_o \sin \nu - e_o \cos 2\omega_o \cos 2\nu \sin \nu + e_o \sin 2\omega_o \sin 2\nu \sin \nu) \delta \omega \\ & - \frac{5}{2} (1 - \cos 2\omega_o \cos 2\nu + \sin 2\omega_o \sin 2\nu + e_o \cos \nu \\ & - e_o \cos 2\omega_o \cos 2\nu \cos \nu + e_o \sin 2\omega_o \sin 2\nu \cos \nu) \frac{\delta p}{p_o} \\ & + \text{terms that vanish upon integration + Higher order terms} \Big] \\ & + \frac{4J^2}{p_o^4} \cos^3 i_o \left[\sin^4 u + e_o^2 \cos^2 \omega_o \sin^4 u \cos^2 u + e_o^2 \sin^2 \omega_o \sin^6 u \right. \\ & \left. + \text{terms that vanish upon integration} \right] \end{aligned} \tag{I. 18}$$

Integration yields:

$$\Delta\Omega = \int_{-\omega}^{2\pi-\omega_o} \frac{d\Omega}{du}\, d\nu = -\frac{2\pi J \cos i_o}{p_o^2} + \frac{\pi J^2}{p_o^4}\cos i_o$$

$$[E_7 - \tfrac{1}{2}\cos 2\omega_o (E_7 + E_9) + \tfrac{1}{2}\sin 2\omega_o (E_2 + E_4) + W_3$$

$$-\tfrac{8}{3}\cos\omega_o\, W_2 + \tfrac{1}{2}\cos 2\omega_o (W_3 - W_5) + \tfrac{1}{2}\sin 2\omega_o (W_8 - W_{10})$$

$$-\tfrac{5}{3}\sin^2 i_o (2P_1 - \cos 2\omega_o P_6 + \sin 2\omega_o P_3 + e_o P_5$$

$$-\tfrac{1}{2} e_o \cos 2\omega_o (P_5 + P_7) + \tfrac{1}{2} e_o \sin 2\omega_o (P_2 + P_4))$$

$$+ \cos^2 i_o (3 + \tfrac{1}{2} e_o^2 (1 + 4\sin^2\omega_o))] \qquad \text{(I. 19)}$$

This reduces to the final form of perturbation of Ω accurate to second order, (Eq. (1. 29) in the text):

$$\Delta\Omega = -\frac{2\pi J \cos i}{p_o^2} + \frac{\pi J^2}{p_o^4}\cos i_o [1 - \tfrac{20}{3}\sin^2 i_o + e_o \cos\omega_o (\tfrac{16}{3} - \tfrac{40}{3}\sin^2 i_o)$$

$$+ e_o^2 (-\tfrac{1}{3} - \tfrac{7}{6}\cos 2\omega_o + \sin^2 i_o (-\tfrac{5}{12} + \tfrac{5}{2}\cos 2\omega_o))] \qquad \text{(1. 29)}$$

The derivation of the perturbation of the argument of perigee (ω) accurate to second-order is accomplished by substituting Eqs. (I. 13), (I. 14), (I. 15), and (1. 24) into Eq. (1. 17c) in the same manner as in the derivation of Δp and $\Delta\Omega$. The result of this substitution is:

$$\frac{d\omega}{du} = \frac{J}{e_o p_o^2}\{(1 - \frac{\delta e}{e_o})(1 - \frac{2\delta p}{p_o})(\cos\nu + \sin\nu\,\delta\omega)(1 + e_o\cos\nu + \cos\nu\,\delta e$$

$$+ e_o \sin\nu\,\delta\omega)^2 - (\sin^2 i_o + (1 - 3\sin^2 i_o)\frac{\delta p}{p_o} - \sin^2 i_o \frac{\delta e}{e_o})\cdot$$

$$\cdot[-\tfrac{3}{2}(\cos\nu + \sin\nu\,\delta\omega)(\cos 2\omega_o \cos 2\nu - \sin 2\omega_o \sin 2\nu)\cdot$$

(continued)

$$\cdot (1 + e_o \cos\nu + \cos\nu\,\delta e + e_o \sin\nu\,\delta\omega)^2 + \frac{3}{2}(\cos\nu + \sin\nu\,\delta\omega)\cdot$$

$$\cdot (1 + e_o \cos\nu + \cos\nu\,\delta e + e_o \sin\nu\,\delta\omega)^2 + (\sin\nu - \cos\nu\,\delta\omega)\cdot$$

$$\cdot (\cos 2\omega_o \sin 2\nu + \sin 2\omega_o \cos 2\nu)(1 + e_o\cos\nu + \cos\nu\,\delta e + e_o\sin\nu\,\delta\omega)^2$$

$$+ (\sin\nu - \cos\nu\,\delta\omega)(\cos 2\omega_o \sin 2\nu + \sin 2\omega_o \cos 2\nu)(1 + e_o \cos\nu$$

$$+ \cos\nu\,\delta e + e_o \sin\nu\,\delta\omega)]\} - \cos i_o \frac{d\Omega}{du} - \frac{J\cos^2 i_o}{2p_o^2}$$

$$\{[1 - \cos 2\omega_o \cos 2\nu + \sin 2\omega_o \sin 2\nu + e_o\cos\nu - e_o\cos 2\omega_o\cos 2\nu\cos\nu$$

$$+ e_o \sin 2\omega_o \sin 2\nu \cos\nu]\frac{\delta p}{p_o}\} - \frac{J^2}{e_o p_o^4}\cos^2 i_o$$

$$\{(2\cos\omega_o \sin^2 u\cos u + 2\sin\omega_o \sin^3 u)(1 + e_o\cos\omega_o\cos u + e_o\sin\omega_o \sin u)^3$$

$$+ \sin^2 i_o\,(-10\cos\omega_o\sin^4 u\cos u - 6\sin\omega_o\sin^5 u + 4\sin\omega_o\sin^3 u\cos^2 u)\cdot$$

$$\cdot (1 + e_o\cos\omega_o\cos u + e_o\sin\omega_o\sin u)^3 + \sin^2 i_o\cdot$$

$$\cdot(-4\cos\omega_o\sin^4 u\cos u + 4\sin\omega_o\sin^3 u\cos^2 u)(1 + e_o\cos\omega_o\cos u$$

$$+ e_o\sin\omega_o\sin u)^2\}$$

(I. 20)

Expanding:

$$\frac{d\omega}{du} = \frac{J}{e_o p}\{+2e_o\cos^2\nu - \sin^2 i_o[3e_o\cos^2\nu - 3e_o\cos 2\omega_o\cos 2\nu\cos^2\nu$$

$$+ 3e_o\cos 2\omega_o \sin 2\nu \sin\nu\cos\nu] + [(-\frac{1}{e_o} + \frac{1}{2}e_o)\cos\nu$$

$$+\frac{1}{2}e\cos 2\nu\cos\nu - \sin^2 i_o((\frac{3}{4}e_o - \frac{3}{2}\frac{1}{e_o})\cos\nu + (\frac{3}{2}\frac{1}{e_o}\cos 2\omega_o + \frac{3}{4}e_o$$

(continued)

$$-\frac{3}{4}e_o\cos 2\omega_o)\cos 2\nu\cos\nu-\frac{3}{4}e_o\cos 2\omega_o\cos 2\nu\cos 2\nu\cos\nu$$

$$+\left(-\frac{3}{2}\frac{1}{e_o}\sin 2\omega_o+\frac{3}{4}e_o\sin 2\omega_o\right)\sin 2\nu\cos\nu+\frac{3}{2}e_o\sin 2\omega_o\cos 2\nu\cos^2\nu\cdot$$

$$\cdot\sin\nu+\left(-\frac{2}{e_o}\cos 2\omega_o+\frac{1}{2}e_o\cos 2\omega_o\right)\sin 2\nu\sin\nu$$

$$+e_o\cos 2\omega_o\cos 2\nu\sin^2\nu\cos\nu+\left(-\frac{2}{e_o}\sin 2\omega_o+\frac{1}{2}e_o\sin 2\omega_o\right)\cos 2\nu\sin\nu$$

$$+\frac{1}{2}e_o\sin 2\omega_o\cos 2\nu\cos 2\nu\sin\nu)]\cdot\delta e+[(1+\frac{1}{2}e_o^2)\sin\nu+2e_o\sin 2\nu$$

$$+e_o^2\sin 2\nu\cos\nu+\frac{1}{2}e_o^2\cos 2\nu\sin\nu-\sin^2 i_o((\frac{3}{2}+\frac{3}{4}e_o^2)\sin\nu$$

$$+3e_o\sin 2\nu+(\frac{3}{2}e_o^2-2\cos 2\omega_o-\frac{1}{2}e_o^2\cos 2\omega_o)\sin 2\nu\cos\nu$$

$$-6e_o\cos 2\omega_o\cos 2\nu\sin\nu\cos\nu-4e_o^2\cos 2\omega_o\cos 2\nu\cos^2\nu\sin\nu$$

$$+6e_o\sin 2\omega_o\sin 2\nu\sin\nu\cos\nu+3e_o\cos 2\omega_o\sin 2\nu\sin^2\nu$$

$$+3e_o^2\sin 2\omega_o\sin 2\nu\sin\nu\cos^2\nu+(\frac{3}{4}e_o^2-\frac{3}{2}\cos 2\omega_o-\frac{3}{4}e_o^2\cos 2\omega_o)\cdot$$

$$\cdot\cos 2\nu\sin\nu+2e_o^2\cos 2\omega_o\sin 2\nu\sin^2\nu\cos\nu+3e_o\sin 2\omega_o\cos 2\nu\sin^2\nu$$

$$-\frac{3}{4}e_o^2\cos 2\omega_o\cos 2\nu\cos 2\nu\sin\nu+(\frac{3}{2}\sin 2\omega_o+\frac{3}{4}e_o^2\sin 2\omega_o)\sin 2\nu\sin\nu$$

$$-3e_o\cos 2\omega_o\sin 2\nu\cos^2\nu+(-2\sin 2\omega_o-\frac{1}{2}e_o^2\sin 2\omega_o)\cos 2\nu\cos\nu$$

$$+\frac{7}{2}e_o^2\sin 2\omega_o\cos 2\nu\sin^2\nu\cos\nu-3e_o\sin 2\omega_o\cos 2\nu\cos^2\nu$$

$$-\frac{1}{2}e_o^2\sin 2\omega_o\cos 2\nu\cos 2\nu\cos\nu)]\cdot\delta\omega+[(-2-e_o^2)\cos\nu-4e_o\cos^2\nu$$

$$-e_o^2\cos 2\nu\cos\nu-(1-3\sin^2 i_o)((\frac{3}{2}+\frac{3}{4}e_o^2)\cos\nu+3e_o\cos^2\nu$$

$$+(\frac{3}{4}e_o^2-\frac{3}{4}e_o^2\cos 2\omega_o-\frac{3}{2}\cos 2\omega_o)\cos 2\nu\cos\nu$$

$$-3e_o\cos 2\omega_o\cos 2\nu\cos^2\nu-\frac{3}{4}e_o^2\cos 2\omega_o\cos 2\nu\cos 2\nu\cos\nu$$

(continued)

$$+\left(\frac{3}{2}+\frac{3}{4}e_o^2\right)\sin 2\omega_o \sin 2\nu \cos\nu + 3e_o \sin 2\omega_o \sin 2\nu \cos^2\nu$$

$$+\frac{3}{2}e_o^2 \sin 2\omega_o \cos 2\nu \cos^2\nu \sin\nu + \left(2\cos 2\omega_o + \frac{1}{2}e_o^2 \cos 2\omega_o\right)\sin 2\nu \sin\nu$$

$$+ 3e_o \cos 2\omega_o \sin 2\nu \sin\nu \cos\nu + e_o^2 \cos 2\omega_o \cos 2\nu \sin^2\nu \cos\nu$$

$$+\left(2\sin 2\omega_o + \frac{1}{2}e_o^2 \sin 2\omega_o\right)\cos 2\nu \sin\nu + 3e_o \sin 2\omega_o \cos 2\nu \sin\nu \cos\nu$$

$$+\frac{1}{2}e_o^2 \sin 2\omega_o \cos 2\nu \cos 2\nu \sin\nu)] \cdot \frac{\delta p}{p_o} + \text{Higher order terms}$$

$$+ \text{terms that vanish upon integration}\} - \cos i \frac{d\Omega}{du}$$

$$-\frac{J\cos^2 i_o}{2p_o^2}\{[1-\cos 2\omega_o \cos 2\nu + \sin 2\omega_o \sin 2\nu + e_o \cos\nu$$

$$- e_o \cos 2\omega_o \cos 2\nu \cos\nu + e_o \sin 2\omega_o \sin 2\nu \cos\nu]\frac{\delta p}{p_o}\}$$

$$-\frac{J^2}{e_o p_o^4}\cos^2 i_o \{(2\cos\omega_o \sin^2 u \cos u + 2\sin\omega_o \sin^3 u)(1+e_o \cos\omega_o \cdot$$

$$\cdot \cos u + e_o \sin\omega_o \sin u)^3 + \sin^2 i_o(-10\cos\omega_o \sin^4 u \cos u - 6\sin\omega_o \cdot$$

$$\cdot \sin^5 u + 4\sin\omega_o \sin^3 u \cos^2 u)(1+e_o \cos\omega_o \cos u + e_o \sin\omega_o \sin u)^3$$

$$+ \sin^2 i_o(-4\cos\omega_o \sin^4 u \cos u + 4\sin\omega_o \sin^3 u \cos^2 u)(1+e_o \cos\omega_o \cos u$$

$$+ e_o \sin\omega_o \sin u)^2\} + \text{Higher order terms}$$

(I. 21)

Hence:

$$\Delta\omega = \int_{-\omega_o}^{2\pi-\omega_o} \frac{d\omega}{du}\, d\nu = \frac{\pi J}{p_o^2}(3\cos^2 i_o) - \cos i_o \Delta\Omega$$

$$+\frac{\pi J^2}{p_o^4}\left\{\frac{1}{e_o^2}E_7 - \frac{3}{4}E_7 - \frac{1}{4}E_9 + \sin^2 i_o\left[-\frac{3}{2}\frac{1}{e_o^2}E_7\right.\right.$$

(continued)

$$+\frac{3}{8}(3E_7+E_9)+\frac{1}{4}\frac{1}{e_o^2}\cos 2\omega_o(-E_7+7E_9)+\frac{1}{4}\frac{1}{e_o^2}\sin 2\omega_o(E_2-7E_4)$$

$$-\frac{1}{16}\cos 2\omega_o(8E_7+11E_9+5E_{11})+\frac{1}{16}\sin 2\omega_o(6E_2+11E_4+5E_6)]$$

$$-\frac{1}{e_o^2}W_3-\frac{2}{e_o}W_4-\frac{3}{4}W_3-\frac{3}{4}W_5+\sin^2 i_o[\frac{3}{2}\frac{1}{e_o^2}W_3+3\frac{1}{e_o}W_4$$

$$+\frac{9}{8}(W_3+W_5)-\frac{1}{4}\frac{1}{e_o^2}\cos 2\omega_o(W_3+7W_5)-\frac{1}{4}\frac{1}{e_o^2}\sin 2\omega_o(W_8+7W_{10})$$

$$-3\frac{1}{e_o}\cos 2\omega_o\cdot W_6-3\frac{1}{e_o}\sin 2\omega_o W_{11}+\frac{1}{16}\cos 2\omega_o(4W_3-11W_5-15W_7)$$

$$+\frac{1}{16}\sin 2\omega_o(10W_8-11W_{10}-15W_{12})]+\frac{1}{e_o^2}W_2[2\cos\omega_o+2e_o\cos 2\omega_o$$

$$+2e_o^2\cos^3\omega_o+\sin^2 i_o(-\frac{4}{3}\cos\omega_o-\frac{3}{2}e_o\cos 2\omega_o-\frac{3}{8}e_o^2\cos\omega_o)]$$

$$+\frac{2}{3}\sin^2 i_o[\frac{2}{e_o}P_5+4P_1+2P_6+\frac{1}{2}e_o(3P_5+P_7)+(1-3\sin^2 i_o)\cdot$$

$$\cdot(\frac{3}{2}\frac{1}{e_o}P_5+(3P_1+\frac{3}{2}P_6)+e_o(\frac{9}{8}P_5+\frac{3}{8}P_7)+\frac{1}{4}\frac{1}{e_o}\cos 2\omega_o(P_5-7P_7)$$

$$+\frac{1}{4}\frac{1}{e_o}\sin 2\omega_o(-P_2+7P_4)+\cos 2\omega_o(-\frac{3}{2}P_6)+\sin 2\omega_o(\frac{3}{2}P_3)$$

$$+\frac{1}{16}e_o\cos 2\omega_o(-8P_5-11P_7)+\frac{1}{16}e_o\sin 2\omega_o(6P_2+11P_4))$$

$$+\frac{1}{2}\cos^2 i_o(2P_1+e_oP_5-\cos 2\omega_oP_6+\sin 2\omega_oP_3-\frac{1}{2}e_o\cos 2\omega_o(P_5+P_7)$$

$$+\frac{1}{2}e_o\sin 2\omega_o(P_2+P_4)]-\cos^2 i(3-\frac{3}{2}\cos 2\omega_o+e_o^2(\frac{3}{4}-\frac{1}{2}\cos 2\omega_o)$$

$$+\sin^2 i[-\frac{27}{4}+2\cos 2\omega_o+e_o^2(-\frac{53}{32}+\frac{5}{4}\cos 2\omega_o-\frac{1}{16}\cos^2 2\omega)])\}$$

(I. 22)

Equation (I. 22) reduces to the final form given as Eq. (1. 30) in the text:

$$\Delta\omega = \frac{\pi J}{P_o^2}(3\cos^2 i_o - 1) - \cos i_o \Delta\Omega + \frac{\pi J^2}{P_o^4}\left[\frac{1}{e_o}\cos\omega_o\left(-4 + \frac{23}{3}\sin^2 i_o - \frac{10}{3}\sin^4 i_o\right) + \left(1 - 4\cos 2\omega_o + \sin^2 i_o\left(\frac{49}{6} + \frac{23}{6}\cos 2\omega_o\right) + \sin^4 i_o\left(-\frac{95}{8} + \frac{5}{4}\cos 2\omega_o\right)\right) + e_o\cos\omega_o\left(-4\cos^2\omega_o + \sin^2 i_o(16 + 5\cos^2\omega_o) - 20\sin^4 i_o\right) + e_o^2\left(\frac{5}{6} + \sin^2 i_o\left(-\frac{5}{6} - \frac{35}{12}\cos 2\omega_o\right) + \sin^4 i_o\left(-\frac{25}{48} + \frac{25}{8}\cos 2\omega_o\right)\right)\right]$$

(1.30)

The integration of the perturbation equation for the time of nodal crossing (Eq. (1.17) in the text) is performed in much the same manner as for the preceding orbital elements. The appearance of the instantaneous radius in the numerator of this equation, however, causes functions of the independent variable to remain in the denominator after expanding the equation in terms of small quantities. This slightly increases the complexity of the integration.

Substituting Eqs. (I.13), (I.14), and (I.15) into Eq. (1.17f) gives:

$$\frac{dt}{du} = \left[\frac{1}{\sqrt{GM}} \frac{p_o^{3/2}\left(1 + \frac{3}{2}\frac{\delta p}{p_o}\right)}{\left[(1 + e\cos\nu)^2 + 2\cos\nu(1 + e_o\cos\nu) + 2e_o\sin\nu(1 + e_o\cos\nu)\right]}\right] - \frac{2J}{\sqrt{GMp_o}}\cos^2 i_o\left[\frac{\sin^2 u}{(1 + e\cos\nu)}\right]$$

(I.31)

Expanding we find:

$$\frac{dt}{du} = \frac{p_o^{3/2}}{\sqrt{GM}}\left[\frac{1}{(1 + e_o\cos\nu)^2} + \frac{3}{2}\frac{1}{(1 + e_o\cos\nu)^2}\cdot\frac{\delta p}{p_o} - \frac{2\cos\nu}{(1 + e_o\cos\nu)^3}\delta e - \frac{2e_o\sin\nu}{(1 + e_o\cos\nu)^3}\delta\omega\right] - \frac{2J\cos^2 i_o}{\sqrt{GMp_o}}\left[\frac{\sin^2 u}{1 + e\cos\nu}\right]$$

(I.32)

Thus:

$$\Delta T = \int_{-\omega_o}^{2\pi-\omega_o} \frac{dt}{du}\, d\nu = \frac{p_o^{3/2}}{\sqrt{GM}} \cdot \frac{J}{p_o^2} \left\{ - \sin^2 i_o \left[(P_1 - P_6) \int_o^{2\pi} \frac{d\nu}{(1+e_o \cos\nu)^2} \right.\right.$$

$$+ (P_5 - 3P_7) \int_o^{2\pi} \frac{\cos\nu\, d\nu}{(1+e_o\cos\nu)^2} + 2P_6 \int_o^{2\pi} \frac{\cos^2\nu\, d\nu}{(1+e_o\cos\nu)^2}$$

$$\left. + 4P_7 \int_o^{2\pi} \frac{\cos^3\nu\, d\nu}{(1+e_o\cos\nu)^2} \right] + 2 \left[(W_3 - W_5 + W_7) \int_o^{2\pi} \frac{d\nu}{(1+e_o\cos\nu)^3} \right.$$

$$+ (E_1 - E_8 + E_{10} + 2W_4 - 4W_6) \int_o^{2\pi} \frac{\cos\nu\, d\nu}{(1+e_o\cos\nu)^3} + (E_7 - 3E_9 + 5E_{11} - W_3 + 5W_5$$

$$- 13W_7) \int_o^{2\pi} \frac{\cos^2\nu\, d\nu}{(1+e_o\cos\nu)^3} + (2E_8 - 8E_{10} - 2W_4 + 12W_6) \cdot$$

$$\cdot \int_o^{2\pi} \frac{\cos^3\nu}{(1+e_o\cos\nu)^3}\, d\nu$$

$$+ (4E_9 - 20E_{11} - 4W_5 + 28W_7) \int_o^{2\pi} \frac{\cos^4\nu\, d\nu}{(1+e_o\cos\nu)^3} + (8E_{10} - 8W_6) \cdot$$

$$\cdot \int_o^{2\pi} \frac{\cos^5\nu}{(1+e_o\cos\nu)^3}\, d\nu$$

$$\left. + (16E_{11} - 16W_7) \int_o^{2\pi} \frac{\cos^6\nu}{(1+e_o\cos\nu)^3}\, d\nu + W_2 \cdot \int_{-\omega_o}^{2\pi-\omega_o} \frac{(\sin\nu)\nu\, d\nu}{(1+e_o\cos\nu)^3} \right]$$

$$\left. - 4\pi \cos^2 i_o \left(\frac{1-\sqrt{1-e_o^2}}{e_o^2} \cos 2\omega_o + \frac{\sin^2\omega_o}{\sqrt{1-e_o^2}} \right) \right\}$$

+ Higher order terms

+ Terms that vanish upon integration.

(I. 33)

where:

$$\int_0^{2\pi} \frac{d\nu}{(1+e_o\cos\nu)^2} = \frac{2\pi}{(1-e_o^2)^{3/2}}$$

$$\int_0^{2\pi} \frac{\cos^2\nu\, d\nu}{(1+e_o\cos\nu)^2} = \frac{2\pi}{e_o^2}\left[1-\frac{(1-2e_o^2)}{(1-e_o^2)^{3/2}}\right]$$

$$\int_0^{2\pi} \frac{\cos^3\nu\, d\nu}{(1+e_o\cos\nu)^3} = \frac{2\pi}{e_o^3}\left[\frac{2-3e_o^2}{(1-e_o^2)^{3/2}}-2\right]$$

$$\int_0^{2\pi} \frac{d\nu}{(1+e_o\cos\nu)^3} = \pi\left[\frac{2+e_o^2}{(1-e_o^2)^{5/2}}\right]$$

$$\int_0^{2\pi} \frac{\cos\nu\, d\nu}{(1+e_o\cos\nu)^3} = \frac{-3\pi e_o}{(1-e_o^2)^{5/2}}$$

$$\int_0^{2\pi} \frac{\cos^2\nu\, d\nu}{(1+e_o\cos\nu)^3} = \pi\left[\frac{1+2e_o^2}{(1-e_o^2)^{5/2}}\right]$$

$$\int_0^{2\pi} \frac{\cos^3\nu\, d\nu}{(1+e_o\cos\nu)^3} = \frac{\pi}{e_o^3}\left[\frac{-2+5e_o^2-6e_o^4}{(1-e_o^2)^{5/2}}+2\right]$$

$$\int_0^{2\pi} \frac{\cos^4\nu\, d\nu}{(1+e_o\cos\nu)^3} = \frac{3\pi}{e_o^4}\left[\frac{2-5e_o^2+4e_o^4}{(1-e_o^2)^{5/2}}-2\right]$$

$$\int_{-\omega_o}^{2\pi-\omega_o} \frac{\nu\sin\nu\, d\nu}{(1+e_o\cos\nu)^3} = \frac{\pi}{e_o}\left[\frac{1}{(1+e_o\cos\omega_o)^2}-\frac{1}{(1-e_o^2)^{3/2}}\right]$$

Upon integration and the substitution of the coefficients of the first-order variation of the elements (P_1, P_6, P_7, etc. see Eq. (1.20), (1.21), and (1.22)) the change in time of nodal crossing accurate to first-order reduces simply to (Eq. (1.31)) in the text:

$$\Delta T = 2\pi \sqrt{\frac{p_o^3}{GM(1-e_o^2)^3}} + \frac{2\pi J}{\sqrt{GMp_o}} \left[- \frac{(1 + e_o \cos\omega_o)^3}{(1-e_o^2)^{5/2}} \right.$$

$$\left. + \frac{(-2 + \frac{5}{2}\sin^2 i_o)}{(1 + e_o \cos\omega_o)^2} \right] \qquad (1.31)$$

The derivation of the perturbation of eccentricity (e) and inclination (i) accurate to second-order are given in detail in the text. No integration is required in these derivations because energy and angular momentum are integrals of the motion.

APPENDIX II

General Perturbation Program

II.1 Introduction

The General Perturbation Program (GPP) is a very general and flexible computer program for the study of satellite orbits. It was created at the M.I.T. Lincoln Laboratory by H. Jones and I. Shapiro, and has been extensively modified and extended by both and by the author, and many others. The purpose of this appendix is to give a brief description of the capabilities of this program which is used extensively in Chapters II, III, and IV. The program is coded in IBM 7094 Fortran, and has previously been used to study the effects of solar radiation pressure [II.1], to predict the lifetime of Echo I [II.2], to predict the lifetimes of the West Ford orbiting dipoles [II.3], and for many other general and special orbit perturbation studies.

Orbital elements are computed by this program for the desired number of orbital cycles using an iteration technique (see Ref. II.4). Net perturbations produced during one complete nodal cycle are evaluated to first order (except for the second harmonic of the earth's gravitational field) and the orbital elements are incremented by the respective net change in each element at the end of each nodal period, or by n times these net changes every n nodal periods, where n is a constant integer and depends on the accuracy desired (a large n reduces computation time but also reduces accuracy). This process is repeated by calculating a new set of net perturbations, using the incremented elements as arguments. The whole process is repeated for any desired number of orbit cycles or until the perigee height falls below a certain minimum, at which time the satellite is no longer considered to be orbiting.

Flexibility and generality are attained in the program by extensive input, output, and control features, and by using the fact that, to first order, no cross-coupling exists between the various perturbing accelerations. The absence of cross-coupling allows each perturbing acceleration to be treated as a separate entity, and therefore, its effects can be calculated in a separate subprogram completely independent of the other perturbing accelerations. After the effects of each perturbing acceleration are computed,

a subroutine increments each orbital element by the sum of the effects on that element from all of the perturbing accelerations. This subroutine structure allows several significant advantages: first, many modifications of the program can be made without disturbing the entire program; second, the effects of each perturbing acceleration are computed separately, and therefore, can be studied separately; and third, a number of mathematical models for the effects of each perturbing acceleration can be included in the subroutine and choices can be made by varying certain input constants.

Included below is a brief outline of the perturbations which can be computed by this program in its present form. These are in closed form wherever possible to conserve computational time. Where numerical integration is required, multiple 9-point Gaussian quadratures are used.

II. 2 Outline of Included Pertrubations

I. Solar radiation pressure (Subroutine RADPR)
- A. Features common to all models
  - 1. Earth shadow boundaries
    - a. Computed in a separate subroutine (SUB. SHADOW)
  - 2. Solar constant
    - a. Flux is corrected for varying earth-sun distance
- B. Models included
  - 1. Spherical satellite*
    - a. Closed form expressions
  - 2. Tumbling cylindrical satellite
    - a. Closed form expressions
    - b. Satellite properties
      - 1. Rapidly tumbling
      - 2. X percent absorption ($0 \leq X \leq 100$)
      - 3. 100-X percent specular reflection ($0 \leq X \leq 100$)
    - c. Special effects
      - 1. Tumbling axis change
        - a. random meteroid collisions

*For a sphere, absorption and specular reflection of light in any combination produces the same net force.

3. Aligned cylinder
    a. Numerical integration
    b. Satellite properties
        1. Alignment
            a. local earth magnetic field line
        2. X percent absorption ($0 \leq X \leq 100$)
        3. 100-X percent specular reflection ($0 \leq X \leq 100$)
    c. Assumed magnetic field
        1. Dipole
            a. Displaced from earth's center
            b. Tipped from earth's axis of rotation

II. Gravitational field of the earth (SUB. EARTH)
    A. Closed form expression
    B. Model
        1. Zonal spherical harmonics
            a. Second harmonic
                1. Evaluated to second order in J
            b. Third harmonic
            c. Fourth harmonic
            d. Fifth harmonic

III. Neutral drag (SUB. DRAG)
    A. Features common to all models
        1. Spherical satellite
        2. Free molecular flow
        3. Atmospheric rotation neglected
    B. Computational methods
        1. Numerical integration
            a. Geoid models
                1. sphere
                2. International Ellipsoid of Reference
            b. Density models (SUB. RHO)
                1. power law
                2. parabolic log
                3. Jacchia 1960 (See Chapter III)
                4. Jacchia temperature model (See Chapter III)
                5. Auroral bulge (See Chapter III)

2. Closed form expressions
    a. Assumptions
        1. Power low density model
        2. Spherical geoid

IV. Lunar Gravitational Field (SUB. MOON)
  A. Closed form expressions
  B. Approximations*
    1. $r/r_{moon} << 1$
    2. Moon ephemeris
      a. Polynomials in time

V. Solar Gravitational Field (SUB. SUN)
  A. Closed form expressions
  B. Approximations
    1. $r/r_{sun} << 1$
    2. Apparent solar ephemeris
      a. Polynomials in time

VI. Solar Radiation Reflected from the Earth
  A. Features common to both models
    1. Choice of satellite properties
      a. Spherical
      b. Absorbing cylinder
    2. Constant albedo
  B. Model of reflection properties of the earth
    1. Specular reflection (SUB. SPECRE)
      a. Numerical integrations
      b. A predetermined percentage (f_e) of the albedo is specularly reflected ($0 \leq f_e \leq 100$)
      c. Approximation
        1. Reflection properties of earth are homogeneous
    2. Diffuse reflection (SUB. DIFFRE)
      a. Numerical integration
      b. $100-f_e$ percent (see above) of the albedo is diffusely reflected ($0 \leq f_e \leq 100$)
      c. Approximation
        1. Reflection properties of earth are homogeneous

*This subroutine is being extensively modified to remove these approximations.

VII. Meteoroid Collisions (SUB. METEOR)

A. Transfer of Linear Momentum

1. Random variables

a. Meteoroid mass

b. Meteoroid velocity vector

c. Time of impact

B. Transfer of Angular Momentum

1. Effect on orbit

a. Changes tumbling axis (see I. B. 2)

2. Cylindrical satellite (e. g., West Ford dipole)

3. Random variables

a. Meteoroid mass

b. Meteoroid velocity vector

c. Time of impact

d. Position on cylinder of impact

IX. Coulomb Drag (SUB. CHDRAG)

A. Ad Hoc parameterized model (Ref. II. 4)

1. Numerical integrations

REFERENCES

II. 1 R. W. Parkinson, H. M. Jones, I. I. Shapiro, "Effects of Solar Radiation Pressure on Earth Satellite Orbits," Science 131, No. 3404 (March 25, 1960), pp. 920-921.

II. 2 I. I. Shapiro, H. M. Jones, "Perturbations of the Orbit of Echo Balloon," Science 132, No. 3438 (18 November 1960), p. 1484.

II. 3 I. I. Shapiro and H. M. Jones, "Lifetimes of Orbiting Dipoles," Science 134, No. 3484 (October 1961), pp. 973-979.

II. 4 I. I. Shapiro, "The Prediction of Satellite Orbits," ed. M. Roy, IUTAM Dynamics of Satellites Symposium, Paris, May 28-30, 1962 (1963 Academic Press).

APPENDIX III

Conversion Between Smithsonian Astrophysical Observatory Mean Orbital Elements and Nodal Osculating Orbital Elements

III. 1 Introduction

Smithsonian Astrophysical Observatory (SAO) satellite orbital data were used for the comparison of computed orbital elements with observation because of the standard of excellence set by SAO in measuring and reducing photographic data. The use of the SAO orbital data requires a conversion between the osculating elements at nodal crossing used in the GPP (See Appendix II) and the SAO Mean Elements. The conversion procedure is given in this appendix because the required information is not fully documented in the literature. In general, great care must be exercised in the comparison of computed orbital elements with orbital data from any source, to insure that the exact definitions of the orbital elements involved are known.

Figure III. 1 is a graphical representation of the definition of the various types of orbital elements and the typical variations of the osculating elements over a nodal period. The distance EB is the sum of the secular and long-period changes in the nodal osculating elements (i. e., changes which do not average to zero in a nodal cycle). This distance is of order J for the argument of perigee (ω) and for the right ascension of the ascending node (Ω) and of order J^2 for the semi-major axis (a), eccentricity (e), and inclination (i). The amplitude of the short-period variations of the osculating elements is of order J for all of the elements.

The output of the Differential Orbit Improvement Program (DOI)[III. 1] used by SAO to reduce satellite observational data, is a set of elements referred to an epoch (usually midnight U. T.), from which short-period perturbations caused by the earth's second harmonic have been eliminated (see Refs. III. 1 - III. 5). The inclination and argument of perigee are referred to the true equator of date and the right ascension of the ascending node is referred to the mean equinox of 1950. 0[III. 6]. The eliminated short-period perturbations (e. g., Distance FH in Fig. III-1) have zero

mean values when averaged with respect to the mean anomaly (III. 2) and serve to define Smithsonian mean elements.* These perturbations are not the first-order perturbations presented in Eqs. (1. 20) through (1. 24) (e. g., Distance AH in Fig. III. 1).

Each conversion from a set of SAO mean elements to a set of nodal-crossing elements and vice versa can be made independent of every other conversion. Hence, no error accumulates in conversion, and the accuracy of the conversion need be only of order J for the present comparison. A further increase in accuracy is not justified because short-period terms of order J^2 are smoothed as noise by the DOI program.

The scheme used for the present comparison of the GPP, with SAO, mean elements is to convert the first set of SAO mean elements to the nearest previous nodal-crossing osculating elements. Then, using these elements as input, the GPP computes nodal-crossing osculating elements at every nodal crossing and places on magnetic tape the nearest preceding nodal-crossing osculating elements for each epoch where a comparison is desired. These sets of elements are then reconverted to SAO mean elements at the epochs for comparison.

The equations for the conversion from SAO mean elements to nodal-crossing elements are derived from Kozai's short-period perturbation equations[III. 7] by evaluating these equations at nodal crossing ($v = -\omega$), correcting ω and Ω for the first-order (in J) secular perturbations and computing the time of nodal crossing (T) from the mean anomaly at the epoch. Kozai's short-period perturbation equations evaluated at nodal crossing (distance AG in Fig. III. 1), are:**

$$da = \frac{1}{3}\,\frac{J}{p}\,\frac{1}{(1-e^2)^2}\,\left[2(1+e\cos\omega)^3 + (1-\tfrac{3}{2}\sin^2 i)(1-e^2)^{3/2}\right]$$

(continued)

*If short-period effects of other perturbing forces are also eliminated, the conversion process presented here may no longer be adequate.

**The orbital elements in these equations are taken as nodal osculating; however, to order J it is not necessary to differentiate between osculating and mean elements here.

$$
\begin{aligned}
de &= \frac{J}{ep^2}\left[\frac{1}{3}(1+e\cos\omega)^3 - \frac{1}{3}\left(1-\frac{3}{2}\sin^2 i\right)(1-e^2)^{3/2} - \frac{1}{2}\sin^2 i \cdot \right. \\
&\qquad \left. \cdot (1-e^2)\left(1+\frac{4}{3}e\cos\omega\right)\right] \\
d\omega &= \frac{J}{p^2}\left\{ \left(2-\frac{5}{2}\sin^2 i\right)(-\omega - M(-\omega) - e\sin\omega) + \sin\omega\left[\frac{1}{e}\left(-1+\frac{2}{3}\sin^2 i\right)\right.\right. \\
&\qquad \left.\left. + e\left(-\frac{1}{3}+\frac{1}{6}\sin^2 i + \frac{1}{3}\sin^2\omega\right)\right] - \frac{1}{2}\sin 2\omega \right\} \\
d\Omega &= -\frac{J}{p^2}\cos i\left[-\omega - M(-\omega) - \frac{4}{3}e\sin\omega\right) \\
di &= \frac{J}{2p^2}\sin i\cos i\left[1+\frac{4}{3}e\cos\omega\right] \\
dM &= \frac{J}{ep^2}\sqrt{1-e^2}\left[\sin\omega\left(1-\frac{2}{3}\sin^2 i\right) + \frac{1}{2}e\sin 2\omega \right. \\
&\qquad \left. + e^2\sin\omega\left(\frac{2}{3}\sin^2 i - \frac{1}{3}\sin^2\omega\right)\right]
\end{aligned}
\qquad \text{(III. 1)}
$$

where $M(-\omega) = E(-\omega) - e\sin E(-\omega)$ is the mean anomaly evaluated at $-\omega$ and

$$E(-\omega) = 2\tan^{-1}\left(\sqrt{\frac{1-e}{1+e}}\cdot\frac{-\sin\omega}{1+\cos\omega}\right)$$

is the eccentric anomaly at $-\omega$.

The osculating elements at the nearest nodal crossing preceding the epoch are then:*

$$
\begin{aligned}
a &= a_m + da \\
e &= e_m + de \\
i &= i_m + di \\
\omega &= \omega_m + d\omega - \frac{J}{p^2}\left(2-\frac{5}{2}\sin^2 i\right)\cdot u \\
\Omega &= \Omega_m + d\Omega + \frac{J}{p^2}\cos i \cdot u \\
T &= \text{EPOCH} - (M_m - M(-\omega) + dM)\cdot P\cdot\frac{1}{2\pi}
\end{aligned}
\qquad \text{(III. 2)}
$$

*The secular corrections to ω and Ω correspond to the distance CF in Fig III. 1. The distance GC is always of order J^2 or higher and is neglected here.

where*

$$a_m = \left(\frac{GM}{n^2}\right)^{1/3} \left(1 - \frac{1}{3}\frac{J}{p^2}\left(1 - \frac{3}{2}\sin^2 i\right)\sqrt{1 - e^2}\right)$$

$$P = \frac{2\pi}{\sqrt{GM}}\, a^{3/2} = \text{osculating period at nodal crossing} \qquad \text{(III. 3)}$$

and where the subscript m denotes SAO mean elements. The argument of latitude (u) is obtained by first solving Kepler's equation, $M = E - e \sin E$, for the eccentric anomaly (E) where $M = M_m - dM$. Then, from the eccentric anomaly relation, Eq. (I. 12) of Appendix I, the true anomaly (v) can be obtained, finally, adding the argument of perigee (ω) yields u. The mean motion (n) is a corrected value of the SAO mean motion (n_m) (see below).

The exact meaning of the SAO mean motion (n_m) depends entirely on the numerical procedure used in the DOI program [III. 1] to compute the mean motion and, in fact, may change between sets of reported data at the program operator's whim (e. g., the meaning of n_m for 1961 IOTA 2 reported in Ref. III. 9 is different from that report in Ref. III. 6 and no indication of this fact is given in either reference). The DOI program computes n_m by numerically differentiating the mean anomaly (M) with respect to time. [III. 8]

The SAO mean motion is the reciprocal of the time required for the satellite to travel froma fictitious perigee (the first-order, short-period and secular, perturbations of ω and M caused by the second harmonic have already been eliminated and thus modified the apparent position of perigee) around the orbit to another fictitious perigee displaced from the first by the change in ω caused by all perturbations** except the first-order contribution of the second harmonic. This displacement of perigee is large ($\sim 0.1°$ per day in the case of 1960 IOTA 2) if the eccentricity is small. ***

---

*The equations involving M, n and P in this Appendix are consistent for M in radians, n in radians per second and P in seconds per revolution for GM in earth radii cubed per second squared. In Chapters II and III, M, n and P appear in the units revolutions, revolutions per day and days per revolution, respectively ($n(\text{rev/day}) = \frac{86400}{2\pi} \cdot n(\text{rad/sec})$ etc.).

**For low A/m satellites, this perturbation is mainly caused by the third harmonic of the gravitational field (see the discussion of ω for 1960 IOTA 2 in Chapter II).

***The correction to the mean motion for 1961 DELTA 1($e \approx 0.1$) is small (amplitude $\approx 3 \times 10^{-5}$ rev/day) and is neglected in Chapter II and III.

The mean motion (n) which appears in Eq. (III. 3) is the SAO mean motion (n_m) corrected for this displacement of perigee. We calculate this correction as follows: Let $\delta\omega'$ represent the displacement of perigee (change in the argument of perigee) by perturbations other than the first-order, short-period and secular, perturbations caused by the second harmonic. Then $\frac{1}{n} = \frac{1}{n_m}$ — time (δt) required for the satellite to travel $\delta\omega'$ in the vicinity of perigee. For small δt:

$$n \approx n_m (1 + n_m \delta t) \tag{III. 4}$$

$$n \delta t \approx E(\delta\omega') - e \sin E(\delta\omega') \tag{III. 5}$$

where

$$\tan \frac{1}{2} E(\delta\omega') = \sqrt{\frac{1-e}{1+e}} \tan (\frac{1}{2} \delta\omega') \tag{III. 6}$$

and for small $\delta\omega'$

$$E(\delta\omega') \approx \sqrt{\frac{1-e}{1+e}} \delta\omega' \tag{III. 7}$$

and

$$n \approx n_m (1 + \delta\omega' (1 - e) \sqrt{\frac{1-e}{1+e}}) \tag{III. 8}$$

since in the small correction term we set $n_m = n$.

For the purpose of the comparison presented in Chapter II, $\delta\omega'$ was approximated by subtracting (for each epoch of interest) the first- and second-order second harmonic perturbation from the total computed perturbation of the osculating argument of perigee at nodal crossing computed by the GPP. The second-order second-harmonic effect was subtracted in an attempt to approximate the change in the first-order short-period perturbation of ω at perigee passage which occurs during the smoothing period of the DOI program* because of changes in the orbital elements during this period.

*Eight days in the case of 1960 IOTA 2(III. 6).

To obtain SAO mean elements from nodal-crossing elements, one simply solves Eqs. (III. 2) for the mean elements. The SAO mean motion (to order J) is derived as follows:

$$n = \frac{\sqrt{GM}}{a^{3/2}} \left[1 - \frac{1}{2} \frac{J}{p^2} \left(1 - \frac{3}{2} \sin^2 i\right) \sqrt{1 - e}\right] \tag{III. 9}$$

and

$$n_m = n \left(1 - \delta\omega' \left(1 - e\right) \sqrt{\frac{1-e}{1+e}}\right) \tag{III. 10}$$

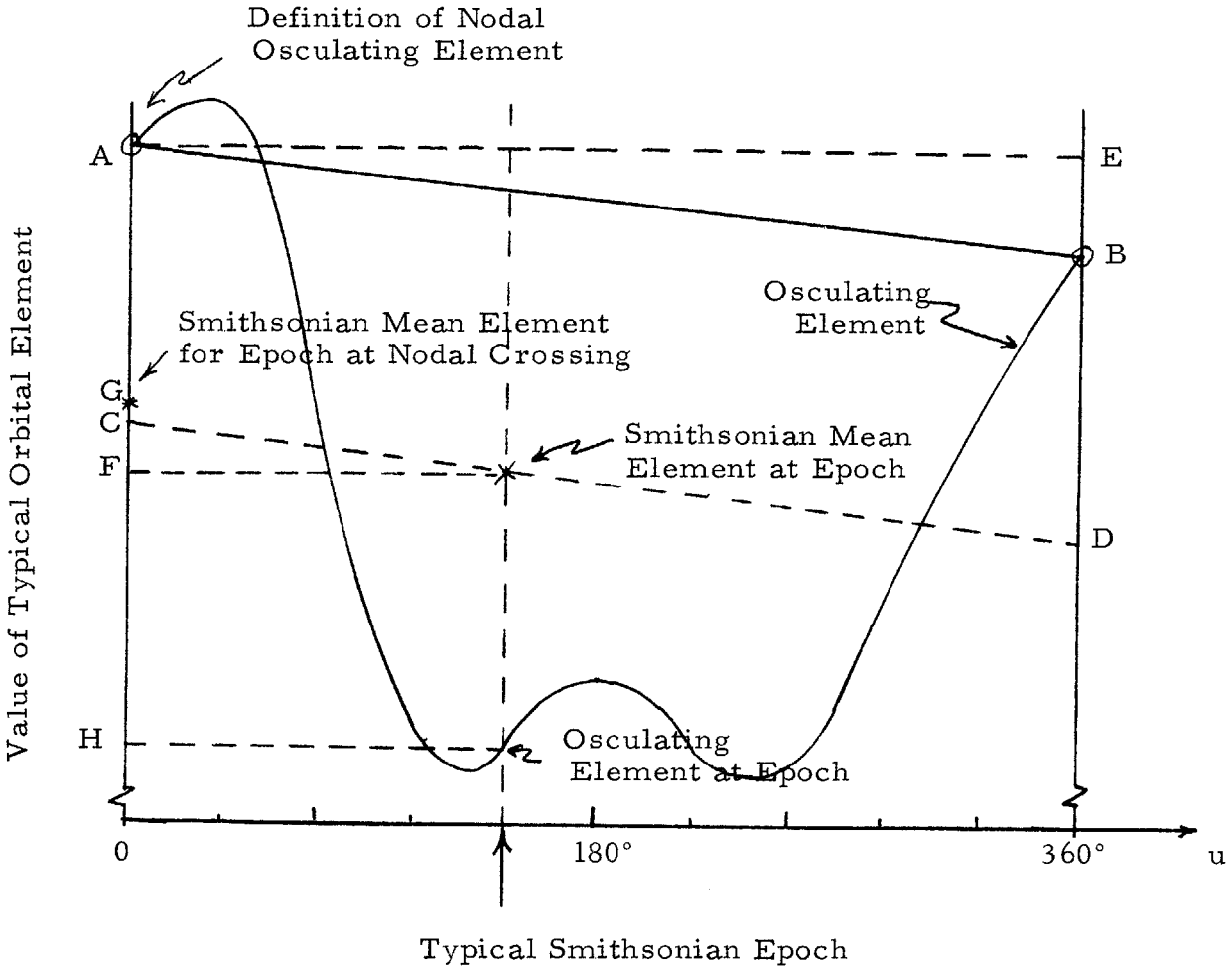

Fig. III.1 The Behavior of a Typical Orbital Element During One Nodal Crossing Orbital Period

REFERENCES

III. 1 Smithsonian Astrophysical Observatory Differential Orbit Improvement Program (DOI and DOI II), unpublished.

III. 2 Yoshihide Kozai, "The Motion of a Close Earth Satellite," The Astronomical Journal 64, No. 9 (November, 1959)~No. 1274.

III. 3 G. Veis, "Geodetic Uses of Artificial Satellites," Smithsonian Contributions to Astrophysics 3, No. 9, Washington, D.C. (1960).

III. 4 P. E. Zadunaisky, "The Orbit of Satellite 1958 Alpha (Explorer I) During the First 10500 Revolutions," Special Report No. 50, Smithsonian Astrophysical Observatory (October 3, 1960).

III. 5 R. Nigam, "The Orbits and the Accelerations of Satellites 1959 Alpha 1 and 1959 Alpha 2," Special Report No. 53, Smithsonian Astrophysical Observatory (December 5, 1960).

III. 6 I. G. Izsak, "Satellite Orbital Data," Special Report No. 119, Smithsonian Astrophysical Observatory (March 15, 1963).

III. 7 Y. Kozai, "Osculation Elements," Special Report No. 31, Smithsonian Astrophysical Observatory (January 18, 1960).

III. 8 Private communication from I. Izsak of the Smithsonian Astrophysical Observatory.

III. 9 I. G. Izsak, "Satellite Orbital Data," Special Report No. 92, Smithsonian Astrophysical Observatory (April 23, 1962).

APPENDIX IV

Calendar

		DAY	M.J.D.			DAY	M.J.D.
0. U.T.*	Jan. '58	0.0	36203.0	O.O. U.T.	Jan. '62	1461.0	37664.
	Feb.	31.	36234.		Feb.	1492.	37695
	Mar.	59.	36262.		Mar.	1520.	37723.
	April	90.	36293.		April	1551.	37754.
	May	120.	36323.		May	1581.	37784.
	June	151.	36354.		June	1612.	37815.
	July	181.	36384.		July	1642.	37845.
	Aug.	212.	36415.		Aug.	1673.	37876.
	Sept.	243.	36446.		Sept.	1704.	37907.
	Oct.	273.	36476.		Oct.	1734.	37937.
	Nov.	304.	36507.		Nov.	1765.	37968.
	Dec.	334.	36537.		Dec.	1795.	37998.
0. U.T.	Jan. '59	365.	36568.	O.O. U.T.	Jan. '63	1826.	38029.
	Feb.	396.	36599.		Feb.	1857.	38060.
	Mar.	424.	36627.		Mar.	1885.	38088.
	April	455.	36658.		April	1916.	38119.
	May	485.	36688.		May	1946.	38149.
	June	516.	36719.		June	1977.	38180.
	July	546.	36749.		July	2007.	38210.
	Aug.	577.	36780.		Aug.	2038.	38241.
	Sept.	608.	36811.		Sept.	2069.	38272.
	Oct.	638.	36841.		Oct.	2099.	38302.
	Nov.	669.	36872.		Nov.	2130.	38333.
	Dec.	699.	36902.		Dec.	2160.	38363.
0. U.T.	Jan. '60	730.	36933.	O.O. U.T.	Jan. '64	2191.	38394.
	Feb.	761.	36964.		Feb.	2222.	38425.
	Mar.	790.	36993.		Mar.	2251.	38454.
	April	821.	37024.		April	2282.	38485.
	May	851.	37054.		May	2312.	38515.
	June	882.	37085.		June	2343.	38546.
	July	912.	37115.		July	2373.	38576.
	Aug.	943.	37146.		Aug.	2404.	38607.
	Sept.	974.	37177.		Sept.	2435.	38638.
	Oct.	1004.	37207.		Oct.	2465.	38668.
	Nov.	1035.	37238.		Nov.	2496.	38699.
	Dec.	1065.	37268.		Dec.	2526.	38729.
0. U.T.	Jan. '61	1096.	37299.	O.O. U.T.	Jan. '65	2557.	38760.
	Feb.	1127.	37330.		Feb.	2588.	38791.
	Mar.	1155.	37358.		Mar.	2616.	38819.
	April	1186.	37389.		April	2647.	38850.
	May	1216.	37419.		May	2677.	38880.
	June	1247.	37450.		June	2708.	38911.
	July	1277.	37480.		July	2738.	38941.
	Aug.	1308.	37511.		Aug.	2769.	38972.
	Sept.	1339.	37542.		Sept.	2800.	39003.
	Oct.	1369.	37572.		Oct.	2830.	39033.
	Nov.	1400.	37603.		Nov.	2861.	39064.
	Dec.	1430.	37633.		Dec.	2891.	39094.
				O.O. U.T.	Jan. '66	2922.	39125.

*Zero day, zero hour Universal Time (i.e., noon on Jan 1, 1958 corresponds to DAY = 1.5). M.J.D. means Modified Julian Day.

Julian Day = 2,400,000.5 + M.J.D. = 2,436,203.5 + DAY

M.J.D. = 36,203.0 + DAY

Courtesy of H. Jones

BIBLIOGRAPHY

C. Allen, Astrophysical Quantities, 2nd edition (Athlone Press, University of London, 1963).

R. M. L. Baker, Jr. and M. W. Makemson, An Introduction to Astrodynamics (Academic Press, New York, 1960).

L. Berkner, editor, Annals of the International Geophysical Year, Vol. VI, "Rockets and Satellites," (Pergamon Press, New York, 1958).

L. Blitzer, "The Orbit of a Satellite in the Gravitational Field of the Earth," Space Technology Laboratories (August, 1960).

J. Britton, H. Jones, I. Shapiro, "Perturbating Forces Affecting the Motion of Artificial Earth Satellites," 7th reference bibliography, M. I. T. Lincoln Laboratory Library (2 October 1961).

D. Brouwer, "Solution of the Problem of Artificial Satellite Theory without Drag," The Astronomical Journal 64, No. 9 (November, 1959)~No. 1274.

J. Chamberlain, Physics of Aurora and Airglow (Academic Press, New York, 1961).

K. A. Ehricke, Space Flight, Vol. I, (D. Van Norstrand Co., Inc., New York, 1960).

B. Garfinkle, "The Orbit of a Satellite of an Oblate Planet," The Astronomical Journal 64, No. 9 (November, 1959)~No. 1274.

I. Harris and W. Priester, "Time-Dependent Structure of the Upper Atmosphere," Technical Note D-1443, NASA, Washington (July, 1962).

I. G. Izsak, "Satellite Orbital Data," Special Report No. 92, Smithsonian Astrophysical Observatory (April 23, 1962).

I. G. Izsak, "Satellite Orbital Data," Special Report No. 119, Smithsonian Astrophysical Observatory (March 15, 1963).

L. G. Jacchia, "Solar Effects on the Acceleration of Artificial Satellites," Smithsonian Astrophysical Observatory, Special Report No. 29 (21 September 1959)

L. Jacchia, "Two Atmospheric Effects in the Orbital Acceleration of Artificial Satellites," Nature 183 (21 February 1959), pp. 526-527.

L. G. Jacchia, "Atmospheric Structure and its Variations at Heights above 200 km," Report to Working Group IV (International Reference Atmosphere) presented at the Fourth International Space Science Symposium, Warsaw, Poland, 1963, Smithsonian Astrophysical Observatory.

L. G. Jacchia, "Corpuscular Radiation and the Acceleration of Artificial Satellites," Nature 183 (13 June 1959), pp. 1662-1663.

L. G. Jacchia, "The Effect of a Variable Scale Height on Determinations of Atmospheric Density from Satellite Acceleration," Special Report No. 46, Smithsonian Astrophysical Observatory (July 11, 1960).

L. G. Jacchia, "A Variable Atmospheric Density Model from Satellite Accelerations," Journal of Geophysical Research 65, No. 9, (September, 1960), p. 2775.

L. G. Jacchia, "The Atmospheric Drag on Artificial Satellites During the October, 1960 and November, 1960 Events," Special Report No. 62, Smithsonian Institute, Astrophysical Observatory (May 26, 1961).

L. G. Jacchia, "A Working Model for the Upper Atmosphere," Nature 192, No. 4808 (December 23, 1961).

L. G. Jacchia, "Variations in the Earth's Upper Atmosphere as Revealed by Satellite Drag," Smithsonian Astrophysical Observatory (December, 1962).

L. G. Jacchia and J. Slowey, "Preliminary Analysis of the Atmospheric Drag of the Twelve-foot Balloon Satellite (1961)," Special Report No. 84, Smithsonian Astrophysical Observatory (February, 1962).

L. G. Jacchia and G. R. Briggs," Orbital Accelerations of Satellite 1958 Beta Two," Special Report No. 18, Smithsonian Astrophysical Observatory (October, 1958).

L. G. Jacchia and J. Slowey, "Accurate Drag Determinations for Eight Artificial Satellites; Atmospheric Densities and Temperatures," Special Report No. 100, Smithsonian Astrophysical Observatory (30 July 1962).

L. G. Jacchia and J. Slowey, "An Analysis of the Atmospheric Drag of the Explorer IX Satellite from Precisely Reduced Photographic Observations," Special Report No. 125, Smithsonian Astrophysical Observatory (1963).

L. G. Jacchia and J. Slowey, "Atmospheric Heating in the Auroral Zones," Special Report No. 136, Smithsonian Astrophysical Observatory (17 September 1963).

H. Jeffreys, The Earth (Cambridge, 1959).

H. Jeffreys, "The Analysis of Gravity," Special Report No. 79, Smithsonian Astrophysical Observatory (October, 1961).

H.M. Jones, C.W. Perkins, I.I. Shapiro, "Orbital Lifetime of the West Ford Dipoles," Science 140, No. 3572 (14 June 1963), p. 1173.

H.M. Jones, I.I. Shapiro, and P.E. Zadunaisky, "Solar Radiation Pressure Effects, Gas Leakage Rates and Air Densities Inferred from the Orbit on Echo I," edited by H.C. Vandehulst, C. DeJager, and A.F. Moore, Space Research II, Proceedings of the Second International Space Science Symposium, Florence, April 10-14, 1961.

W.M. Kaula, "Celestial Geodesy," Technical Note D-1155, NASA, Washington (March, 1962).

Y. Kozai, "The Motion of a Close Earth Satellite," The Astronomical Journal 64, No. 9 (November, 1959)~No. 1274.

Y. Kozai, "Osculation Elements," Special Report No. 31, Smithsonian Astrophysical Observatory (January 18, 1960).

Y. Kozai, "Numerical Results from Orbits," Special Report No. 101, Smithsonian Astrophysical Observatory, Research in Space Science (31 July 1962).

Y. Kozai, "Second-Order Solution of Artificial Satellite Theory without Air Drag," The Astronomical Journal 67, No. 7 (September, 1962)~ No. 1302, pp. 446-461.

W. Liller, "The Optical Effects of the 1963 Project West Ford Experiment," Science, to be published.

D.V. Mechau, "Satellite Orbital Data," Special Report No. 51, Smithsonian Astrophysical Observatory (October, 1960).

W.A. Mersman, "Theory of the Secular Variations in the Orbit of a Satellite of an Oblate Planet," Technical Report R-99, NASA, Washington, (1961).

W.E. Morrow, Jr., "Long Range Communication by Orbiting Dipole Belts (Project West Ford)," presented at the XIV General Assembly of the International Scientific Radio Union, Tokyo, Japan (September 9-20, 1963).

F.R. Moulton, An Introduction to Celestial Mechanics (The MacMillan Co., New York, 1914).

M. Nicolet, "Density of the Heterosphere Related to Temperature," Special Report No. 75, Smithsonial Astrophysical Observatory (September, 1961).

J.N. Nielson, F.I. Goodwin, and W.A. Mersman, "Three-Dimensional Orbits of Earth Satellites, Including Effects of Earth Oblateness and Atmospheric Rotation," Memo No. 12-4-58A, NASA, Washington (December, 1958).

R. Nigam, "The Orbits and the Accelerations of Satellites 1951 Alpha 1 and 1959 Alpha 2," Special Report No. 53, Smithsonian Astrophysical Observatory (December 5, 1960).

R. W. Parkinson, H. M. Jones, I. I. Shapiro, "Effects of Solar Radiation Pressure on Earth Satellite Orbits," Science 131, No. 3404 (25 March 1960), pp. 920-921.

C. Perkins, "Low Thrust Propulsion Requirements for Maneuvering Satellites in Near Circular, Low Inclination Orbits," United Aircraft Co., unpublished (13 September 1960).

S. Ross, "The Orbital Motion of Pellet Clouds," Journal of the Astronautical Sciences VIII, No. 3 (Fall, 1961), p. 79.

P. E. Sandorff, Orbital and Ballistic Flight, Department of Aeronautics and Astronautics, Massachusetts Institute of Technology (1960).

I. I. Shapiro, "The Prediction of Satellite Orbits," ed. M. Roy IUTAM Dynamics of Satellites Symposium, Paris May 28-30, 1962 (Academic Press, 1963).

I. I. Shapiro, "Effects of Sunlight Pressure on Air Density Determinations Involving Cylindrical Satellites," Journal of Geophysical Research 68, No. 19 (October 1, 1963).

I. I. Shapiro, H. M. Jones, "Perturbations of the Orbit of Echo Balloon," Science 132, No. 3438 (18 November 1960), p. 1484.

I. I. Shapiro and H. M. Jones, "Lifetimes of Orbiting Dipoles," Science 134, No. 3484 (October 1961), pp. 973-979.

I. I. Shapiro, I. Maron, I. Kraft, "Experimental Study of Charge Drag on Orbiting Dipoles," Journal of Geophysical Research 68, No. 7 (April 1, 1963).

P. Stern, "Catalog of Precisely Reduced Observations," No. P-8, Special Report No. 118, Smithsonian Astrophysical Observatory (14 February 1963).

T. E. Sterne, An Introduction to Celestal Mechanics, Interscience Tracts on Physics and Astronomy, No. 9 (Interscience Publishers Inc., New York, 1960).

C. Stormer, The Polar Aurora (Oxford Press, London, England, 1955).

G. Veis, "Geodetic Uses of Artificial Satellites," Smithsonian Contributions to Astrophysics 3, No. 9 Washington, D.C. (1960).

C. A. Whitney, "The Structure of the High Atmosphere," Special Report No. 21, Smithsonian Astrophysical Observatory (27 February 1959).

C. A. Whitney, "The Structure of the High Atmosphere-II-A Conduction Model," Special Report No. 25, Smithsonian Astrophysical Observatory (20 April 1959).

S. P. Wyatt, "Effect of the Diurnal Atmospheric Bulge on Satellite Accelerations," Special Report No. 63, Smithsonian Astrophysical Observatory (May, 1961).

P. E. Zadunaisky, "The Orbit of Satellite 1958 Alpha (Explorer I) During the First 10500 Revolution," Special Report No. 50, Smithsonian Astrophysical Observatory (October 3, 1960).